Republic of Iraq
Ministry of Higher Education and Scientific Research
University of Babylon
College of Engineering

An Improved Simulation of Underwater Optical Wireless Communications System

A Thesis
Submitted to the Department of Electrical Engineering College of Engineering University of Babylon in Partial Fulfillment of the Requirements for the Degree of Master in Engineering / Electrical Engineering / Communications

By

Ali Mohammed Abdul Sada Abdul Wahid

Supervised by

Prof. Dr. Haider Jabbar Abd

2023 A.D **1444 A.H**

Copyright © 2022. All rights reserved, no part of this thesis may be reproduced in any form, electronic or mechanical, including photocopy, recording, scanning, or any information, without permission in writing from the author or the department of electrical engineering, faculty of engineering, university of Babylon.

(وَلَمَّا بَلَغَ أَشُدَّهُ وَاسْتَوَى آتَيْنَاهُ حُكْمًا وَعِلْمًا وَكَذَلِكَ نَجْزِي الْمُحْسِنِينَ)

صدق الله العلي العظيم

[القصص: ١٤]

Examining committee certificate

We certify that we have read this thesis entitled **"An Improved Simulation of Underwater Optical Wireless Communications System"** and as an examining committee, examined that student **Ali Mohammed Abdul Sada Abdul Wahid** in its content and that in our opinion it meets a standard of a thesis for the degree of master in engineering/Electrical engineering / Communications.

Signature:

Name: **Prof. Dr. Ibrahim A. Murdas**

(Chairman)

Date: / /2023

Signature:

Name: **Asst. Prof Dr. Hilal Al-Libawy**

(member)

Date: / /2023

Signature:

Name: **Asst. Prof.Dr. Hassanein A. Hasan**

(member)

Date: / /2023

Signature:

Name: **Prof. Dr. Haider J. Abd**

(supervisor)

Date: / /2023

Approval of Head of Department

Signature:

Name: **Prof. Dr. Qais Kareem Omran**

Date: / / 2023

Approval of the Dean of College

Signature:

Name: **Prof. Dr. Hatem Hadi Obeid**

Date: / /2023

Supervisor's Certification

I certify that this thesis **"An Improved Simulation of Underwater Optical Wireless Communications System"** and submitted by the student ***Ali Mohammed Abdul Sada Abdul Wahid*** was prepared under my supervision at the Department of Electrical / College of Engineering/ University of Babylon as a part of requirements for a master degree of science in Electrical Engineering/Communications.

Signature:

Supervisor: ***Prof. Dr. Haider Jabbar Abd***

Date: / / 2023

I certify that this thesis mentioned above has been completed in Electrical Engineering in the College of Engineering/ University of Babylon

Signature:

Head of Department: ***Prof. Dr. Qais Kareem Omran***

Date: / / 2023

Dedication

First and foremost, I would like to dedicate this work Sincerely to Allah Almighty,

then,

To

The reason for creation and existence Fatima al-Zahra,(peace be upon her)

To

the one who gave his life for our happiness ……My father.

To

my mother who stayed up and sacrificed for my success and to reach my goals.

To

my beloved wife, who shared my days with me and was my best support

Ali Mohammed Abdul Sada

2023

Acknowledgment

In the name of God, praise be to God, prayer, and peace be upon the Messenger of Allah .

All praises and thanks be to Allah for easing my task to accomplish this work despite all the hardships.

I would like to express my deepest sincere thanks and gratitude to my supervisor ***Prof. Dr. Haider Jabbar Abd****, I am very proud to work with him, for his supervision, guidance, and constant support in accomplishing this project within the limited time frame.*

I'm so grateful to the faculty and the staff of the Electrical Engineering Department, and colleagues for their eligible help and support that played a key role in finishing this project.

I would like to thank all my family and friends for their constant support and encouragement of me

Also, I would like to thank my friends ***Ali Razzaq*** *and* ***Ali Al-Karkhi*** *who were the best guides and advisors for me in addition to the trust they gave me*

Ali Mohammed Abdul Sada

2023

Abstract

The sending and receiving of information wirelessly underwater are called underwater wireless communication (UWC), there is done through the use of wireless carriers. Which are divided into three types: acoustic waves, radio waves, and optical waves. This work focused on the use of optical waves as wireless carriers for the design of an Underwater Wireless Optical Communication (UWOC) system. The purpose of employ this type of carrier is because it has a wider transmission bandwidth and therefore it provides a very high data rate much higher than acoustic and radio carriers. In recent years, because of this feature (high-speed transmission) that has attracted the interest of many researchers to study the (UWOC) system. Several (UWOC) systems have been proposed for disaster prevention, marine exploration, environmental monitoring, and military operations. However, despite these advantages of the (UWOC) system, the problems of light absorption and scattering by the water channel and the noise are limitations and obstacles to this system.

In this current work, two main types of modulation have been proposed. The first one is named Quadrature Phase Shift Keying (QPSK-OFDM) while the second one is named On Off Keying (OOK) modulation with different pulse shapes Non Return to Zero (NRZ), Carrier-Suppressed Return to Zero (CSRZ), and Manchester code. The effectiveness of the UWOC system is investigated over a range of transmission distances and different water kinds (clear, coastal, and turbid). In addition to that, the optical transmission systems were simulated with 1×1SISO and different MIMO configurations with selective data rates. The suggested system offered maximum communication link distance and better performance. The results show that the 8 × 8 MIMO technology used in the

Abstract

UWOC system is better than the rest of the other techniques used in all types of modulation in terms of link range and bit error rate BER. Moreover, the performance of the proposed QPSK-OFDM and OOK-Manchester code with 8×8MIMO is better than OOK-NRZ and OOK-CSRZ with 8×8MIMO under the same parameters. For instance, QPSK-OFDM with 8×8 MIMO, at 20Gbps data rate, and under clear water, achieved (230m with BER equal to 3×10^{-8}) and OOK-Manchester code with 8×8 MIMO, at 10Gbps data rate, and under clear water, achieved (257m with BER equal to 1.5×10^{-7}).

List of Contents

List of Contents

List of Contents

List of Contents

List of Figures

List of Figures

List of Figures

List of Figures

List of Figures

List of Tables

List of Tables

List of Tables

List of Abbreviations

Abbreviation	Definition
APD	Avalanche Photodiode
ASK	Amplitude Shift Keying
AUV	Autonomous Underwater Vehicle
BER	Bit Error Rate
BPSK	Binary Phase Shift Keying
CD	Coherent Detection
CSRZ	Carrier-Suppressed Return to Zero
DAB	Digital Audio Broadcasting
DAC	Digital to Analogue Convertor
DD	Direct Detection
DPSK	Differential Phase Shift Keying
DVB	Digital Video Broadcasting
FDM	Frequency Division Multiplexing
FEC	Forward Error Correction
FFT	Fast Fourier Transform
FOV	Field of View
FSK	Frequency Shift Keying
FSO	Free Space Optical
IF	Intermediate Frequency
IFFT	Inverse Fast Fourier Transform
IM	Intensity Modulation
ISI	Inter-Symbol Interference
LD	Laser Diode

List of Abbreviations

LED	Light Emitting Diode
LO	Local Oscillator
LOS	Line of Sight
LPF	Low-Pass Filter
LTE	Long-Term Evolution
MCM	Multi-Carrier Modulation
MIMO	Multiple In Multiple Out
MISO	Multiple In Single Out
MZDI	Mach-Zehnder Interferometer
MZM	Mach-Zehnder Modulator
NLOS	Non-Line of Sight
NRZ	Non-Return to Zero
OFDM	Orthogonal Frequency Division Multiplexing
OOFDM	Optical Orthogonal Frequency Division Multiplexing
OOK	On-Off Keying
OSNR	Optical Signal-To-Noise Ratio
OWC	Optical Wireless Communications
PAPR	Peak to Average Power Ratio
PDF	Probability Density Function
PIN	Positive-Intrinsic-Negative
PolSK	Polarization Shift Keying
PRBS	Pseudo-Random Bit Sequence
PSK	Phase Shift Keying
P/S	parallel to serial
QAM	Quadrature Amplitude Modulation

List of Abbreviations

QPSK	Quadrature Phase Shift Keying
RF	Radio Frequency
RZ	Return to Zero
S/P	Serial to Parallel Converter
SISO	Single Input Single Output
SIMO	Single Input Multiple Output
UOWN	Underwater Optical Wireless Network
UAWC	Underwater Acoustic Wireless Communication
UWC	Underwater Wireless Communication
UWOC	Underwater Wireless Optical Communication
VLSI	Very Large-Scale Integration
WDGF	Weighted Double Gamma Function
WLAN	Wireless Local Area Networks

Chapter One

Introduction and Literature Review

Chapter One

Introduction and Literature Review

1.1 Overview

Earth is a planet covered by water on two-thirds of its surface. Thus, the presence of a wireless communication system in the aquatic environment is important and necessary. The field of underwater communications has expanded quickly due to rapid technological advancements, and it now has a wide range of use for both commercial and military systems. Applications for underwater wireless communications include underwater surveillance, disaster discovery, national protection and security, control for pollution in environmental systems, collecting scientific data from deep-sea stations, and new resource discovery. Thus, in oceans and other aquatic environments, research into new wireless communication systems has been important [1].

Contrary to terrestrial wireless communication, the marine environment effected by noise, limited power, bandwidth, and the difficult underwater conditions. Thus, the underwater channel of communication often shows high attenuation, multipath effect, frequency dispersion, limited bandwidth and power resources. Making the underwater wireless channel is one of the most complex and difficult in nature. Future underwater wireless networks in optical, acoustic, and Radio frequency (RF) communications face many additional obstacles as a result of these particular circumstances in many underwater applications that have not been seen in wireless terrestrial communications. In recent years, there has been several of studies deals with underwater wireless networks. However, given the difficulties in the past with utilizing acoustic and optical wireless channels, further

advancements in underwater wireless systems remain difficult. Underwater communications can be done in three different ways[2][3]:

- RF by transmitting radio frequency waves.
- acoustic by transmitting sound vibrations.
- Transmission of optical waves for optical communication.

Each of these techniques has advantages and limitations.

Optical waves are electromagnetic waves between 400 nm (blue light) and 700 nm (red light) of wavelength. Because of its very short wavelength, high frequency and high bandwidth, optical waves are capable of communicating at extremely high speeds (above 1Gbps) [3]. The optical waves used as wireless communication carriers, usually for short destances due to strong water absorption and strong backscatter of suspended particles in the optical frequency band.

Table (1.1) shows the comparison between the three techniques [4]. Radio waves suffer from a high attenuation in water and at low frequencies require large antennas and high transmission power. Which makes it unsuitable for use underwater. Underwater sound propagation is influenced by high noise level propagation delay, path loss, multi-path, high bit error rate which is in the order of 10^{-2}-10^{-5} bps and limited bandwidth which depends on the range and frequency. In addition, acoustic communications is not the best to use underwater particularly with applications that need high data rates, multipath and real time operation. Therefor; underwater optical communications is a feasible solution because of the high data rate, high bandwidth. However, the absorption and scattering have an effect on the optical propagation path[5][6].

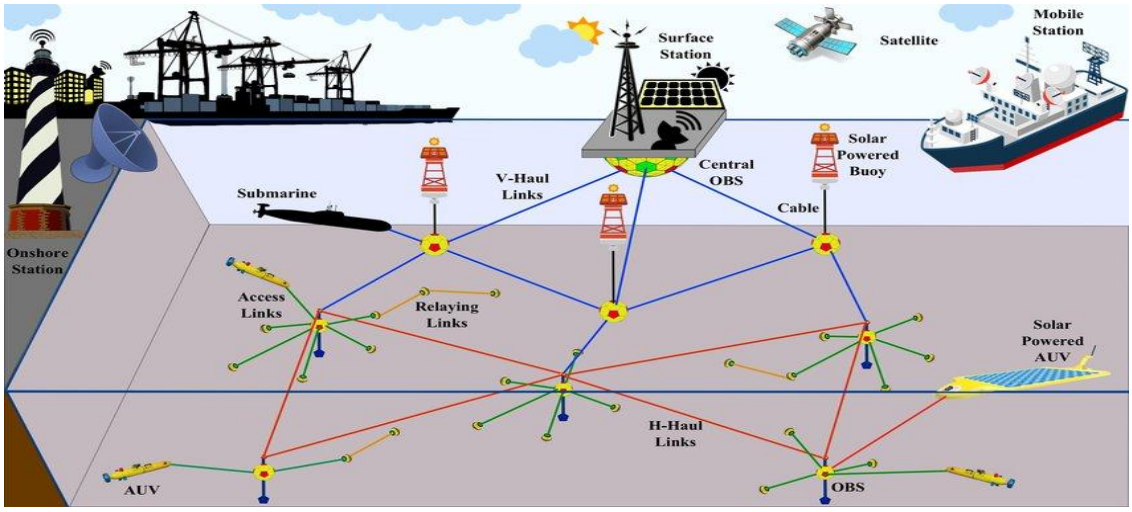

Fig.1.1: Shows the architecture of the underwater optical wireless network (UOWN) [7].

Table (1.1): Compares Acoustic, Radio Frequency, and Optical Techniques [4].

Parameters	**RF**	**Acoustic**	**Optical**
Attenuation	(3.50 – 5) dB/m	(0.10 – 4) dB/km	0.39dB/m (coastal) 3 dB/m (turbid)
Attenuation dependent	Frequency and Conductivity	Frequency and Distance	Distance and Type of water
Speed(m/s)	$2.225 * 10^8$ m/s	$1.5 * 10^3$ m/s	$2.225 * 10^8$ m/s
Data rate	(Mbps)	(Kbps)	(Gbps)
Latency	Moderate	High	Low
Range	10 meters or less	Around of km_s	10 – 100 meters
Bandwidth	MHz	KHz	10 – 170 MHz
Transmission power	mW-W	Tens of Watts	mW-W
antenna length	0.50m	0.10m	0.10m
Efficiency	_	100 bits /J	$3×10^4$ bits/J
Performance Parameters	permittivity and conductivity	salinity temperature, and pressure	Absorption and Scattering

1.2 Motivation

UWOC is a cost-effective, energy-efficient option for high data rates and minimal latency. In underwater propagation, light is absorbed, scattered, and subjected to multipath effects, causing signal distortion in the form of Inter Symbol Interference (ISI) and reducing the system's overall performance. Therefore, there is a need for a technique that can adapt to such a severe environment [4].

OFDM-MIMO exemplifies the advantages of wireless communication in the air. It is an available option for use in underwater wireless communication system. A popular type of multiple optical transmitters is MIMO, and multiple photodetector technology is an efficient way to dramatically increase system performance in terms of improving the channel capacity and data rate [8].

1.3 Problem Statement

The UWOC system seeks to solve the problems and limitations of Underwater Acoustic Wireless Communications (UAWC) systems, attractively and encouragingly addressing them. Although optical carriers can achieve high data rate communications at Gbps, but the high attenuation (scattering and absorption) in the water remain obstacles and thus, it is only useful for short-distance communications. Transmission length and underwater attenuation are impediments to the deployment of underwater optical networks in UWOC that must be overcome (scattering, absorption, and multipath)[9].

1.4 Literature Review

This section relates to the reviews and research about underwater wireless communication and some of the techniques used with it.

In 2015, H. M. Oubei, et. al. [10] used the NRZ-OOK modulation method, high-speed underwater wireless optical communication was demonstrated. The experiment was conducted in a 7-meter water pool. A laser diode (LD) with a bandwidth of 1.2 GHz and an avalanche photodiode (APD) generating at 520nm served as the transmitter. During the experiment, the BER was measured to be 2.23×10^{-4}.

In 2016, J. Xu, et. al. [11] developed and experimentally demonstrated an (IM/DD) OFDM-based optical wireless communication system for use underwater. The transmitter consisted of a single small LED, while the receiver was an inexpensive PIN photodiode. In addition to employing QAM modulation. The 40-meter transmission link in coastal water operated. The testing results indicated the bit rates were 225.9Mb/s with BER of 1.540×10^{-4} using 16QAM and 231.9Mb/s with BER of 3.280×10^{-3} using 32QAM at a link distance of 2 meters.

In 2016, M. V. Jamali, et. al. [12] Under coastal water, employing OOK modulation and the MIMO technique. The simulation findings show that spatial variety can greatly improve the system's performance in tandem with reducing the effect of turbulence; utilizing the 3X1MISO technique, MIMO technique performance improvement at the target BER of 10^{-9} over a 25meter coastal water connection range.

In 2018, F. Wang, et. al. [13] presented a QAM and Multi PIN photodetector-based underwater visible light communication system. A silicon substrate LED served as the transmitter. The transmitter's wavelength was 521nm. A 1.3m pool was used to test the proposed method. They concluded that choosing the appropriate value might enhance communication and that the ratio of two

receivers could have a substantial impact on the system's performance. The experiment's top data rate was 2.175Gbps.

In 2019, J. Wang, et. al. [14] designed and demonstrated in the lab a high-speed, long-distance UOWC system employing a low-cost LD with power-efficient OOK-NRZ modulation. Using 520nm blue LD, the system was able to achieve a data throughput of 500 Mbps over a 100-meter channel of tap water. The measured system BER value was $2.5x10^{-3}$.

In 2020 H. M. Azzawi, et. al. [15] used 4QAM-OFDM modulation with 4x4 MIMO technique and data rate 40Gbps. The photo source type is LD with 450nm wavelength and 100mw light power. The performance of the system has been examined in three types of water and has achieved 12m in turbid water with BER is 10^{-5}

In 2020, M. N. Hasan, et. al. [16] MIMO in addition to Direct Detection (DD-OFDM) with DPSK modulation used with data rate=10 Gbps. Under clear ocean water, simulations and evaluations of the system's performance have been conducted. 50 m for 1x1 SISO and 131 m for 4x4 MIMO is the maximum distance of a communication link that can be achieved with the proposed system and a bit error rate of 10^{-5}, as determined by comparing the bit error rate imposed by each configuration.

In 2021, S. Chakri D, et. al. [17] proposed an underwater wireless communication system using QAM modulation designed and implemented with OFDM. And the use of 8×8MIMO technology with different data rates (10, 20, 40, 80, and 100) Gbps and use of the CW laser diode with a wavelength of 532nm, and the use of a simple pin photodetector. The experiment was carried out under turbid

water conditions and obtained BER =0.00013 at a distance of 30m and a data rate of 40Gbps.

In 2022, F. Kaeib, et. al. [18] an underwater wireless communication design was made using Mach-Zehnder Modulator (MZM) and a laser diode as a light source and using OOK modulation. In this simulation, three types of water were used: pure water, coastal water, and turbid water. The results were compared between different wavelengths to compare the attenuation rates for each wavelength, and a distance was reached. More than 100 meters in pure water with a capacity of 1mW and the same distance was also reached with 0.35mW using wavelengths of low attenuation.

After reviewing all these studies, it was noted that the use of QPSK-OFDM modulation and OOK modulation can be relied upon in designing a wireless communication system suitable for the aquatic environment. Therefore, these two types of inclusion were proposed for this work.

1.٥ Thesis Objectives

In order to improve the system's performance against underwater restrictions, this study intends to create and evaluate the UWOC system's performance. The following objects might be listed:

- ❖ To design and simulate QPSK-OOFDM with direct detection (DD) based on a different MIMO configurations and 1×1SISO technique.
- ❖ To design and simulate OOK-NRZ, OOK-CSRZ, and OOK-Manchester code based on a 1×1SISO technique and different MIMO configurations.
- ❖ The goal BERs are 10^{-8} in order to maximize link ranges and execute the system performance in various water conditions (clear, mid-turbulence (coastal), and turbid).

- To compare the suggested and recently completed works using the same input parameters.

1.6 Thesis Layout

This thesis consists of five chapters:

Chapter One " Introduction and Literature Review " provides an overview of the UWOC system, motivation, Problem Statement, literature review, thesis objectives, and thesis layout.

Chapter Two "Theoretical Background of UWOC" discusses the fundamental concepts that utilized in the implementation of the proposed work.

Chapter Three "Design and Testing of the Proposed Systems " presents the system design and key parameters for QPSK-OFDM and OOK based on various MIMO configurations with various data rates. The material offered in the preceding two chapters serves as the design's foundation.

Chapter Four "Results and discussions " Presents and compares the simulation results for evaluating the performance of the UWOC suggested system under different water types and transmission distances using the simulation provides by Optisystem software.

Chapter Five "Conclusion and Suggestions for Future Work " presents a summary of the simulation's results as well as suggestions for future work that will help the system function better.

Chapter Two

Theoretical Background of UWOC

Chapter 2

Theoretical Background of UWOC

2.1 Introduction

Optical Wireless Communications (OWC) has become a favorable complementary technology to RF wireless technologies for future communication networks. OWC technologies possess many features such as a wide spectrum, high data rate, low latency, high security, low cost, and low energy consumption. In recent years, the use of OWC is not limited within the free space only, but also to the aquatic environment. Because of this, the UWOC system is a attracted many researchers to develop this system and overcome the obstacles in the aquatic environment.

This chapter, provides a general theoretical context, such as a description of the UWOC system. In addition, it describes the QPSK and OOK modulation formats, the attenuation underwater such as turbulence, absorption, scattering, underwater signal noise sources. In this part, the configurations of the underwater path are presented. In addition, this chapter describes the various fundamental types of Optical OFDM and a summary of the theoretical notions of the MIMO technique for improving the performance of the UWOC system.

2.2 UWOC System

A typical UWOC system's components are shown in Figure (2.1). It consists of a source for data generation that is modulated in an optical transmitter and transmitted over long distances at a high rate of data. The transmitter has a projection lens and beams steering components to focus the optical wave on the position of the receiver. The data carrying wave can then propagate along the water channel with characteristics unique to a particular geographic region[10] [4]. An

optical wave at the receiving end is converted from optical to electric by the photodetector. A demodulator and a signal processor can then process the electric signal to recover the original signal.

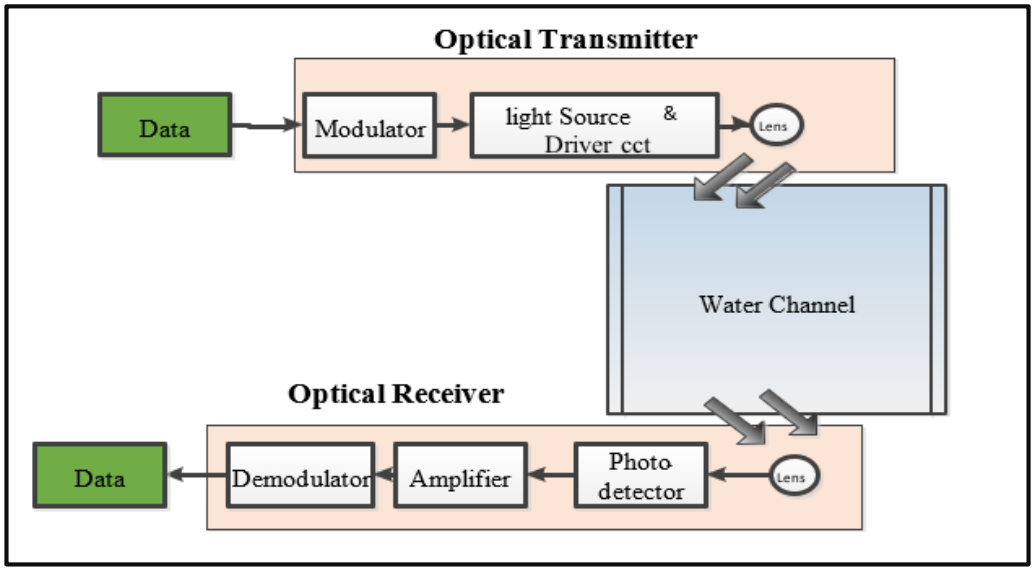

Fig.2.1: Block Diagram of UWOC System [4].

2.2.1 Transmitter of UWOC system

The electrical data signal is transformed into an optical signal and projects the optical signal into a transmission channel. Figure (2.2) shows a standard optical transmitter with an original wave, an optical driver system, a source of light, and additional optics components for the focusing and conditioning of light beams (lenses and reflectors)[19][20].

(Optical Transmitter)

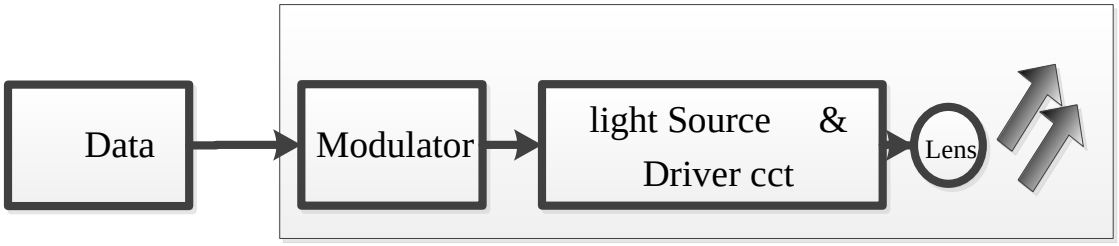

Fig.2.2: A Typical Optical Transmitter [19].

The role of the optical source is to convert an electrical input signal into the corresponding optical signal. There are two available types of optical transmitter device based on photon source: LEDs and LDs [19][20].

2.2.1.1 Laser Diode (LD)

LASER is the acronym for Light Amplification by Stimulated Emission of Radiation [21]. Stimulated emissions are a process in which the photon incident causes the stimulated electron to go down and radiates a photon with the same phase and frequency of the incident photon throughout this transition.

The basic diagram of a semiconductor optical amplifier, which is the main concept used in LASER technology is shown in Figure (2.3). Direct bias voltage is applied to the diode for a coherent photon beam. This causes electrons to flow into the p-type region and holes into the n-type region and therefore a pair of electron holes is generated, which is called pumping in laser applications. In this case, photon emission leads to electron-hole pairs being recombined. As a result, an additional photon with the same frequency and phase as the initial photon is produced.

These photons can be guided from the semiconductor, the input and the generated photon or can be used to produce more photons. Two mirrors are used, the first mirror that shows the photons incidentally, and a partial mirror (second mirror) that shows just part of the photos and transmits the rest, is one common way to achieve this objective. Trapped photons can be used to stimulate additional electrons and thus to produce more photons. The laser beam output is the photons passing through the partial mirror[22].

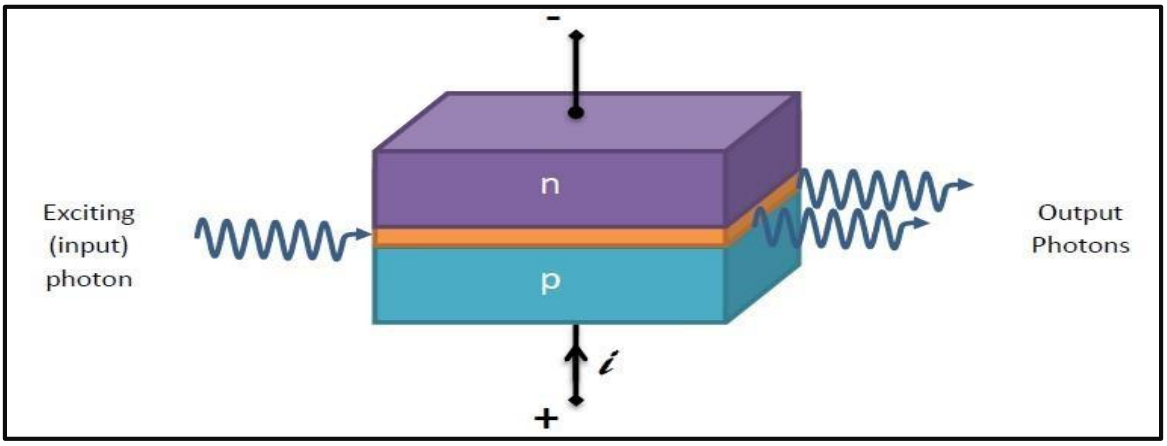

Fig.2.3: Shows the diagram of the Laser Diode [22].

2.2.2 Optical Receiver

The role of an optical receiver is to convert the optical signal back into electrical form and recover the data transmitted through the light wave system. Its main component is the photodetector that converts light into electricity through the photoelectric effect [10]. It consists of an optical signal detector that transform into an electric current. Figure (2.4) shows the system-level receiver design. Two popular examples of photodetector currently in use include p-i-n photodiodes (PIN) and avalanche photodiodes (APD) [19][20].

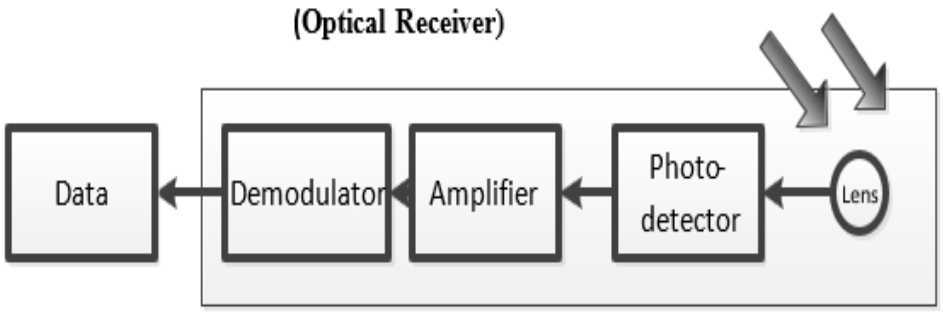

Fig. 2.4: A Typical Optical receiver [19].

The PIN photodetector includes semiconductor materials p and n type, which are separated by a very small intrinsic area of n-doped material. The reverse biases voltage is generated on the device under normal operating conditions.

The reverse bias ensures that the intrinsic region has been depleted by any charging carrier to convert an incident photon into an electron / electric current. The photon incident uses its energy to excite an electron from the valence band to the conductive band and generate a free pair.

The incident light is usually focused on the intricately depleted area. The high electric field in this disintegrated region separates and collects the generated charging carriers through the opposite partition junction. This gives rise to a current flow in an external circuit there is one electron flowing for every carrier pair generated. PIN photo-detector is reactivity always below the unit, and PIN photo detectors can work at very high rates of over 100 Gbit [23][24].

2.2.3 Mach-Zehnder Modulator (MZM)

For external optical modulation, the most popular modulator is the MZM. Ernst Mach and Ludwig Zehnder proposed it in 1891. The Mach-Zehnder Interferometer (MZDI) is comprised of two 3 dB couplers and two interconnection waveguides with waves of similar length, as displayed in Figure (2.5).

Typically, two waveguides are constructed for the MZM from an electro-optical substance like Lithium Niobate (LiNbO3). In addition, Phosphide Indium (InP) and Gallium Arsenide (GaAs) are included in the MZM creation process. The refractive index of an electro-optical material is dependent on an electric field applied. Thus, an electrical wave can alter the crystal's refractive index, thereby altering the speed of light propagation throughout the waveguide. The combination of two waveguide signals via the second coupler may be either constructive or destructive, depending on the level of electrical power chosen. The voltage of the modulator ($V\pi$) indicates the difference in voltage that enables a change from a maximum (constructive interference to a minimum (destructive interference)[25].

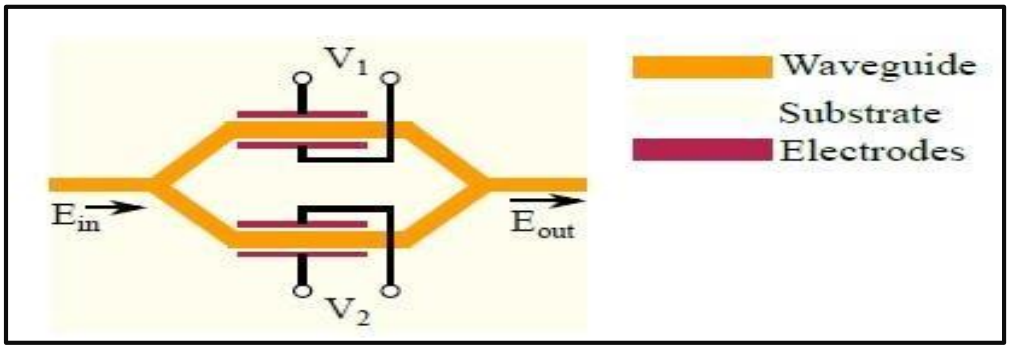

Fig.2.5: The Interferometer of MZM [25].

The MZM optical output field is given by [25]:

$$E_{out} = \frac{E_{in}(t)}{2} \left(e^{i\emptyset 1\,(t)} + e^{i\emptyset 2\,(t)}\right) \tag{2.1}$$

where ($\emptyset_1(t)$ & $\emptyset_2(t)$) are phases produced in the lower and upper arms of the MZM that are computed as:

$$\emptyset_1(t) = \frac{V_1(t)}{V_{\pi 1}}\pi \tag{2.2}$$

$$\emptyset_2(t) = \frac{V_2(t)}{V_{\pi 2}}\pi \tag{2.3}$$

where ($V_{\pi 2}$ & $V_{\pi 1}$) are the voltages necessary to generate a phase shift π of relative to the input for each arm. The MZM can be utilized in either push-pull or push-push mode.

Considering($V_1(t) = V_2(t) = V(t)$) and ($V_{\pi 1} = V_{\pi 2} = V_\pi$), the phase shift that is produced on the traveling light wave by the MZM is the same in both of its arms, resulting in a phase-modulated output upon combination. In push-push mode, the MZM behaves as a phase modulated device, with the output in this case being:

$$E_{out}\,(t) = E_{in}\,(t) e^{i\frac{V_1(t)}{V_\pi}\pi} \tag{2.4}$$

In the push-pull state, the voltage applied to both sides of MZM is similar, but with opposing signs. Therefore, the phase caused by the MZM arms becomes

opposite, resulting in amplitude modulation when combined in the output arm. Considering the voltage applied throughout the MZM sides ($V_1(t)= -V_2(t)= \frac{V(t)}{2}$), following is the relation between output and input:

$$E_{out}(t) = \frac{E_{in}(t)}{2}\left(e^{i\frac{V(t)}{2V_\pi}\pi} + e^{-\frac{V(t)}{2V_\pi}\pi}\right) = E_{in}(t).\cos\frac{V(t)}{2V_\pi}\pi \quad (2.5)$$

By quadrupling Eq (2.5), the relation between output and input power can be determined as follows:

$$P_{out}(t) = P_{in}(t)(0.5 + 0.5\cos(\frac{V(t).\pi}{V_\pi})) \quad (2.6)$$

2.3 Optical Communication Modulation Scheme

In optical communication systems, one of the most important factors is the modulation of the transmitted wave, which encodes information onto the light carriers as well as various digital communications systems. Modulation formats used for optical communication systems are similarly to those employed in radio frequency communication systems, with the phase, amplitude, and frequency relating to an optical wave containing data [26]. Optical modulation technology enables the modulation of optical waves and the transmission of data through optical systems.

The digital modulation technology includes different forms of modulated variables, including ASK, FSK, and PSK. Depending on modulating variables, the ASK modulation is the simplest type of modulation. In FSK, there is a frequency difference surrounding a center frequency, while in PSK, the phase of the carrier signal is moved 180° based on the information bit (1,0). In addition to amplitude, phase, and frequency, polarization states for (PolSK) can be used to modulate

signals. In addition, polarizing statements can be multiplexing various forms of optical signals that generate new signals[26].

2.3.1 PSK

Different digital modulation methods can be used for an analog signal. PSK, FSK, and ASK are the 3 fundamental types. Figure (2.6) displays their differences. The carrier signal is used to transmit bits with different amplitudes in ASK modulation. The PSK signal phase is altered, whereas the FSK differences center around the central frequency. As binary bits are encoded by using two separate phases, this modulation's phase shift is likely to be referred to as BPSK. The phase difference between the 2 nations is Ø=π. The terminology for BPSK's representation is [27]:

$$S(t) = \begin{cases} A\cos(2\pi fct)\ for\ binary\ 1 \\ -A\cos(2\pi fct)\ for\ binary\ 0 \end{cases} \quad (2.7)$$

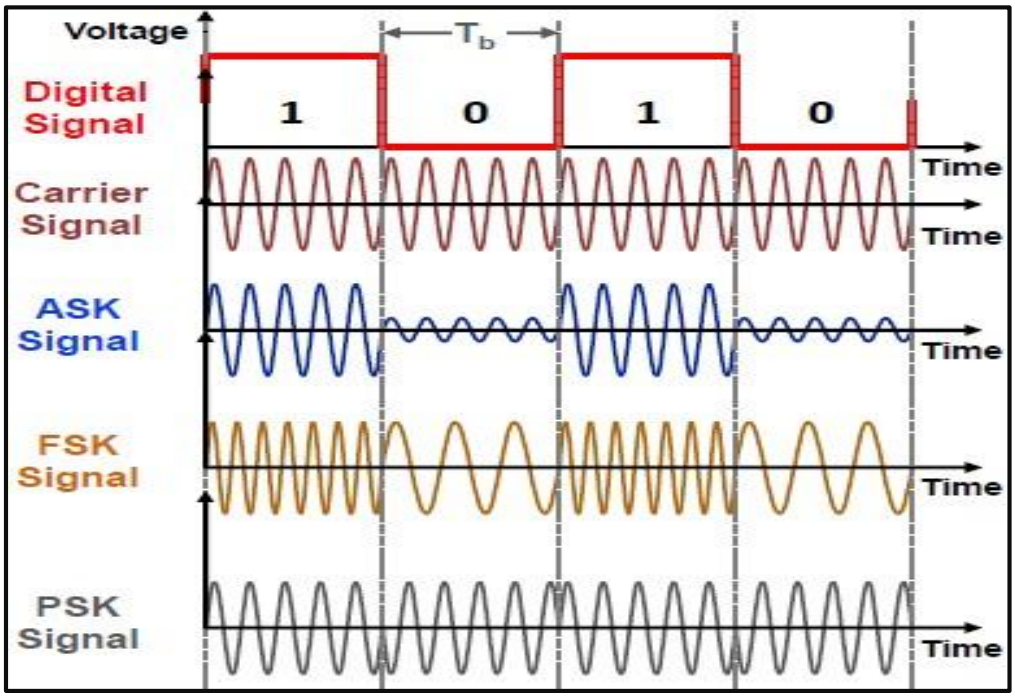

Fig.2.6: Three Modulations Techniques, ASK, FSK and PSK [27].

2.3.1.1 QPSK

In QPSK, two bits of a signal's information can be represented by a single symbol. The QPSK constellation is depicted in the diagram (2.7). When it shows that, information is allocated to the ($\pi/4$, $3\pi/4$, $-\pi/4$ and $-3\pi/4$) phases of the carrier signal are represented as (00, 01, 11 and 10) respectively.

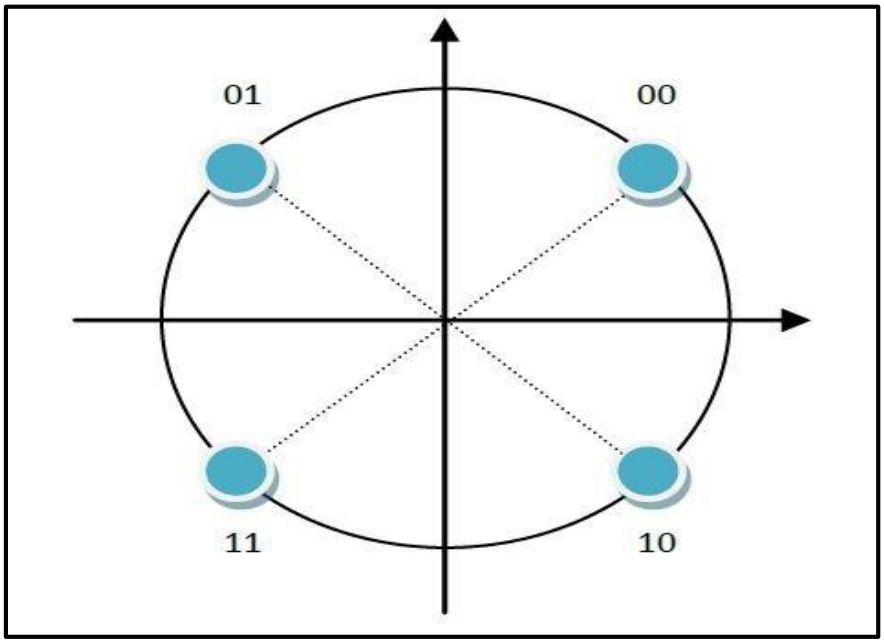

Fig.2.7: QPSK constellation diagram[28].

Each dibit (two bits) transmits a single symbol. A way for producing the QPSK waveform is to split the input binary stream of data into two streams: the odd-bit and even-bit streams, which are comprised of the odd- and even-numbered bits, respectively. Then, every one of these binary streams can be modulated using BPSK, and upon addition, the QPSK waveform is produced[29]. This procedure is depicted in the figure below (2.8).

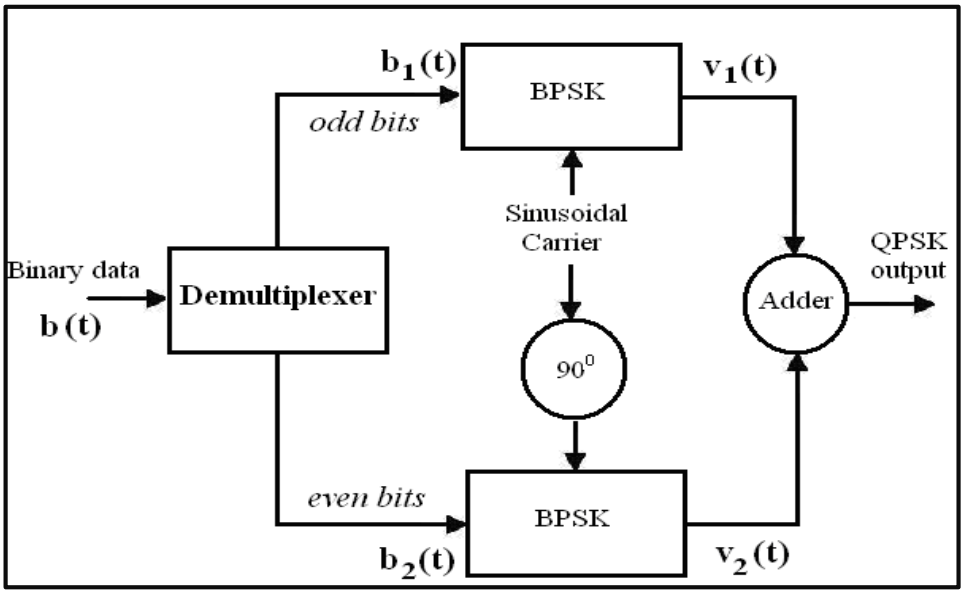

Fig.2.8: Method for producing the QPSK waveform for the digital data stream[28].

For QPSK differential encoding, a set of four bits is mapped to one of 2^2 possible transitions between two successive complex symbols S(i-1) and S(i). The transition can be described by the differential angle Δθ. The table (2.1) shows the dibit for differential angle mapping:

Table (2.1): Dibit for differential angle mapping.

Dibit	Δθ
0 0	*0*
0 1	*π/2*
1 1	*Π*
0 1	*3π/2*

As an updating formula, the differential QPSK encoding principle can be stated[30]:

$$s(i) = s(i-1)\, e^{j\Delta\theta(i)} \qquad (2.8)$$

The initial symbol $s(0)$ is set by letting $s(0) = re^{j\pi/4}$, with:

$$r = \sqrt{2} \tag{2.9}$$

where r represents the distance between center of the origin and the point of the constellation. Each symbol can be represented as:

$$s(i) = a(i) + jb(i) \tag{2.10}$$

where $\{a, b \in \pm 1\}$

QPSK modulation consists of two BPSK modulation on in-phase and quadrature components of the signal and the BER equation for QPSK modulation given by:

$$BER_{QPSK} = Q\left(\sqrt{\frac{2E_b}{N_\circ}}\right) \tag{2.11}$$

Where $Q \approx \frac{1}{x\sqrt{2\pi}} exp\left(-\frac{x^2}{2}\right)$ is the complementary error function of a normal distribution, E_b is the signal energy per binary bit, and $N_\circ$ is a single-sided noise power spectral density[31].

2.3.2 On-Off Keying (OOK)

In optical wireless communication systems, OOK is the principal pulse modulation format. It employs the straightforward amplitude-shift keying (ASK) modulation technique that represents digital data based on the existence of an optical pulse[32][33]. In its most basic form, the presence of a pulse for a particular bit length is represented by '1', whilst its absence for the same bit duration is represented by '0'.

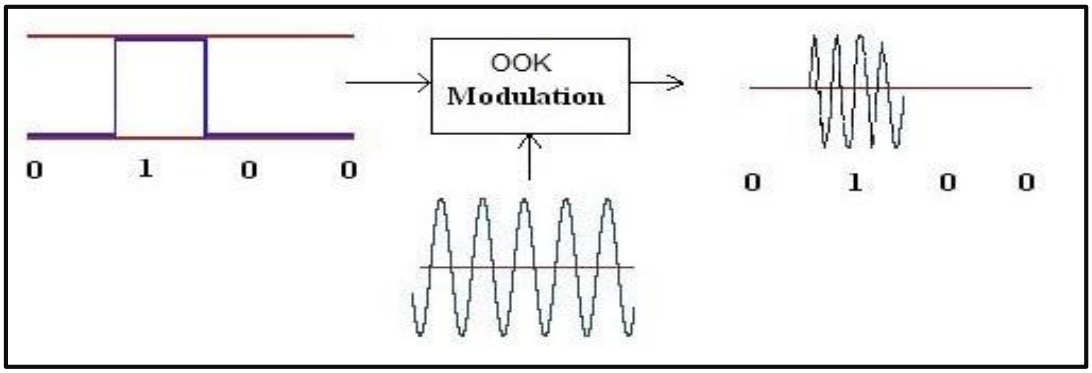

Fig.2.9: Modulation Technique of OOK[33].

The BER equation for OOK modulation given by:

$$BER_{OOK} = Q\left(\sqrt{\frac{E_b}{N_\circ}}\right) \tag{2.12}$$

Where Q is the complementary error function of a normal distribution, E_b is the signal energy per binary symbol, and $N_\circ$ is a single-sided noise power spectral density[31].

2.3.2.1 OOK-NRZ

Ones are represented by a single significant condition in an NRZ line code, typically, a positive voltage, whereas zeros are represented by another significant condition, typically a negative voltage, with no neutral or rest condition in between [34].

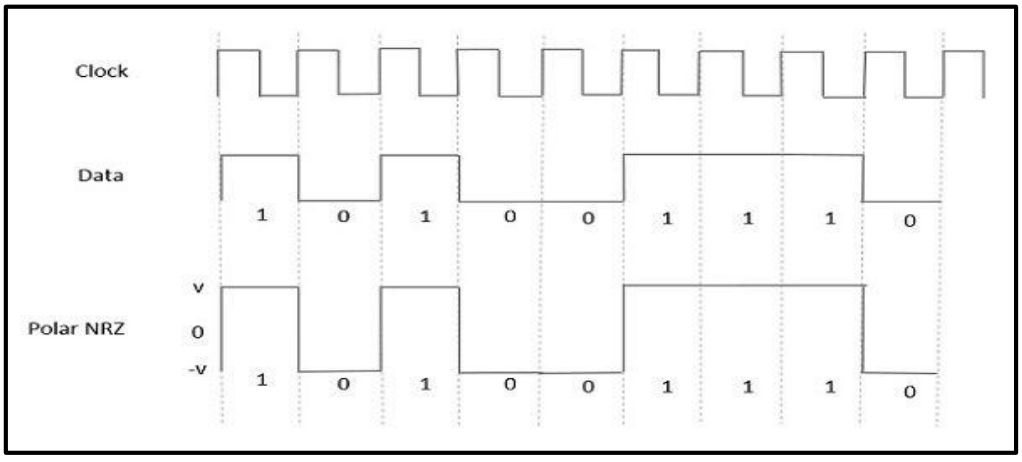

Fig.2.10: NRZ Encoding.

2.3.2.2 OOK-CSRZ

CSRZ modulation (carrier-suppressed RZ modulation) has a recently suggested as a modulation form for high data rate transmission systems that have been thoroughly examined in computational and experimental investigations[35].

The primary goal of this modulation style is to reduce nonlinear effects in transmission lines. Because of its smaller spectral width in comparison with standard RZ modulation, CSRZ modulation is predicted to increase transmission dispersion tolerance.

In CSRZ, a factor of two-spectrums decrease occurs when compared to the RZ scenario, as illustrated in figure (2.11). The RZ signal form of CSRZ pulses has an optical phase difference between consecutive bits. This condition of the inter-pulse phase can help to boost nonlinear tolerance. A carrier-suppressed RZ pulse is a kind of RZ pulse in which the carrier is turned off. The CSRZ signal differs from normal RZ in that consecutive bits in the CSRZ signal have a phase shift. In the optical domain, this phase change yields no DC component, hence there is no carrier component for CSRZ. Return to zero pulse modulation is used in CSRZ modulation. It also changes the optical signal's phase.

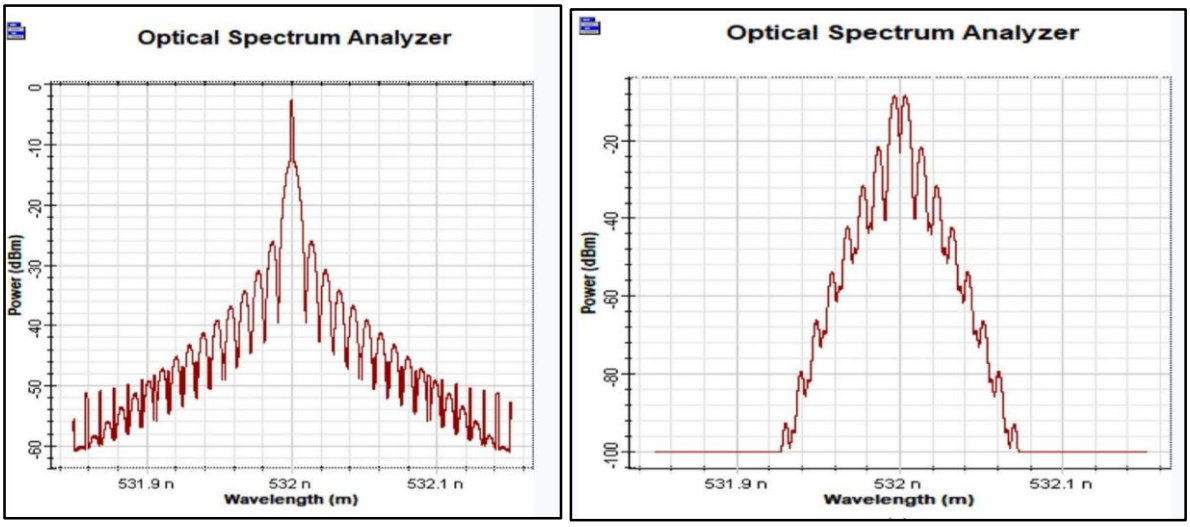

Fig.2.11: The optical spectrum of RZ and CSRZ Modulation format[35].

2.3.2.3 OOK-Manchester code

In data transmission, Manchester encoding is a form of digital encoding in which data bits are represented by transitions from one logical state to the other. This is different from the more common method of encoding. When the Manchester code is used, the length of each data bit is set by default which makes the signal self-clocking. The state of a bit is determined according to the direction of the transition. In some systems, the transition from low to high represents logic 1, and the transition from high to low represents logic 0. In other systems, the transition from low to high represents logic 0, and the transition from high to low represents logic 1.

The main advantage of Manchester encoding is that it is self-synchronizes. This minimizes the error rate and optimizes reliability. The main disadvantage is the fact that a Manchester-encoded signal requires that more bits be transmitted than those in the original signal [36].

The Manchester code is created from a non-return-to-zero (NRZ) data stream by a binary XOR (exclusive OR) with a clock signal having twice the frequency of the bit stream. When XORed with the ‘0’ (low) level, a low-to-high transition occurs, representing a logic ‘0’. If a data bit is XORed with the ‘1’ (high) level, an inversion occurs and the signal makes a high-to-low transition, corresponding to a logic ‘1’ [37].

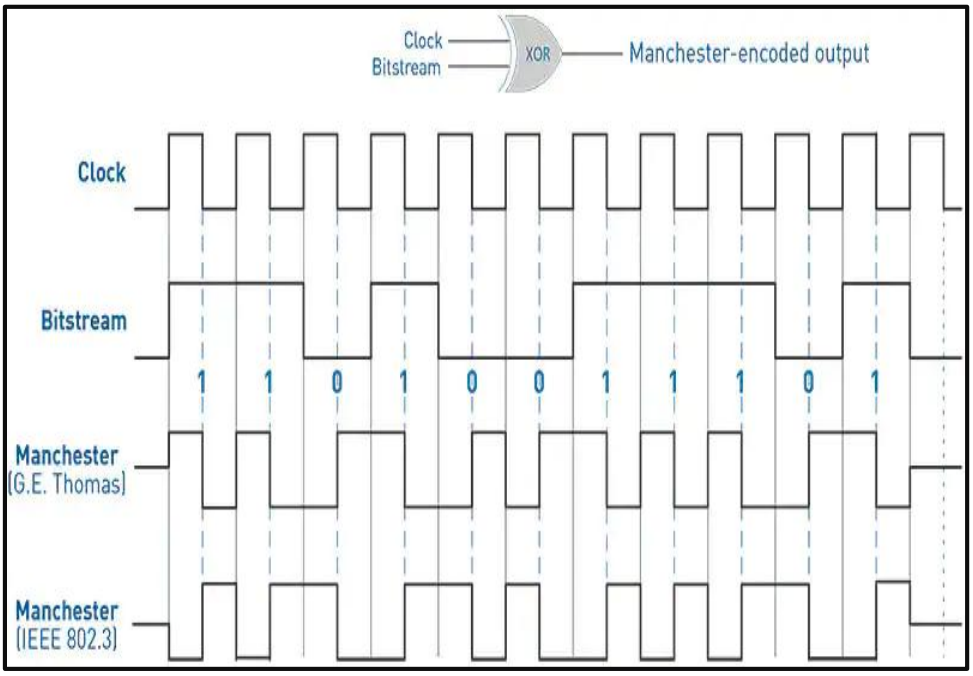

Fig.2.12: Waveform for the Manchester code[36].

2.4 Factors That Effect on UWOC system

Attenuation (scattering and absorption), turbulence, background noise, thermal noise , current shot noise , and dark current noise are the important facets that have an impact on UWOC systems[4].

2.4.1 Attenuation

Because of the high absorption of water applied to optical frequencies and strong particle backscattering, typically, the range of optical signals used as wireless carriers is extremely constrained. The fact that light waves often heavily absorbed by water one of the major issues, and the other is that all particles in the ocean diffuse optically. However, in the (green-blue) area of the visible light, absorption is diminished. As demonstrated in Figure (2.13), the minimum attenuation is centered in 450nm [26][7].

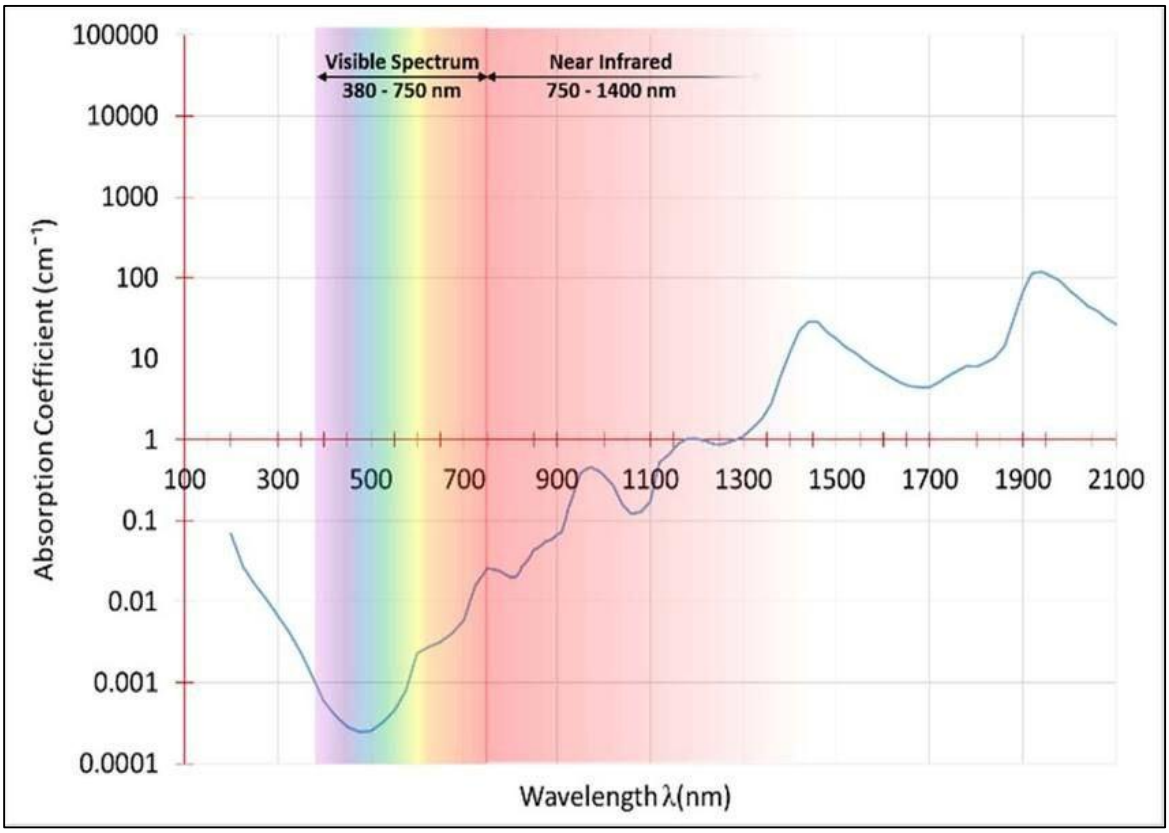

Fig.2.١3: The Transparent Window for Light Aquatic Attenuation is Shown with Blue and Green Colors [38].

2.4.1.1 Absorption

Absorption as the coefficient of spectral absorption (α(λ)), which is the change of the beam of light because the medium is absorbed per meter of the path length. The total absorbance is a linear mixture of the absorption of clean seawater, wavelength, concentration of chlorophyll, and dissolved organically colored chemicals. The absorption factor $\alpha(\lambda)$ is provided by:

$$\alpha(\lambda) = acl(\lambda) + aw(\lambda) + ah(\lambda) + af(\lambda) \quad (2.13)$$

Where $acl(\lambda)$ is the acid chlorophyll absorption factor as a wavelength dependence, $aw(\lambda)$ is the water absorption factor in relation to wavelength (m^{-1}),

$af(\lambda)$ Absorption ratio of fulvic acid and $ah(\lambda)$ is the absorption coefficient of humic acid and both depend upon wavelength [7] [39].

2.4.1.2 Scattering

Amount of optical flux that is lost as a consequence of the scattering of photons is denoted by the scattering factor β(λ). Overall scattering is a convolution of water's scattering coefficient, $b_w(\lambda)$, scattering caused by minute particles, $b_s{}^o(\lambda)$ depending upon wavelength and concentration, and scattering by substantial particles, $b_l{}^o(\lambda)$ depending upon concentration and wavelength. The scattering factor β(λ) is described by:

$$\beta(\lambda) = b_w(\lambda) + b_{s^\circ}(\lambda)Cs + b_{l^\circ}(\lambda)Cl \quad (2.14)$$

Where Cs represents a little particle concentration and Cl represents a big particle concentration[7] [39].

The route loss factor is displayed in Eq. 2.15 as a function of wavelength λ and distance z [26]

$$L(\lambda, z) = L^\circ e^{-c(\lambda)z} \quad (2.15)$$

Where L_0 is optical wave power before transmission, L (λ, z) is optical wave power after transmission, and c(λ) is the factor of extinction indicating the total attenuation caused by undersea propagation. Absorption plus scattering constitutes total attenuation. The total attenuation factor in eq. (2.16) It is employed in a completely scattering or absorbing medium. The scattering factor (β) or the absorption factor (α), respectively can be substituted. The product of c(λ) and z, commonly known as length of the attenuation, contributes to a reduction in received power using an exp factor.

On this will the extinction coefficient be calculated [40][38]:

$$C(\lambda) = \beta(\lambda) + \alpha(\lambda) \qquad (2.16)$$

Where $\alpha(\lambda)$ represents the absorption factor, $\beta(\lambda)$ represents the scattering factor, and λ represents the wavelength. Table (2.1) provides average values for $\alpha(\lambda)$, $\beta(\lambda)$, and C(λ) for the three most common forms of water. Clear ocean water has a larger concentration of dissolved particles, which impacts scattering. In coastal (mid turbulence) water, significant quantities of plankton, trash, and minerals are the primary causes of absorption and scattering. The greatest amount of dissolved substances can be found in the turbid water, which drastically limits light propagation[38]. Table 2.2 displays standard values for the factors C(λ), $\alpha(\lambda)$, and $\beta(\lambda)$ in consideration of the water classification. The 3 main kinds of water, together with their extinction values, are as follows:

Table 2.1: Standard extinction coefficient values (absorption and scattering)[26] [38].

Types of water	α(λ) (m^{-1})	β(λ) (m^{-1})	c(λ) (m^{-1})
Clearwater	0.114	0.037	0.151
Coastal Water	0.179	0.220	0.399
Turbid Water	0.366	1.829	2.195

2.4.2 Background Noise

The background noise consists of the blackbody radiation and the ambient light under water whose primary source is the refracted sunlight from the surface of the water. The background noise power can be written as [41]:

$$P_{BG} = P_{BG(blackbody)} + P_{BG(Solar)} \qquad (2.17)$$

In the equation above, the power of solar background noise, $PBG_{(Sol)}$, is given by:

$$P_{BG\ (sol)} = (\pi FOV)^2 A_R \Delta_\lambda T_F L_{(sol)} \quad (2.18)$$

Where Δ_λ bandwidth of an optical filter, A_R is the receiver area, FOV is the visual field, and the optical filter's transmissivity is denoted by the symbol T_F. The solar radiance, $L_{(sol)}$ W/m^2 is[41]:

$$L_{sol} = \frac{ERL_f e^{-dk}}{\pi} \quad (2.19)$$

where R is reflection of downwelling irradiance by water, *E* is downwelling irradiance W/m^2, L_f is the factor defining the dependence of undersea radiation on direction, K refers to the factor of diffuse attenuation, while d refers to the depth of the water (m).

2.4.3 Dark Current Noise

The noise that is being produced by the detector (photodiode) right now is called dark current noise. The variance of the noise of the dark current is [41]:

$$\sigma_{DC}{}^2 = 2qI_{DC}B \quad (2.20)$$

Where B is the bandwidth, and $I_{DC} = 12.26 \times 10^{-10}$ (Ampere).

2.4.4 Thermal Noise (Johnson Noise)

The variance of Johnson noise is [41]:

$$\sigma_{TH}^2 = \frac{4KT_eFB}{R_L} \quad (2.21)$$

Suppose that the equivalent temp T_e is 290K, that the system's noise figure is F = 4, B is the bandwidth, and that the load resistance RL = 100 Ω.

2.4.5 Current Shot Noise

When the received signal is there, shot noise is present. Variance for current shot noise is [41]:

$$\sigma_{ss}^2 = 2q\Re P_S B \qquad (2.٢2)$$

Where q is the charge of the electron (1.6×10^{-19}), P_s is the signal power, B is the bandwidth and $\Re$ is the responsivity.

The sum of all noise sources constitutes the total noise variance. Therefore, the variance of current noise in the detector in the absence of an optical signal can be calculated as:

$$\sigma_{0^2} = \sigma_{TH^2} + \sigma_{DC^2} + \sigma_{BG^2} \qquad (2.٢3)$$

Due to the existence of shot noise the variation of current noise within the detector that is used for the detection of an optical wave is computed as follows:

$$\sigma_{1^2} = \sigma_{TH^2} + \sigma_{DC^2} + \sigma_{BG^2} + \sigma_{SS^2} \qquad (2.24)$$

2.4.٦ Turbulence

Variation in the refraction index along the transmission path caused by fluctuations in the underwater environment. Salinity, density and temperature leads to large fluctuations in the receiver signal intensity. This fact is called scintillation, and it reduces UOWC's efficiency. As such, there is no specific model for underwater turbulence as in the case of free space optical (FSO) communication because of the dynamic nature of the underwater environment[4].

2.5 Configurations for Underwater Links

Underwater optical link configurations can be classified into one of three types [42][43]: (a) direct links (LOS), (b) Non direct links, and (c) retroreflector links.

2.5.1 Direct Links LOS

Figure (2.14) depicts a direct link LOS, which is the most elementary, unhindered, and point-to-point undersea connection between receiver and transmitter. This connection is especially well implemented in the situation of static receivers or transmitters, such as multiple sensor nodes at the ocean's bottom. When the transmitter in clear oceans transmits a narrow wave to the receiver, it works well. The likelihood of obscuration is significant, however, because of fish populations, marine life expansion, and other obstacles.

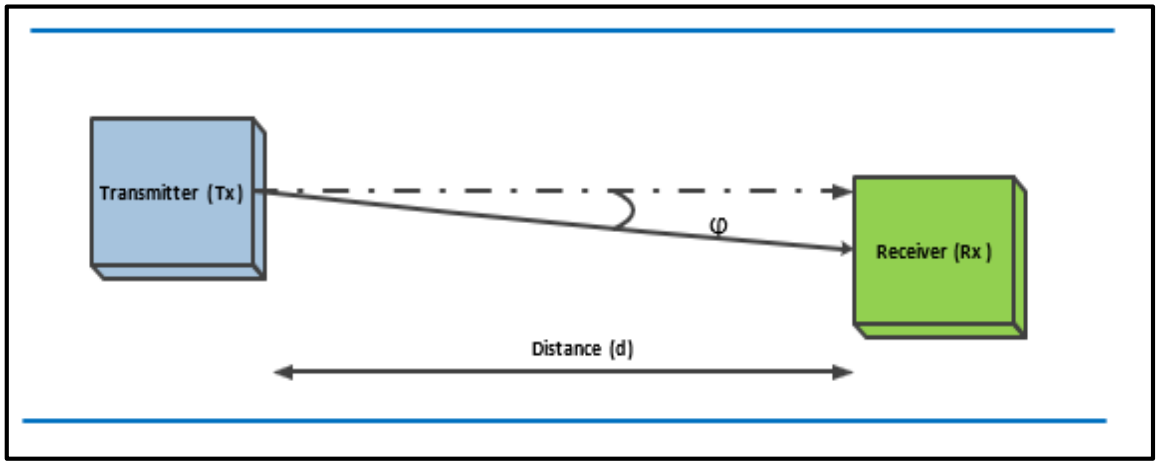

Fig.2.14: LOS Link Configuration [43].

Therefore, to construct a LOS link, a system must be developed that avoids marine life from obstructing the propagation path. The ideal lighting for optical communication underwater also attracts schools of fish. While fish favor yellow and green wavelengths, marine fish prefer blue and green wavelengths. As a result,

erratic or flashing lights are preferred to keep fish out of the LOS area. The authority derived from P_R ($_{Los}$) is granted by[43].

$$P_{R-los} = P_T \eta_T \eta_R L_{pr}\left(\lambda, \frac{d}{\cos\theta}\right).\frac{A_r.\cos\emptyset}{2\pi d^2(1-\cos\theta_\circ)} \qquad (2.25)$$

Where P_T is an average transmission power, η_T is the transmitters optical efficiency, η_R is the receiver's optical efficiency, d represents the perpendicular space between the planes of the transmitter and receiver, Ø angle formed by the reception plane and the trajectory of the transmitter and receiver, A_r area of the receiver aperture, while θ_0 is the angle of beam divergence. In situations where the angle of divergence of the laser light is extremely narrow ($\theta_0 << \pi/20$) equation (2.25), approximated as [43]:

$$P_{R-los} = P_T \eta_T \eta_T L_{pr}\left(\lambda, \frac{d}{\cos\emptyset}\right).\frac{A_r.\cos\emptyset}{\pi.(d.\tan\theta_\circ)^2} \qquad (2.26)$$

2.5.2 NLOS Links

Non-Los arrangement overcomes the alignment of LOS links at UWOC, as depicted in Figure (2.15). A transmitter in this design emits the light beam toward the surface of the water at an incidence angle bigger than the angle of critical incidence. In order to ensure the proper receipt of signal, the receptor should continue to face the water surface in a direction approximate to the reflected light. Random water surface slopes resulting from wind or other types of turbulence pose the greatest obstacle for non-LOS connections. These unwanted occurrences are seen as a reflection in the light emitted by the transmitter, resulting in severe signal dispersion[43].

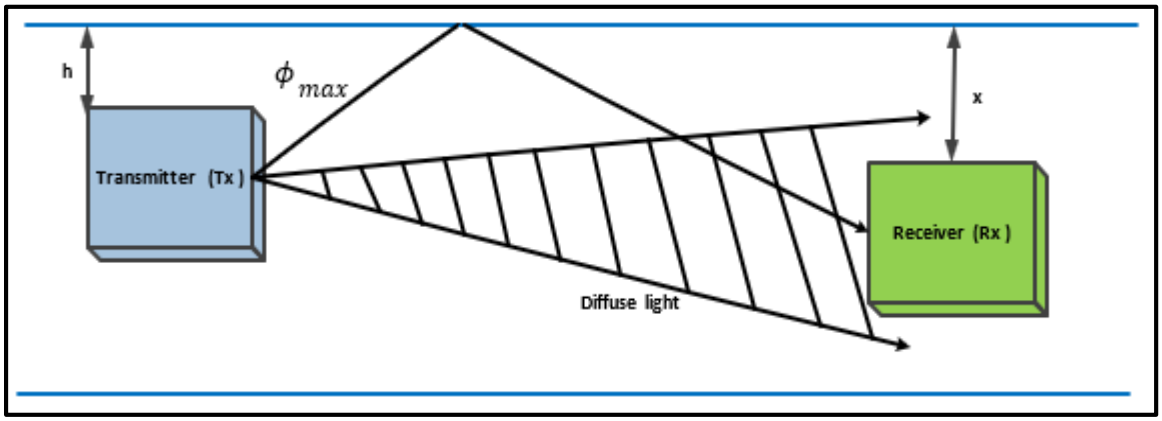

Fig.2.15: Configuration of a Non-LOS Link [43].

When the transmitter is located at depth h, an illuminated annular area with a similar power density at depth z can be calculated as follows[4]:

$$A_{(ann)} = 2\pi\,[(h+z)^2(\cos\emptyset - \cos\emptyset\max)] \quad (2.27)$$

The received power P_R offered by:

$$P_{R(\text{non-Los})}(\emptyset) = A_r f_R(\emptyset) \quad (2.28)$$

where $f_R(\phi)$ is an extra function dependent on η_T, η_R, P_T, (h + z), A_{ann}, and ϕ_t transmitting angle.

2.5.3 Retroreflector Links

In a restricted duplex communication situation with a low capacity of receivers' power to support full transceiver operations, retroreflector links are used, as shown in figure (2.16). Here, the source has more power and load capability than the receiver; hence, it acts as a transmitter of modulated light signals to the remote receiver. The receiver is equipped with a small optical retro-reflector which upon sensing the incoming beam from the source reflects it back to the same source. The received power in this case is given as [4]:

$$P_{R-Retro} = P_T \eta_T \eta_{Retro} L_{pr}\left(\lambda, \frac{d}{\cos\emptyset}\right) . \frac{A_{Retro} . \cos\emptyset}{2\pi d^2 (1-\cos\theta_\circ)} . \left[\frac{A_{Rero}}{\pi (d \tan\theta_{Retro})^2}\right] \quad (2.29)$$

Where η_{Retro} optical efficiency of the retro-reflector, θ_{Retro} is the divergence angle of the retroreflector, A_{Retro} is the area of the retro-reflector's aperture, and other parameters were previously defined.

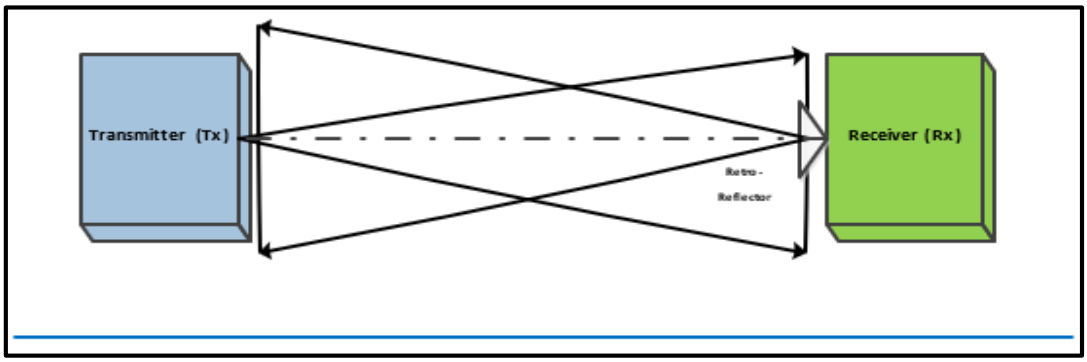

Fig.2.16: Configuration of Retroreflector Links [4].

2.6 UWOC Channel Model Turbulence

Early studies of underwater channels frequently employed basic models, like Beer Lambert's rule, to simulate the underwater light propagation. Despite the change, Beer Lambert's rule cannot adequately explain the channel characteristics for UWOC systems since it only accounts for range dependence and does not address spatial and temporal features[44].

Undersea turbulence can be divided into three channels based on the value of the light scintillation index (σ_I^2), which is defined as the typical fluctuation of the laser radiance: low turbulence (clear water), mid-turbulence (coastal water), and strong turbulence (turbid water). This is a measurement of turbulence intensity. The mathematical definition of the scintillation index is[45]:

$$\sigma_I^2 = \frac{E[I^2] - E^2[I]}{E^2[I]} = \left[\frac{E[h^2]}{E^2[h]} - 1\right] \quad (2.30)$$

Where $E[x]$ represented the expectation of random variable x, and I_0 is the non-fading intensity. A high scintillation index denotes a strong turbulent channel, whereas a low scintillation index defines an ineffective turbulent channel. A channel with ineffective turbulence is specified for $\sigma_I^2 \ll 1$. The designation given to the mild turbulence channel as $\sigma_I^2 \sim 1$. Intense fluctuations usually referred to as saturation channel, are attained when $\sigma_I^2 \gg 1$.

It is important to examine and comprehend the statistical distribution for optical signal fluctuations caused by undersea optical turbulence in order to create strong and reliable UOWC systems. The majority of the early work on underwater optical turbulence was theoretical, describing changes in irradiance in the maritime environment using models of air turbulence, including the lognormal distribution. The spectrum of salinity or temperature in the atmosphere, however, greatly contrasts with the variety of refractive index changes caused by pressure inhomogeneities or temperature in water. Because of this, the lognormal distribution cannot accurately represent how irradiance fluctuates in turbid water. It investigated whether the Gamma-gamma distribution might be used to describe the channel of UWOC system.[45].

2.6.1 Gamma-Gamma Model

The Gamma-gamma scintillation model is based on Doubly Stochastic theory and it has weak to strong turbulence condition so the PDF (Probability Density Function) of its intensity (I) is product of two gamma random variables which represents fluctuations from small and large turbulence. The two random variables are X and Y and the received intensity I, is [46]:

$$I = XY \tag{2.31}$$

The PDF for I is:

$$p(I) = \frac{2(ab)^{\frac{a+b}{2}}}{\Gamma(a)\Gamma(b)} . I^{\left(\frac{a+b}{2}\right)-1} . K_{a-b}\left(2\sqrt{abI}\right), I > 0 \quad (2.32)$$

Where r(.)is the function of gamma, I is a radiance, and $K_{(a, b)}$ is the second order Bessel function. The numbers (a and b) refer to the number of small and large turbulence cells, respectively, and are defined by [46]:

$$a = \frac{1}{\exp\left[\frac{0.49\sigma^2}{(1+1.11\sigma^{\frac{12}{5}})^{\frac{7}{6}}}\right]-1} \quad (2.33)$$

$$b = \frac{1}{\exp\left[\frac{0.510\sigma^2}{(1+0.7\sigma^{\frac{12}{5}})^{\frac{5}{6}}}\right]-1} \quad (2.34)$$

Where σ^2 is the variance. For the channel model, the scintillation index used to determine the amount of turbulence is calculated by [46]:

$$\sigma^2 = \left(\frac{1}{a}\right) + \left(\frac{1}{b}\right) + \left(\frac{1}{ab}\right) \quad (2.35)$$

2.7 Fundamentals of MIMO and OFDM Optical Communications Techniques

During underwater propagation, light rays are absorbed and scattered, causing ISI and reducing the total performance. Consequently, it is solve by a technique that adjusts to this type of environment. Multi Input Multi Output (MIMO-OFDM) has demonstrated the benefits of wireless communication inside the air. It is a technology that could be utilized in an undersea communication system. The MIMO technique is a commonly employed multi transmitters and

photodetectors technique that effectively improves performance of the system in terms of data rates and performance.

MIMO is a commonly used technique, in contrast to the typical SISO technique, the MIMO technique offers substantially higher data rates across greater distances and increases the transmission's efficiency and reliability. The OFDM may be considered since it is not only an effective method for minimizing ISI but also a simple technique to be implemented in a practical systems. In Multi-Carrier Modulation (MCM), that mean the transmits data over a lot of lower-rate subcarriers, OFDM is characterized as a type of multicarrier modulation. OFDM's resistance to channel dispersion and flexibility in a time-varying system are its two main advantages [47][8].

2.7.1 MIMO Techniques with Optical Communication

In the underwater communication, the signal attenuation is large due to the physical and chemical properties of water such as the sea surface and bottom reflection, sea temperature, and the dynamics of oceans, etc. Therefore, it is motivated a technique that adapt to such environment. MIMO has proved the advantages in wireless communication in atmosphere. It will be a potential technique to use in underwater communication system. In the fading channels, MIMO system improves significantly channel capacity. This means that the transmission rate is significantly increased. In addition, MIMO system also creates the spatial diversity which reduces BER when the system is operated. The MIMO technique will combine above mentioned advantages of techniques to achieve the reliable transmission for underwater wireless communication[8].

2.7.2 MIMO System Mathematical Model

Figure (2.17) displays the MIMO system model. Any communication system includes transmission antennas N_T and receive antennas N_R. The antennas (Tx1, Tx2…, TxN_R) respectively transmit signals (x1, x2…, xN_T) to receive antennas (Rx1, Rx2…, RxN_R). Each receiving antenna mixes the coherently adding incoming signals. The signals received by antennas (Rx1, RX2…, RxN_R) are respectively symbolizes them (y1, y2…, yN_R). Received signal on the antenna Txq; q = 1, 2…, N_R [32]:

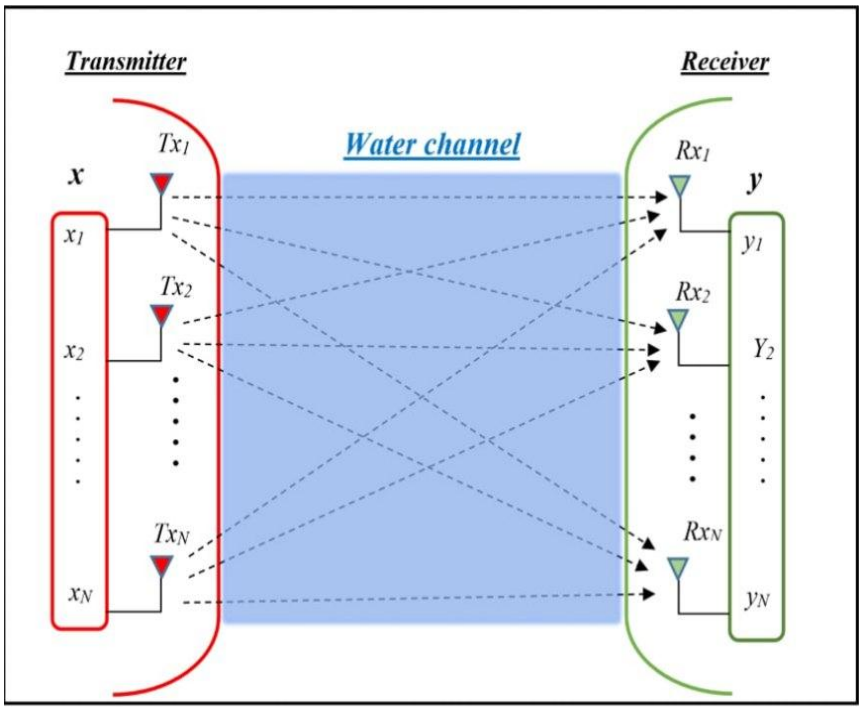

Fig.2.17: Multi-Input Multiple-Output (MIMO) System Model [48].

$$y_q = \sum_{p=1}^{N_T} h_{qp}.x_p + b_q; q = 1, \dots, N_R \quad (2.36)$$

The relation with both input and output is what defines the flat fading for the MIMO channel model as [42]:

$$y = b + x.H \quad (2.37)$$

Where H is the complex channel matrix ($N_R \times N_T$) generated from:

$$H = \begin{pmatrix} h_{11} & \cdots & h_{1NT} \\ \vdots & \ddots & \vdots \\ h_{N_R 1} & \cdots & h_{N_R N_T} \end{pmatrix} \quad (2.38)$$

Where $p = 1, 2\ldots, N_T$; $q = 1, 2\ldots, N_R$ is the complicated channel gain that connects the transmit antenna Tx_p with the receive antenna Rx_q., $x = [x_1, x_2\ldots, x_{NT}]^T$ is the ($N_T \times 1$) Complex signal transmission Vector, $y = [y_1, y_{2\ldots,} y_{NR}]^T$ is the ($N_R \times 1$) vector of complex received signal and $b = [b_1, b_2\ldots, b_{NR}]^T$ is the ($N_R \times 1$) complex additive noise signal vector.

2.8 OFDM with optical communication

OFDM is a frequency-division multiplexing (FDM) scheme that was introduced by Robert W. Chang of Bell Labs in 1966 was the first to propose the OFDM idea. OFDM gain over the most development part in military applications, because the lack of broad band applications for OFDM and powerful integrated electronic circuits to support the complex computation is required by OFDM. However, the development in broadband digital applications and the Very Large-Scale Integration (VLSI) CMOS chips in the 1990 brought OFDM into the spotlight[47].

The first (DAB) Digital Audio Broadcasting standard was OFDM in 1996, and it later became the most major modulation technique in many other standards, Wireless Local Area Networks (WLAN), including Digital Video Broadcasting (DVB), long-term evolution (LTE), wireless metropolitan area networks (WAN), and the 4G mobile communication systems. It was previously unknown of in optical communications prior to 2005, when Dixon suggested utilizing OFDM to resolve modal dispersion. Therefore, the first optical OFDM

developments focused on multimode fiber applications. OFDM is used for transmission over large distances, Direct Detection (DD-OFDM), and Coherent Detection (CD-OFDM) are the three areas in which optical OFDM is of most interest[47][49].

2.8.1 OFDM Basics

In this study, the water channel can have multipath impacts. The modulations mentioned so far suffer a great deal in such an environment and multipath that could even impair communication to a point in which the message is unusable. When multipath impacts are existent, it is necessary to look at more reliable modulations.

Now days, OFDM is thought to be a strong option to be used in such situations. A type of MCM known as OFDM divides a data stream moving at one rate into many, parallel streams moving at lower rates. The bits stream is then individually modulated into various frequency carrier waves, called subcarriers, and sent over the same channel. Although OFDM has just recently been used in optical communication, there are increased numbers of studies on its theoretical and practical performance in a variety of optical communication systems, it includes multimode optical fiber, single mode fiber, and wireless optical[49].

A modified form of frequency division multiplexing (FDM) is known as OFDM. The FDM technique transmits various information for several users concurrently over multiple frequency carriers, as depicted in Figure (2.18). After being modulated by the user's data at the transmitter, each subcarrier has a wide guard band to prevent it from interfering with other subcarriers. This guard band will, however, reduce the spectral efficiency of the system. The oscillator banks at the receiver and then demodulate the signals that were just received[49].

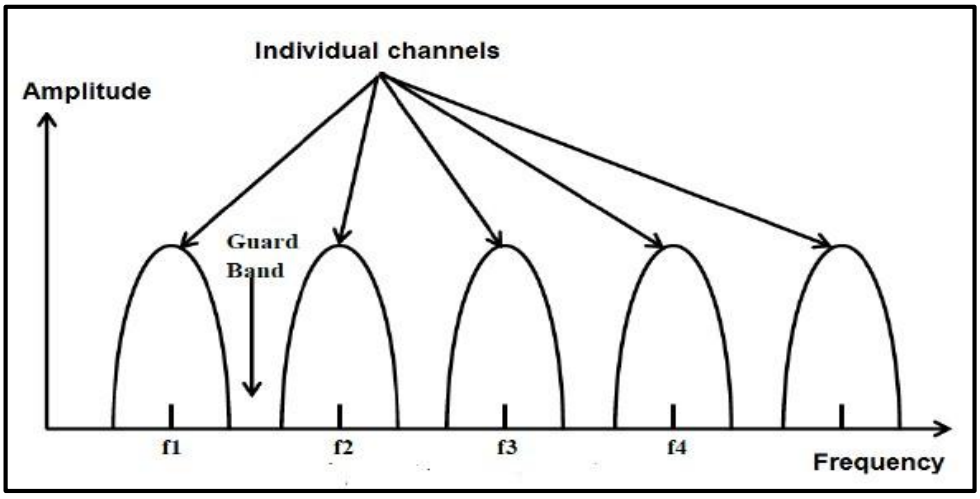

Fig.2.18: Spectral FDM [49].

In OFDM, as a special case of FDM, OFDM uses many carriers per a given spectrum that are very close to each other, However, they maintain orthogonality at a precise distance from one another. Even when there is overlap between the subcarrier, FFT and IFFT are used to demodulate and build the original signal as shown in Figure (2.19).

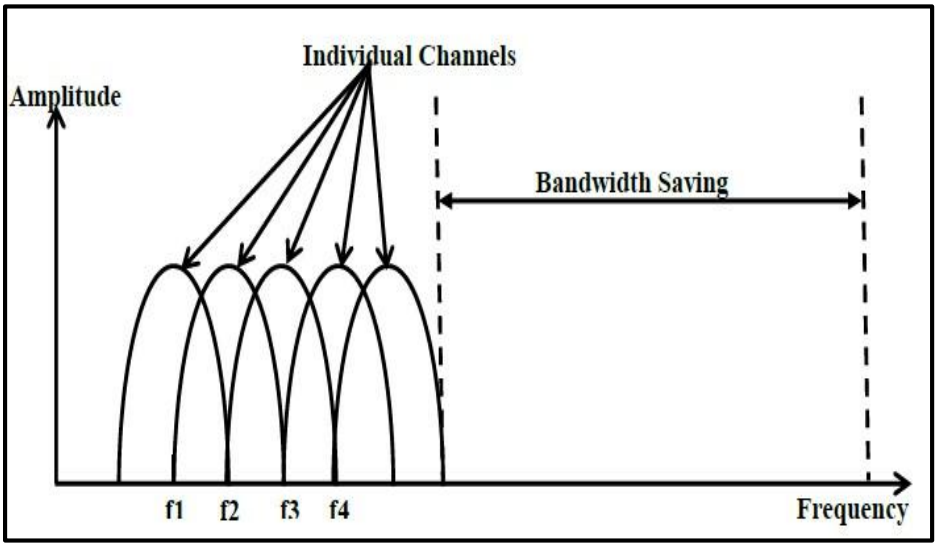

Fig.2.19: Spectral OFDM [49].

An accumulation of sinusoids, which each corresponds to a subcarrier, produces OFDM signals. Subcarriers can also be mathematically expressed as [50]:

$$S_k(t) = \begin{cases} \sin(2\pi k \Delta f t), & 0 < t < T, k = 1,2,\dots,N \\ 0, & otherwise \end{cases} \quad (2.39)$$

where N refers to the number of subcarriers, Δf is the subcarrier spacing, and the symbol T represents the symbol period. Considering the highest frequency component to be NΔf, the bandwidth of the transmission is about NΔf. If signals are mutually independent, they are orthogonal. All subcarriers are orthogonal to one another since the following criterion has been met [50].

$$\int_0^T S_i(t) S_j(t) d(t) = \begin{cases} C, i = j \\ 0, i \neq j \end{cases} \quad (2.40)$$

The orthogonality property of OFDM signals is to look at its spectrum. The orthogonal nature of the transmission is a result of the peak of each subcarrier corresponding to the nulls of all other subcarriers

2.٨.2 OFDM System Description

A typical OFDM wireless system's transmitter and receiver are shown in block diagram form in Figure (2.20). At the transmitter side, (S/P) serial to parallel converter divides the data rate of digital stream into N parallel streams. Each stream is assigned a symbolic stream by the modulation scheme (PSK, QAM, etc.). Using IFFT on the sub-carrier, the symbols are modulated to convert the OFDM signal from the frequency domain to the time domain. After IFFT, the guard interval or cyclic prefix is added to stop sub-band carriers from overlapping, and the OFDM signal is then converted to analog signal by the (DAC) digital to analog converter.

After converting from (P/S) parallel to serial, the signal is then transmitted through the channel using a local oscillator. An analog to digital converter removes the cyclical prefix on the receiver side before converting the received wave to digital in parallel. Following that, the FFT technique will be

utilized in order to demodulate the signal and either the PSK/QAM data symbol selections. To obtain the original data, the data is transformed to serial. [51].

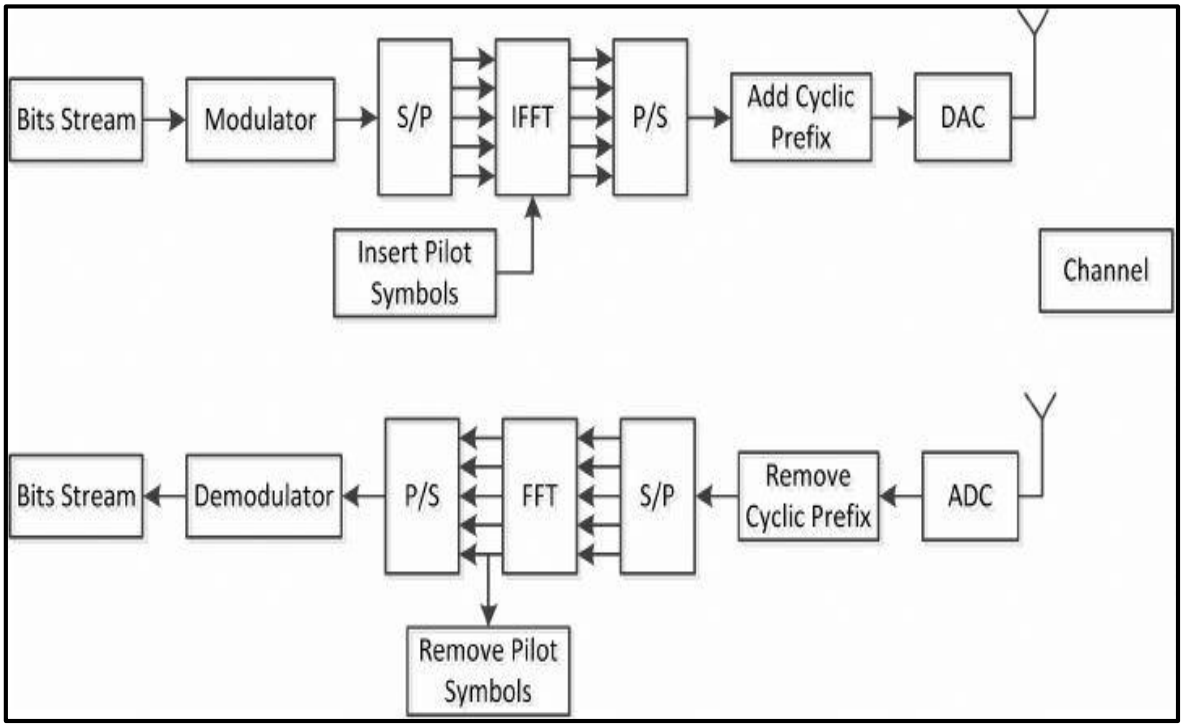

Fig.2.20: OFDM System Block Diagram [51].

Chapter Three

Design and Testing of the Proposed Systems

Chapter Three

Design and Testing of the Proposed Systems

3.1 Introduction

In this chapter, the proposed UWOC system is performed based on the principles which discussed in the previous chapters. The system simulation was tested under three types of water (clear, coastal, and turbid). This chapter is divided into four main sections. A simulation of the QPSK-OFDM modulation is shown in the first section. The second is a simulation of the OOK-NRZ modulation, the third is a simulation of the OOK-CSRZ modulation, and the fourth section is a simulation of the OOK-Manchester code modulation. The simulation of the above systems was carried out using the OptiSystem program. Figure (3.1) shows the steps of the proposed work, which include.

All of the above types of modulation have been used with various techniques: (1×1SISO, 1×2SIMO, 2×1MISO, 2×2MIMO, 1×4SIMO, 4×1MISO, 4×4MIMO, 1×8SIMO, 8×1MISO, 8×8MIMO).

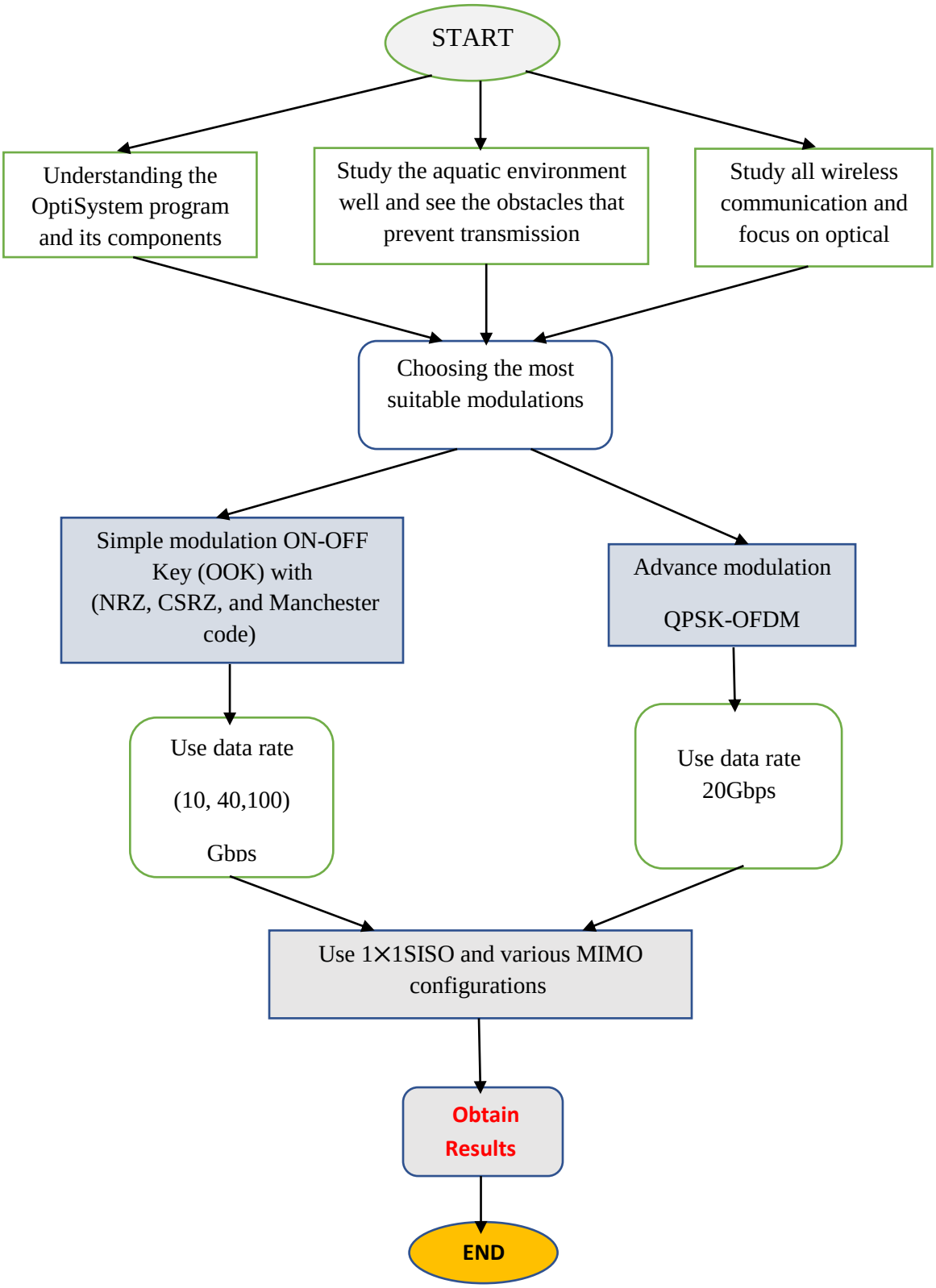

Fig.3.1: Shows a scheme to describe the proposed current work.

3.2 System Design of QPSK-OFDM

To display the performance of the undersea optical communication network under the influence of different water conditions. Different types of modulations were proposed. The first method was proposed and designed by using QPSK-OFDM. The three parts transmitter, water channel, and receiver of the QPSK-OFDM design are depicted in Figure (3.2).

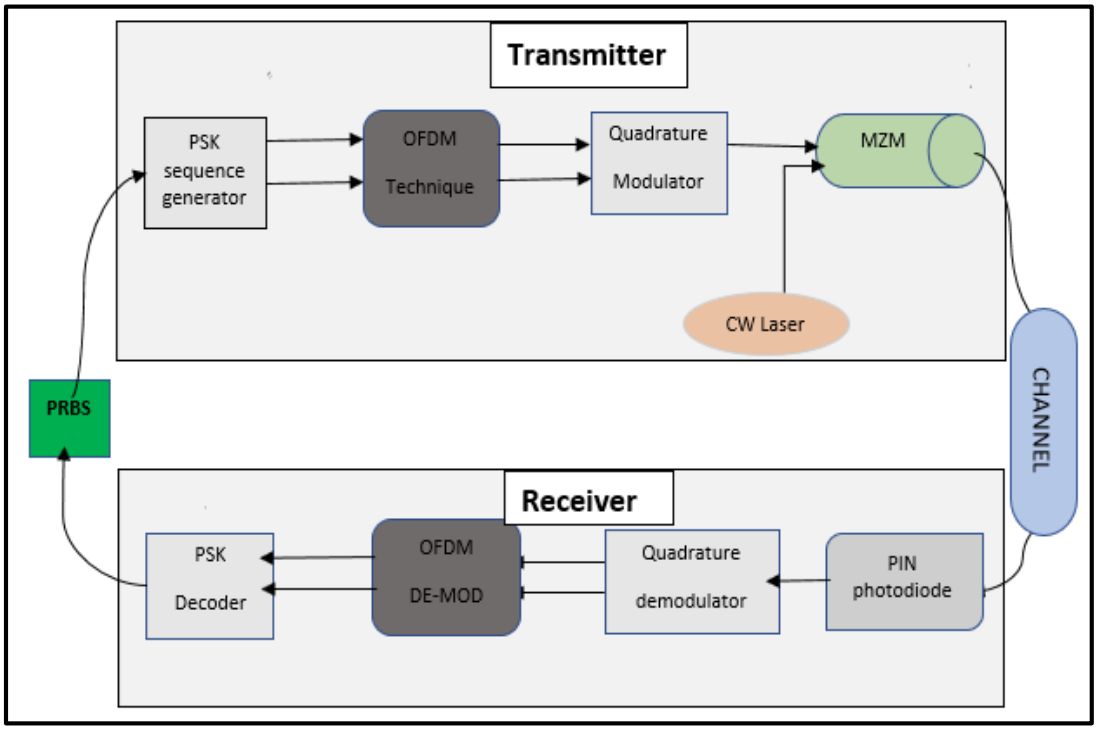

Fig.3.2: Block diagram of QPSK-OFDM modulation.

The transmitter part consists of binary signals generator, a PSK sequence generator, an OFDM technique component, a quadrature modulation component, and an optical source with MZM. The channel part uses the wireless water channel, and the receiver consists of the simplest PIN photodetector and decoder. Figure (3.3) shows how the QPSK-OFDM system was designed by the OptiSystem program. In transmitter part, the input data sequence length is set to 2^{15}-1 and it is built with a Pseudo Random Binary Sequence (PRBS) to generate a bit sequence

which is then fed into the QPSK encoder to produce M-Array sequences. The M-Array sequence is serial-to-parallel converted into blocks of symbols; each may comprise two bits for M-array coding.

These information symbols are mapped into two-dimensional complex signal. The IFFT is applied to produce the time-domain samples. The DAC convert the digital OFDM signal into analog form and by using low-pass filter to remove the unwanted alias sideband signals. The OFDM baseband signal is then converted to an Intermediate Frequency (IF) signal through an IQ modulator, then to an optical domain, or converted, according to system configuration, directly to the optical domain. In-phase (I) and quadrature (Q) of the resulting OFDM signal are transmitted parallel to overlap orthogonal subcarriers, whereby their (I) and (Q) electrical inputs are modulated with an RF carrier of 7.5 GHz by a quadrature modulator unit.

The output RF signal is then fed to intensity modulation /direct detection (IM/DD). The MZM will modulate the electrical signal from the OFDM modulator to the optical carrier with 450nm laser source. The power of the laser source is 20dBm.

The resulting optical signal from the MZMs is then transmitted through the underwater channel. In the receiver, the decoding process takes place, which is the opposite of the encoding process. The quadrate demodulator duplicates the electrostatic input signal, multiplies it by sinusoidal and cosine carriers. The optical signal sent from a laser to a receiver by the optical link is detected by PIN detector with responsivity of 1 A/W, thermal noise of 1×10^{-22} W/Hz, dark current of 10nA, and a center frequency of 450nm. After the optical signal converted to electrical signal, the signal will be down converted from 7.5 GHz RF carrier to OFDM signal stage. The OFDM demodulator removes the guard periods then applies the FFT

process for each OFDM symbol and regenerates the transmitted spectrum. The QPSK decoder decodes the two M-array inputs into one binary output and BER of the system is calculated. Table (3.1) shows the global parameter settings of the proposed QPSK-OFDM system.

Table (3.1): Principal parameters of Proposed QPSK-OFDM Modulation.

Parameters	Value	Notes
Data rate	20Gbps	high data rate[52]
Modulation	QPSK-OFDM	Low PAPR[53]
Symbol Rate	10 G S/s	2 bits per symbol
Optical Transmitter Laser Diode (LD)	Wavelength=450nm	Poor scattering and absorption[4]
	Power=20dBm	Economical in power [53]
	Transmitter aperture=50mm	Light Divergence = 2mrad [54]
Optical Receiver Photo Detector (PIN)	Responsivity =1A/W[55]	High
	Dark current = 10 nA[54]	Low
	Thermal noise =$1x10^{-22}$ W/Hz[54]	Low
Subcarrier for OFDM	1024 [49]	$N_{(FFT/IFFT)}$ = 2048[56]
Channel	Water	(turbid, coastal, and clean) water[4]
Length of Sequence	2^{15}-1 =32767 bits	optional
Link Configuration	LOS	A direct link between the transmitter and receiver[4].

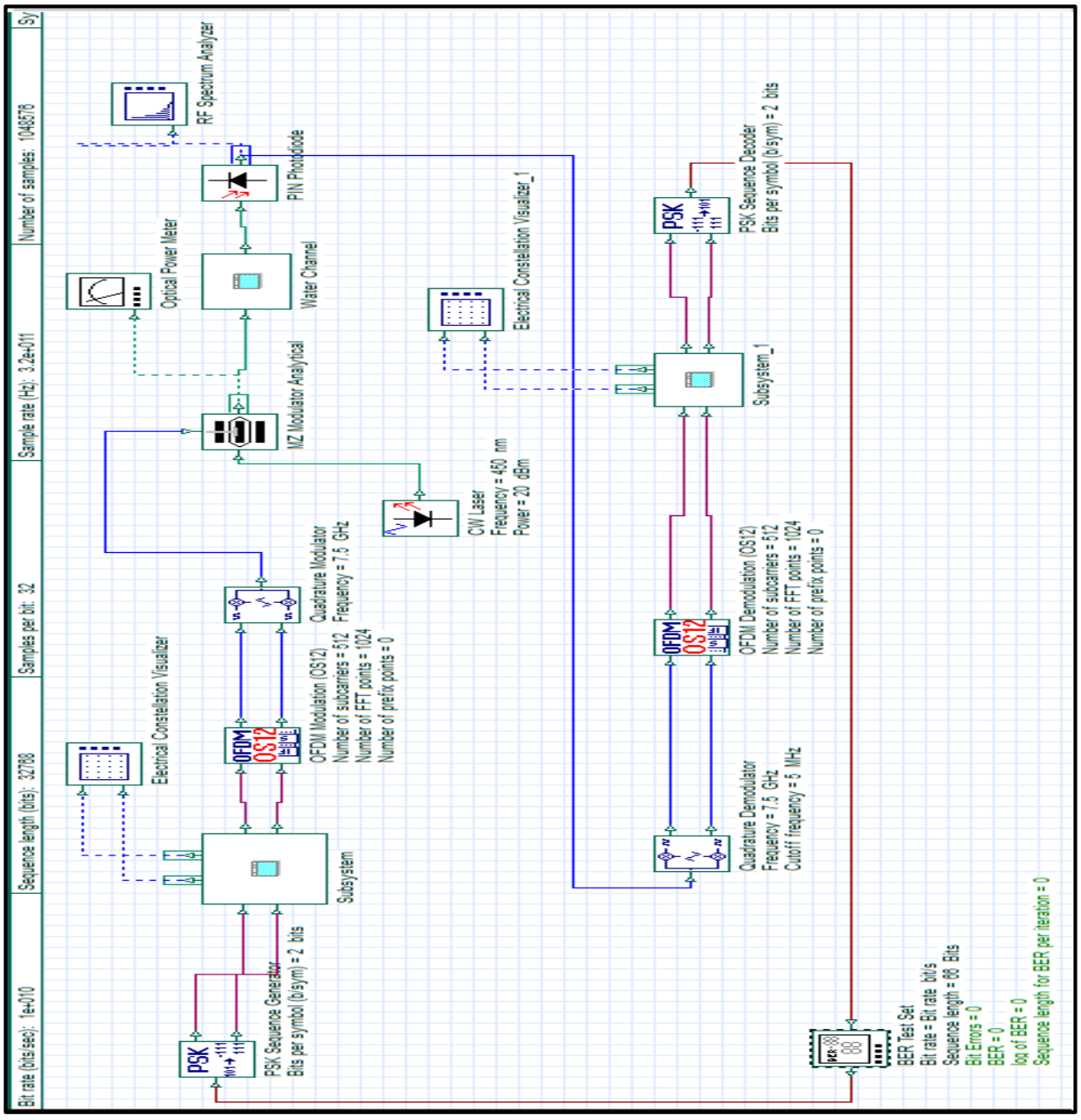

Fig.3.3: Simulation of QPSK-OFDM System by Optisystem

3.3 System Design of OOK-NRZ

Figure (3.4) displays the block diagram of the second proposed model, which was built on OOK modulation using NRZ pulse generator and shows the main parts of the system (transmitter, water channel, and receiver).

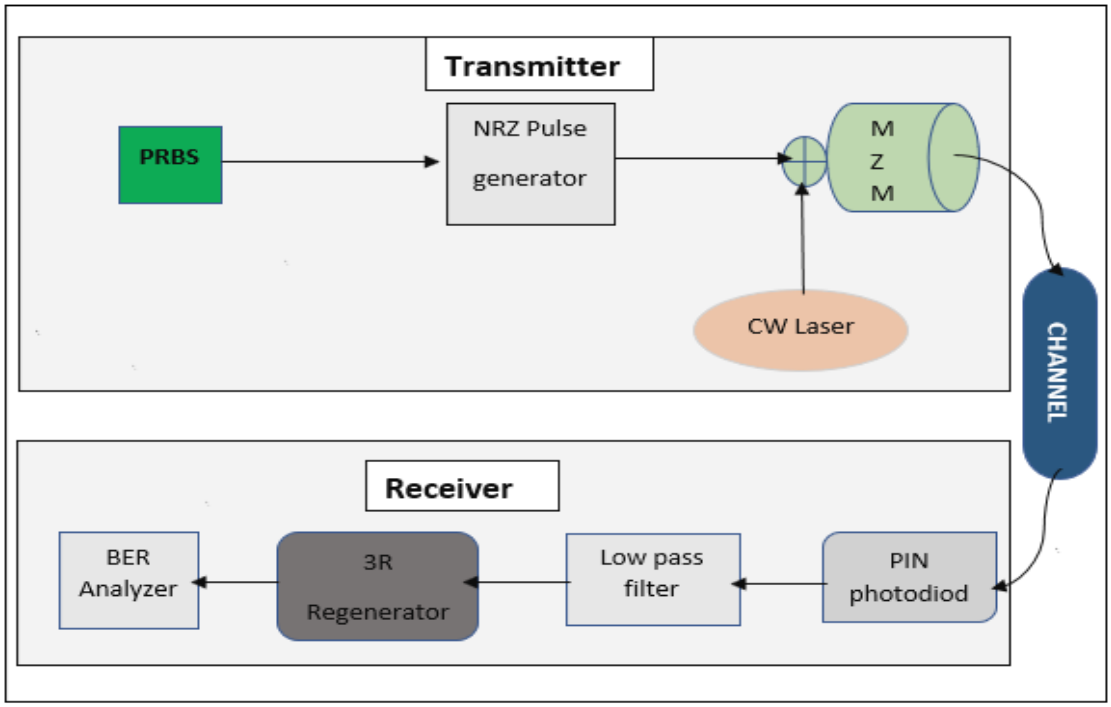

Fig.3.4: Displays the block diagram of the OOK-NRZ System.

It can be seen that the system generally consists of several parts, i.e., transmitter, underwater channel and receiver, where the UWOC signal is generated by the transmitter part; and broadcast over the underwater channel. Finally, the received signal is demodulated by the receiver and BER of the system is calculated by the BER analyzer.

In figure (3.5) the input data sequence length is built with a Pseudo Random Binary Sequence (PRBS) to generate a bit sequence that will be converted to NRZ electrical pulses. This signal directly drives the laser CW (continuous wave). The CW emits the modulated optical output with a laser source of 450nm. The power of the laser source is 20dBm and this CW establishes the connection with photo detector which is located several meters away from the transmitter through underwater channel. The turbulence model used in water channel is gamma-gamma model. The thermal noise is set to 1 10^{-22} W/Hz, the responsivity is 1A/W, and the dark current is 10nA. After all of these operations, the electrical signal separated from the light fed

to the 3R generator component. This component regenerates an electrical signal. It generates the original bit sequence, and a modulated electrical signal to be used for BER analysis. It is a subsystem based on the Data Recovery component and a NRZ Pulse Generator and then analyze it through BER analyzer.

Table (3.2): Principal parameters of Proposed OOK-NRZ Modulation.

parameter	Value	Note
Data rate	(10, 40,100) Gbps	High data rate[52]
Modulation	OOK-NRZ	
Symbol Rate	(10, 40,100) G S/s	each symbol contains 1 bit
Optical Transmitter (LD)	LD Wavelength=450nm	Poor scattering and absorption[4]
	Transmitter Power=20dBm	Low power consumption [53]
	Transmitter aperture=50mm	Light Divergence = 2mrad [54]
Optical Receiver Photo Detector (PIN)	Responsivity =1A/W [55]	High
	Dark current = 10 nA [54]	Low
	Thermal noise =$1x10^{-22}$ W/Hz[54]	Low
Channel	Water	(Clean, coastal, and turbid) water[4]
Sequence Length	1024	optional
Link Configuration	LOS	The point-to-point link between the transmitter and receiver[4].

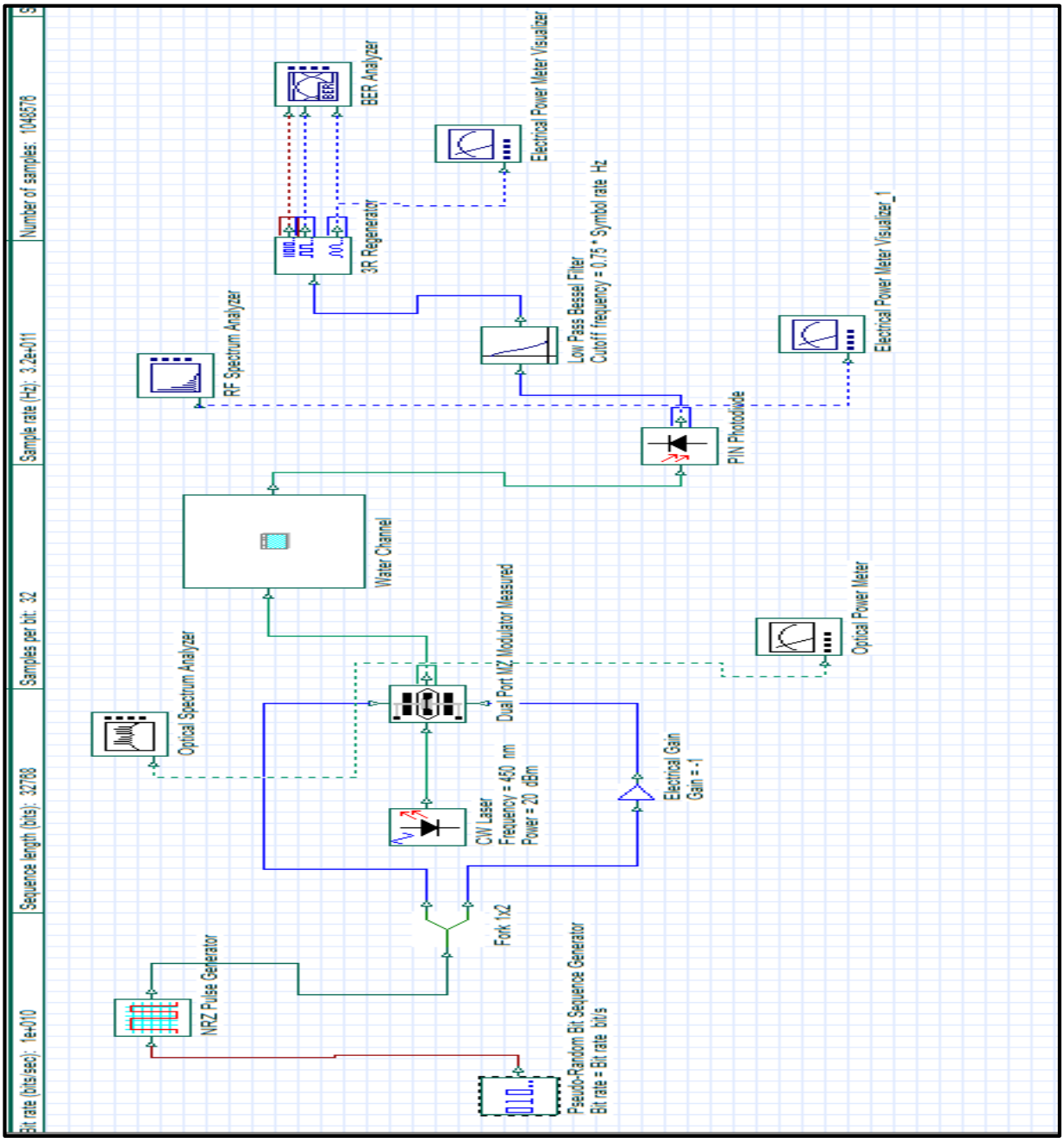

Fig.3.5: Simulation of OOK-NRZ System by Optisystem.

3.4 System Design of OOK-CSRZ

In Figure (٣.6) displays the block diagram of the third proposed model, which was built on OOK modulation using CSRZ technique and shows the main parts of the system (transmitter, water channel, and receiver).

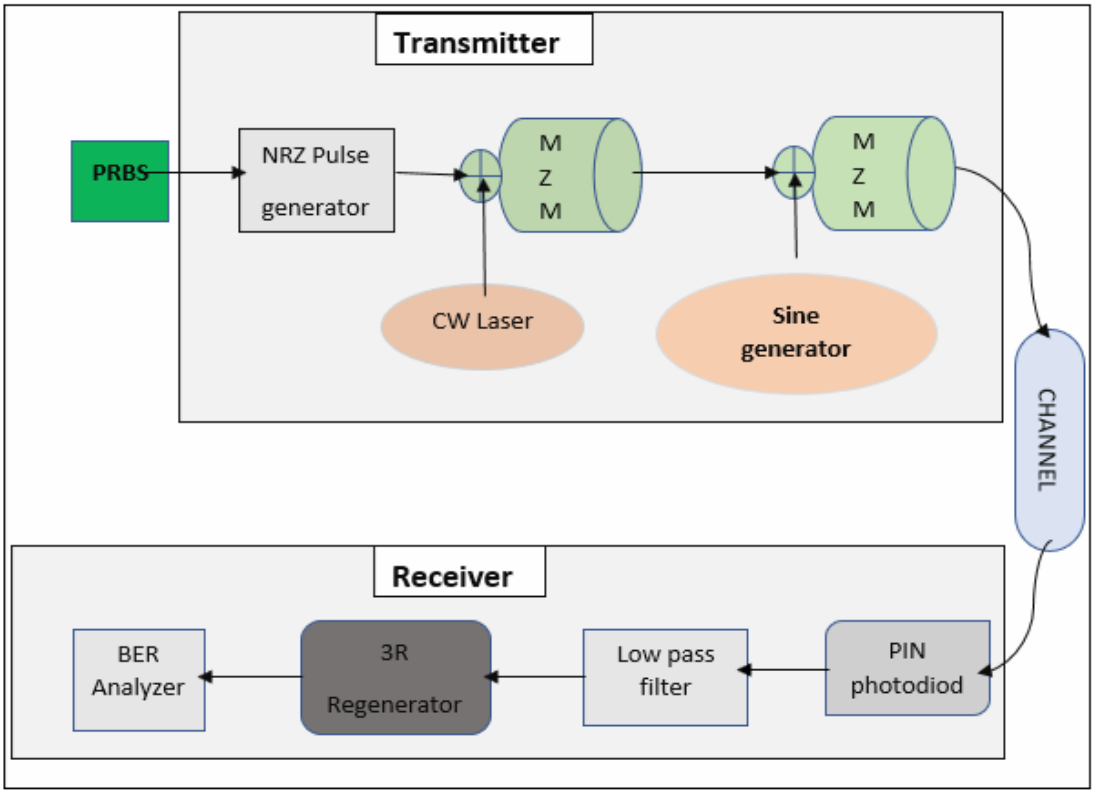

Fig.3.6: Displays the block diagram of the OOK-CSRZ System.

The sequence length in this system, as illustrated in Figure (3.7), is set to 1024 which is constructed using a pseudo-random bit sequence generator (PRBS). The data is then interred into NRZ Pulse generator to create the (NRZ) coded signal. The resultant signal is modulated onto a light wave with a wavelength of 450nm and 20dBm power by the first MZM modulator, and the light wave then enters the second MZM modulator along with a sine signal generated by a sine generator at a frequency of 32GHz to create a phase shift about 90° between adjacent bits.

The data on the light is transmitted through a water channel towards the receiver. The PIN photodetector, which is the initial component of the receiver, uses the device's responsiveness to transform an optical signal into an electrical

current. The electric pulse enters a filter to remove noise and other undesired frequencies. After all of these operations, the electrical signal separated from the light enters the 3R generator component to extract data from it and then analyze it through BER analyzer.

Table (3.٣): Principal parameters of Proposed OOK-CSRZ Modulation.

Parameter	Value	Note
Data rate	(10, 40,100) Gbps	High data rate[52]
Modulation	OOK-CSRZ	
Symbol Rate	(10, 40,100) G S/s	each symbol contains 1 bit
Optical Transmitter (LD)	LD Wavelength=450nm	Poor scattering and absorption[4]
	Transmitter Power=20dBm	Reduced power consumption[53]
	Transmitter aperture=50mm	Light Divergence = 2mrad[54]
Optical Receiver Photo Detector (PIN)	Responsivity =1A/W [55]	High
	Dark current = 10 nA [54]	Low
	Thermal noise =$1x10^{-22}$ W/Hz[54]	Low
Channel	Water	(Clean, coastal, and turbid) water[4]
Sequence Length	1024	optional
Link Configuration	LOS	The point-to-point link between the transmitter and receiver[4].

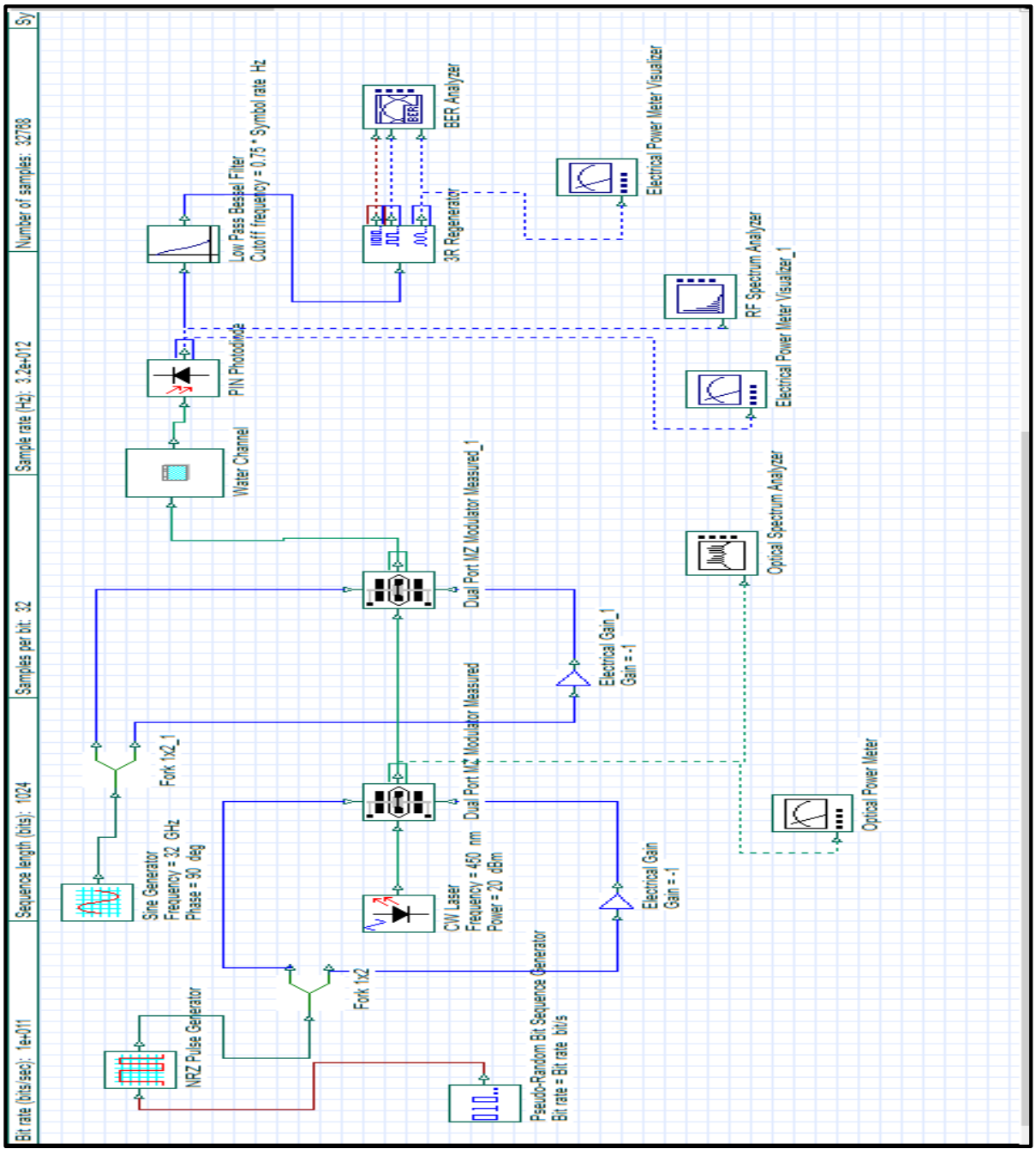

Fig.3.7: Simulation of OOK-CSRZ System by Optisystem.

3.5 System Design of OOK-Manchester Code

Figure (٣.8) shows the block diagram of the fourth proposed model, which was built on OOK modulation using Manchester code and shows the main parts of the system (transmitter, water channel, and receiver).

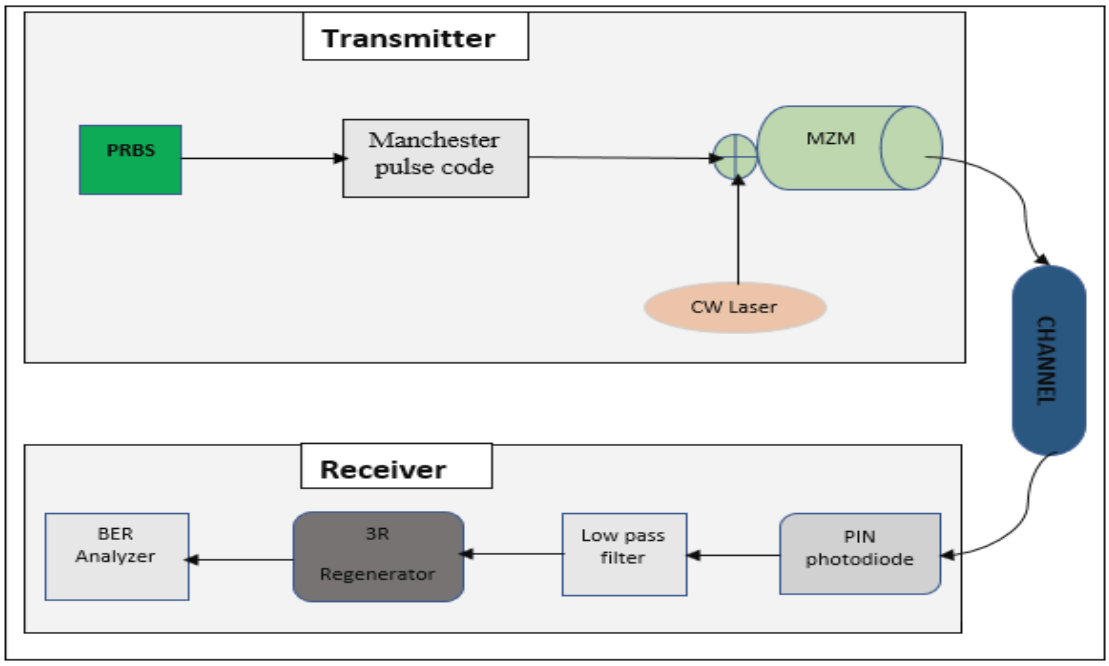

Fig.3.8: Displays the block diagram of the OOK-Manchester code system.

In this model, as demonstrated in Figure (3.9), A user-defined bit pattern, commonly known as data, is initially created using a user-defined bit sequence generator with (10, 40, and 100) Gbps data rates (110011). To provide a clock signal, another user-defined bit sequence generator with (10, 40, and 100) Gbps data rates is created (101010).

To create a binary output, the data and clock signals are inputted through the binary XOR component. To create a binary value of the Manchester signal, this output is fed via a binary NOT gate. Through the NRZ pulse generator, this Manchester signal is converted into an electrical signal. Then, MZM modulator modulates this signal into an optical signal by this modulator using a CW laser source with a wavelength 450nm and 20dBm power. Then the optical wave passes through the water channel.

When the signal reaches to the receiver end, the receiver is the PIN photodetector that transforms an optical signal into an electrical current. The

electric wave enters a filter to remove noise and other undesirable frequencies after separating the data from the light. After all of these operations, the electrical signal separated from the light enters the 3R generator component to extract data from it and then analyze it through BER analyzer.

Table (3.4): Principal parameters of Proposed OOK-Manchester code modulation.

Parameter	Value	Note
Bit rate	(10, 40,100) Gbps	High data rate[52]
Modulation	OOK-Manchester code	
Symbol Rate	(10, 40,100) G S/s	each symbol contains 1 bit
Optical Transmitter (LD)	LD Wavelength=450nm	poor scattering and absorption[4]
	Transmitter Power=20dBm	reduced power consumption[53]
	Transmitter aperture=50mm	Light Divergence = 2mrad [54]
Optical Receiver Photo Detector (PIN)	Responsivity =1A/W[55]	High
	Dark current = 10 nA [54]	Low
	Thermal noise =$1x10^{-22}$ W/Hz[54]	Low
Channel	Water	(Clean, coastal, and turbid) water[4]
Sequence Length	1024	optional
Link Configuration	LOS	The point-to-point link between the transmitter and receiver[4].

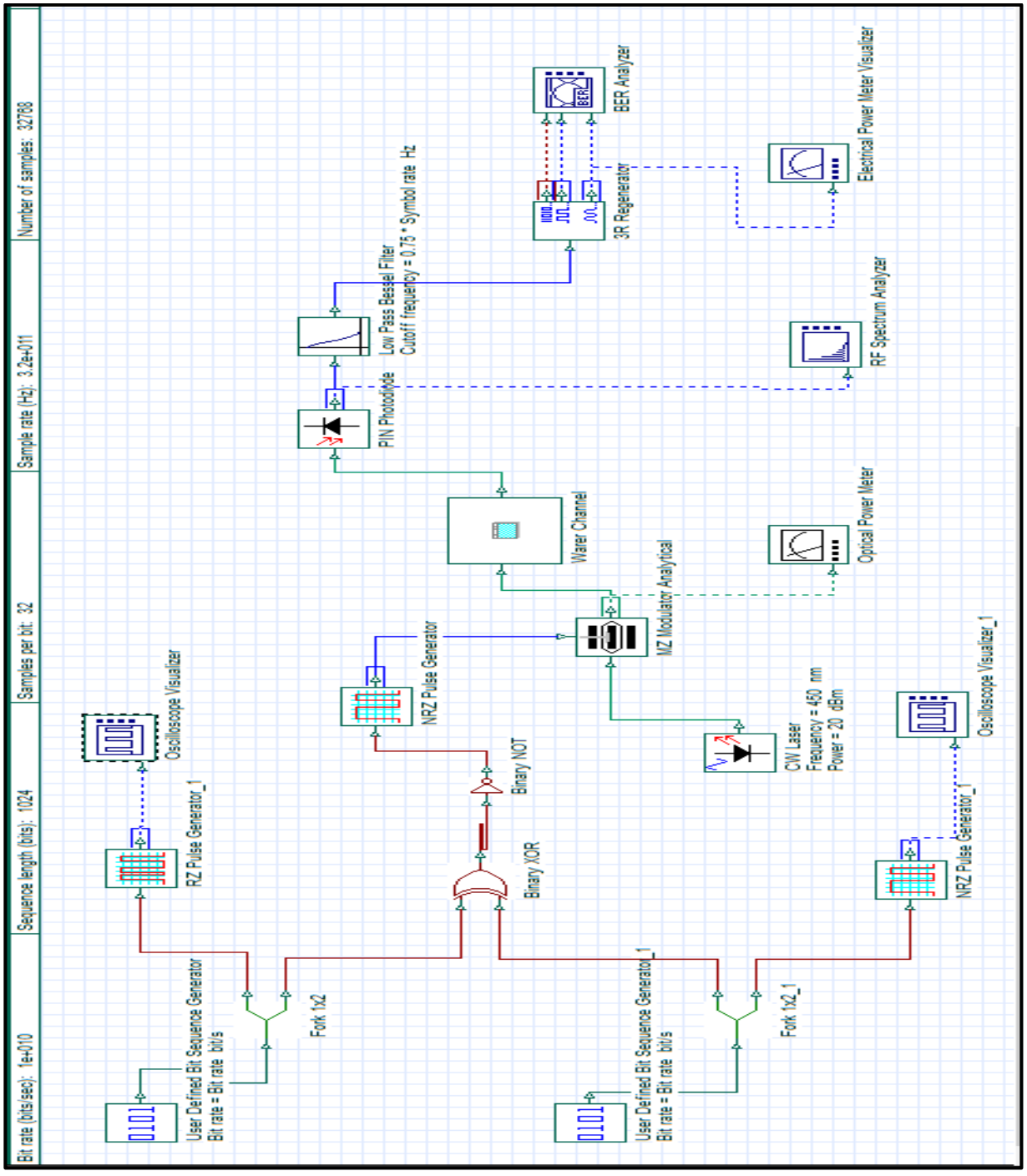

Fig.3.9: Simulation of the OOK-Manchester code System by Optisystem

3.6 Water Channel Techniques

Several aqueduct techniques have been used with all kinds of modulation to achieve high transmission rates and reach good distances. The techniques used are:

3.6.1 SISO Technique

The SISO technique or the single input single output communication system is the simplest type of communication technique out of every four in which there is one transmitting antenna at the source and one receiving antenna, at the receiver.

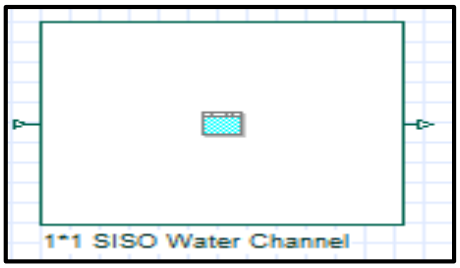

Fig.3.10: Shows the Simulation Setup for 1x1 SISO.

3.6.2 SIMO Technique

In this technique, the transmission is from a single transmitter antenna, but the data is received from multiple receiver antennas, the number of receiver antennas equal to 2^n, where (n= 1, 2, 3, 4...) figure (3.11) shows SIMO types.

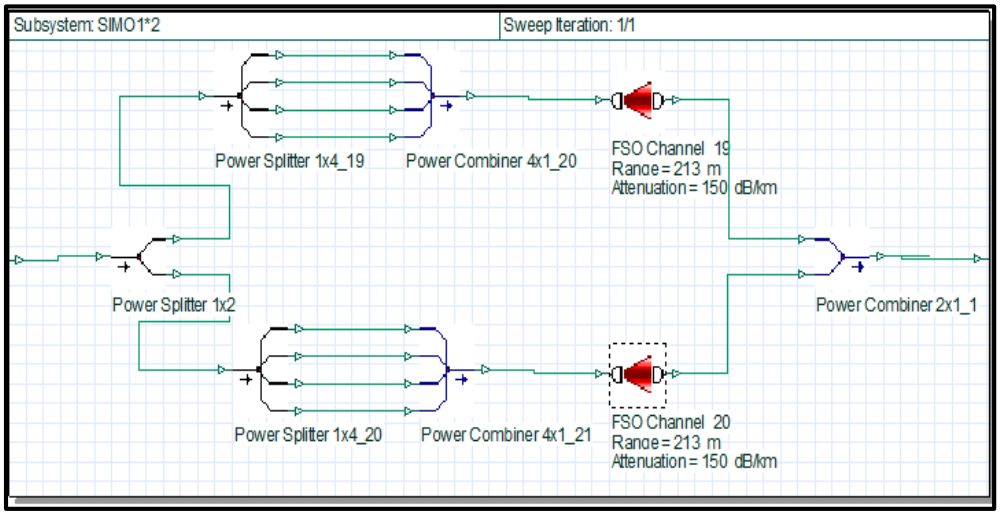

(a)

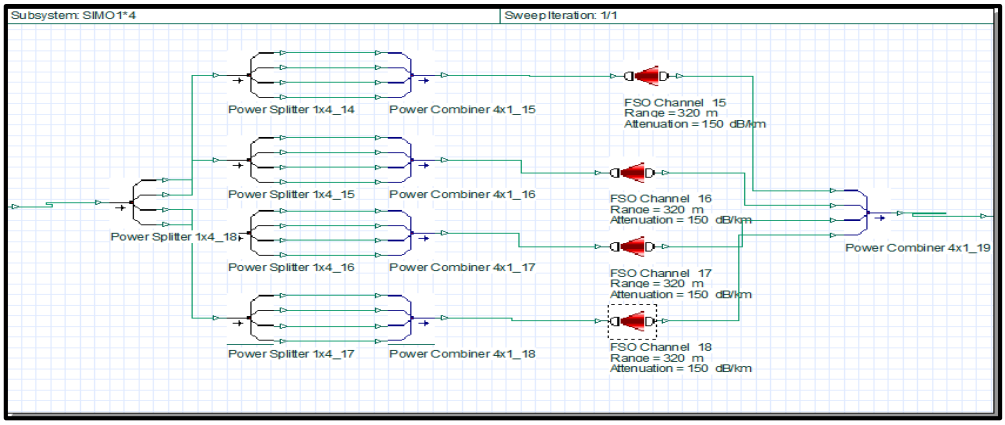

(b)

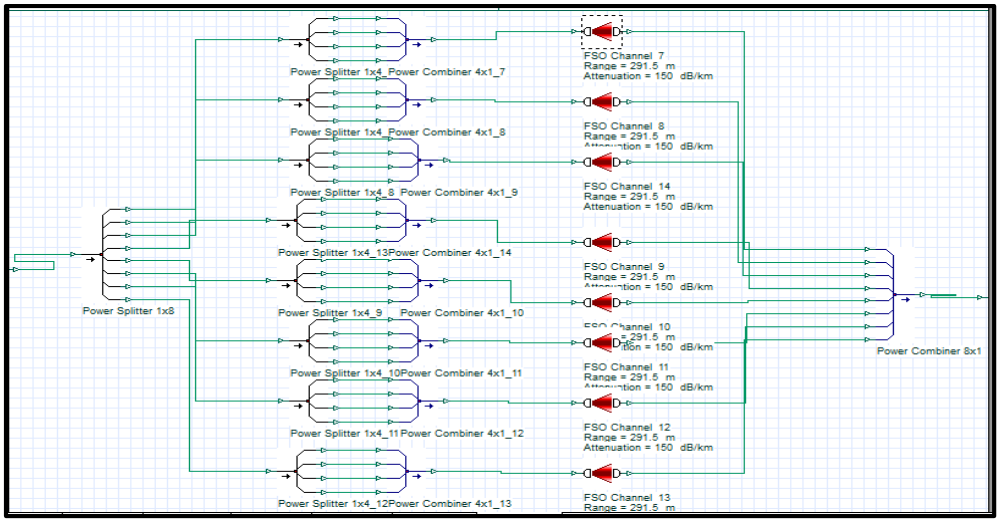

(c)

Fig.3.11: Shows the Simulation Setup for (a) 1x2 SIMO, (b) 1x4 SIMO, and (c)1x8 SIMO.

All scenario depicted in Figure 3.11 (a, b, and c) above, the power splitter splits an optical input signal into (two, four, or eight) output signals, and the divided data is supplied to each output signal over a separate channel before being combined at the receiving end.

3.6.3 MISO Technique

Multiple antennas are employed at the source of wireless communications technology known as MISO (multiple input, single output). To reduce errors and

maximize transmission speed, the antennas are merged. The receiver at the destination only has one antenna and many antennas at the transmitter.

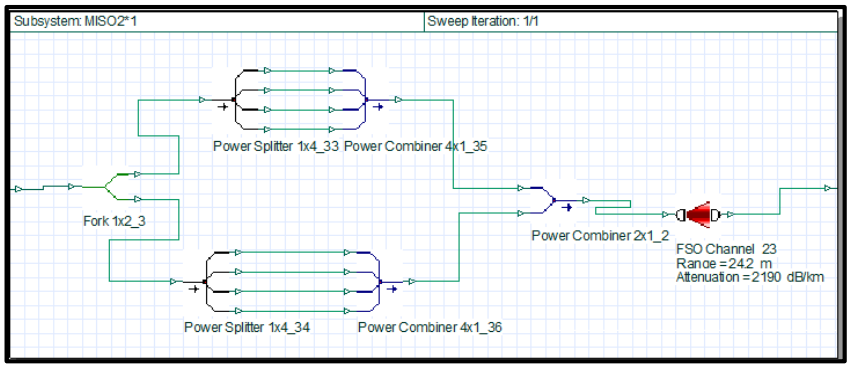

(a)

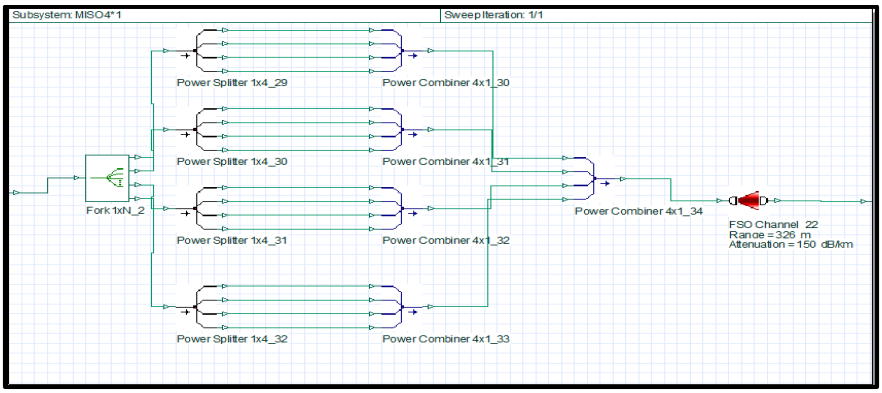

(b)

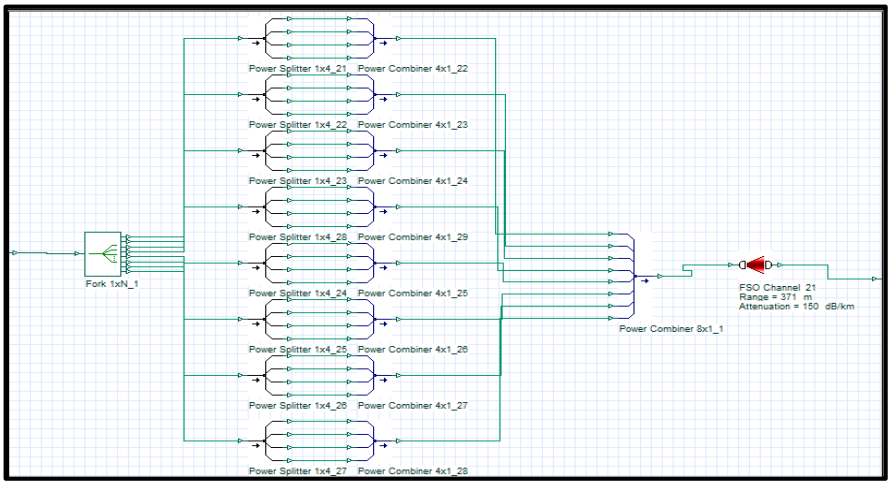

(c)

Fig.3.12: Shows the Simulation Setup for (a) 2x1 MISO, (b) 4x1 MISO, (c) 8x1 MISO.

3.6.4 MIMO Technique

Multiple antennas are utilized at both the transmitter and the destination in wireless communications known as MIMO (multiple input, multiple output). By enabling data to travel through several signal routes at once, the antennas for each end of the communications network are combined in order to eliminate errors, increase data speed, and improve the capacity of optical transmissions. Both the transmitter and the receiver contain an equal number of antennas.

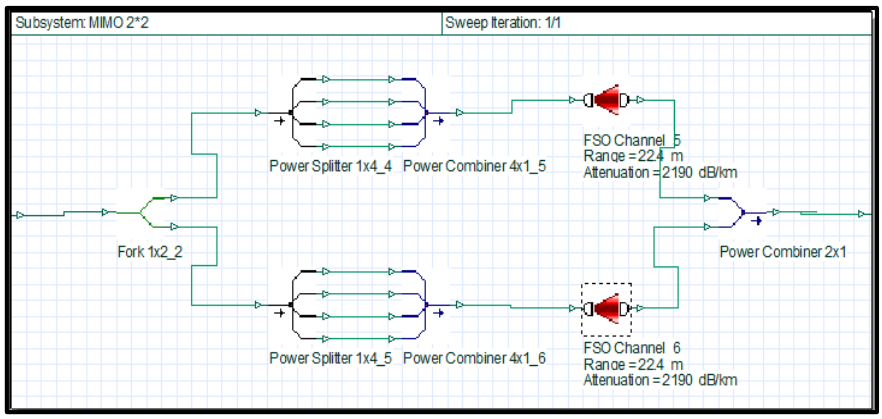

(a)

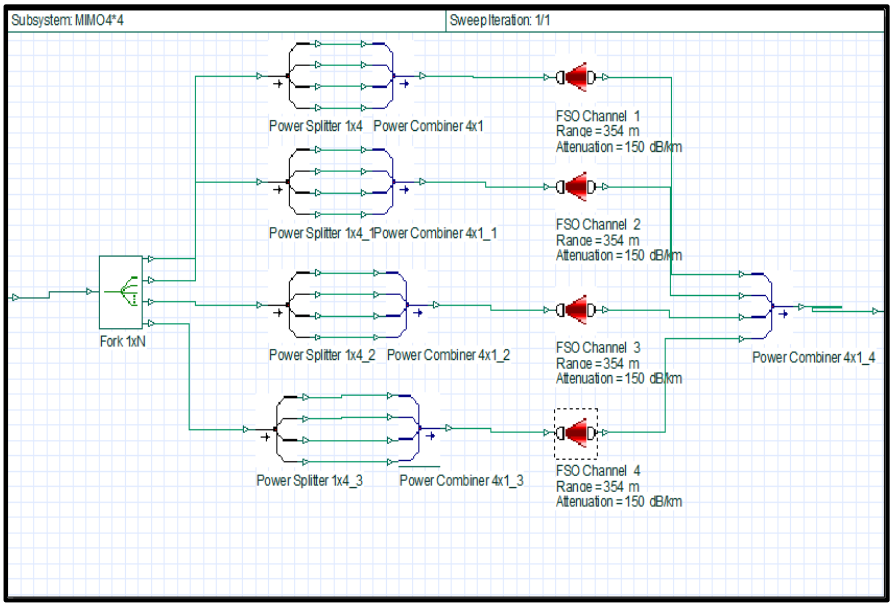

(b)

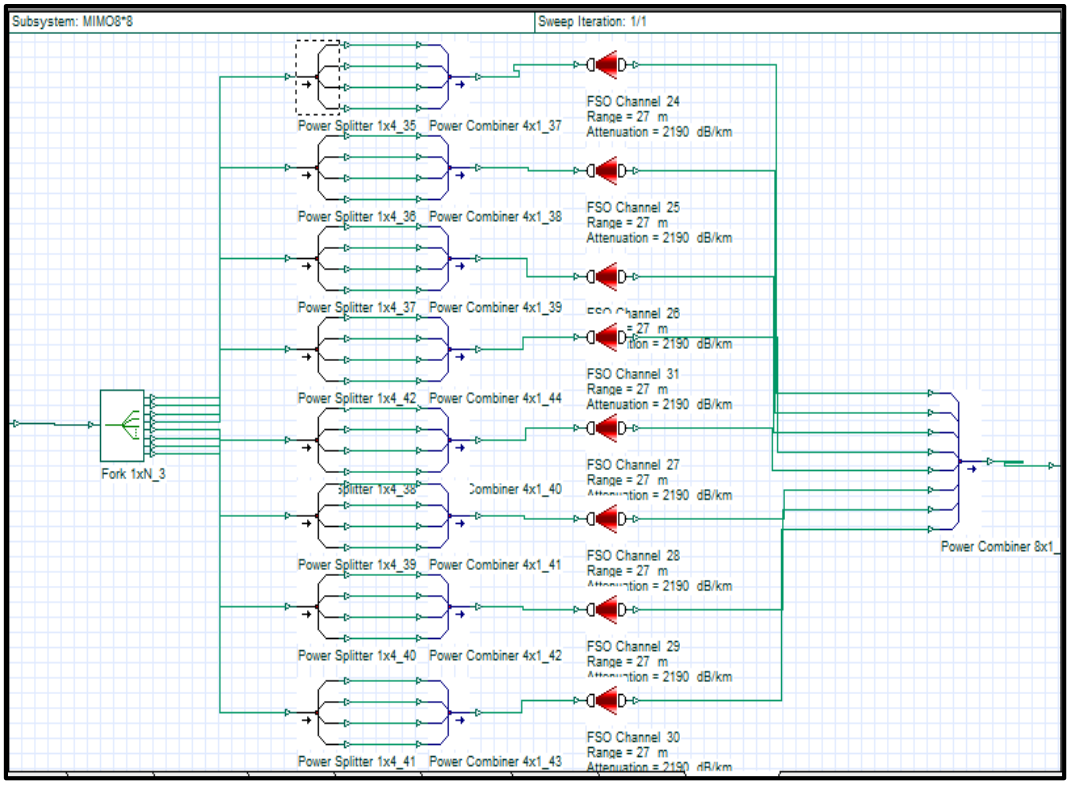

(c)

Fig.3.13: Shows the Simulation Setup for (a) 2x2 MIMO, (b) 4x4 MIMO, (C) 8x8 MIMO.

To simulate MIMO technology, the fork tool may be used, which can multiply the signal several times, and each of the resulting signals has the same power as the original signal. And then each of them enters through a channel to reach the receiver, which has the same number of antennas as the transmitter.

Chapter Four

Results and Discussions

Chapter Four

Results And Discussions

4.1 Introduction

By using the Optisystem program, a UWOC system is simulated and examined. In this chapter, the effectiveness of the UWOC system is investigated over a range of transmission distances and water types. In the simulation, QPSK and OOK are the two primary modulation types. These techniques provide good resistance to signal fading, low PAPR, and low water turbulence. This chapter examines the 20Gbps data rate performance evaluation of the proposed OFDM system with QPSK in various types of water.

Three encoding approaches are used to evaluate the effectiveness of OOK Modulation (NRZ, CSRZ, Manchester). Then, increasing the data rate from 10 Gbps to 40 Gbps and then to 100 Gbps, checking and calculating with each increase in the data rate. In addition to using various MIMO techniques with each type of modulation and also at each increase in the data rate. These comparisons are made in terms of BER and distance, as well as the received power and quality factor.

4.2 QPSK-OFDM Simulation Results

Three different types of water (clear, coastal, and turbid), 20Gbps data rate, and varying transmission lengths are used to determine the BER performances of the proposed QPSK-OFDM.

The simulation results for BERs and distances have been achieved and are presented in table (4.1) for clear water operating at 20Gbps.

Table (4.1): Results from simulations of QPSK-OFDM modulation in clear water

Techniques	Max Link Range(m)	BER
1×1SISO	173	1×10^{-8}
1×2SIMO	177	1×10^{-8}
1×4SIMO	179	1.5×10^{-8}
1×8SIMO	181.5	2×10^{-8}
2×1MISO	190	2.4×10^{-8}
4×1MISO	205	4.2×10^{-8}
8×1MISO	225	1.2×10^{-8}
2×2MIMO	195	2.1×10^{-8}
4×4MIMO	210	1.3×10^{-8}
8×8MIMO	230	3×10^{-8}

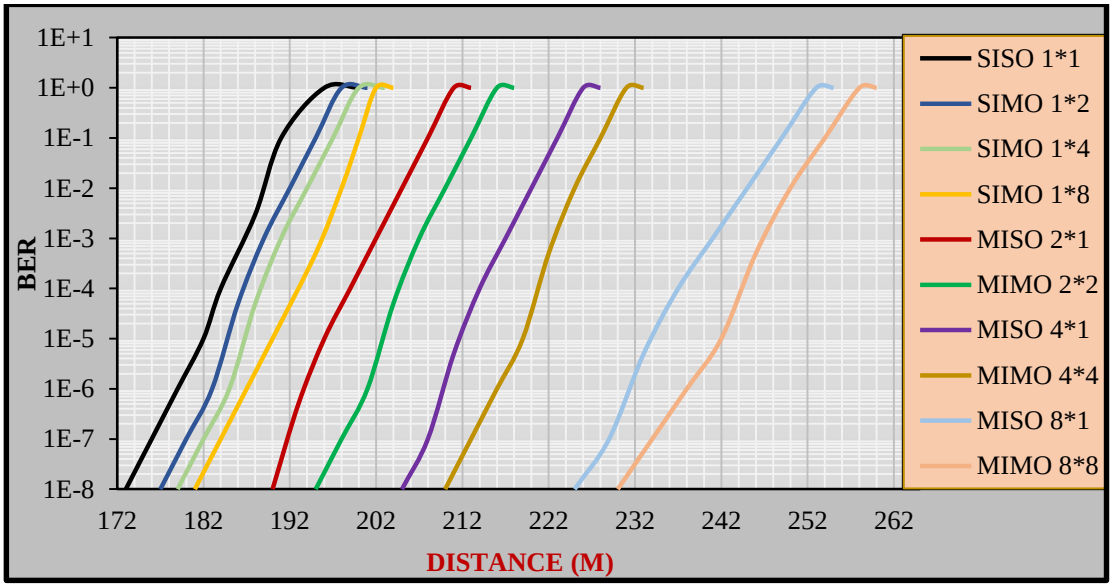

Fig. 4.1: Distance vs. BER for QPSK-OFDM with SISO and various MIMO configurations in clear water.

Figure (4.1) shows the QPSK-OFDM connection range diagram of BER with various MIMO technique combinations and 1×1SISO under a low turbulence channel (clear water). 8×8MIMO was the best in terms of result in clear water, achieving a link range of 230m with a very low BER approximately 10^{-8}.

Table (4.2) below presents the numerical results of BERs and link distances that have been obtained in coastal water when transmitting at 20Gbps.

Table (4.2): The results of a simulation of QPSK-OFDM modulation.

Techniques	Max Link Range(m)	BER
1×1SISO	74	1.9×10^{-8}
1×2SIMO	75.8	1.7×10^{-8}
1×4SIMO	78.1	3.2×10^{-8}
1×8SIMO	81.1	2.2×10^{-8}
2×1MISO	84.7	9.1×10^{-9}
4×1MISO	91	1.4×10^{-8}
8×1MISO	98	2×10^{-8}
2×2MIMO	87.6	3.6×10^{-8}
4×4MIMO	94	1.5×10^{-8}
8×8MIMO	101	1.9×10-8

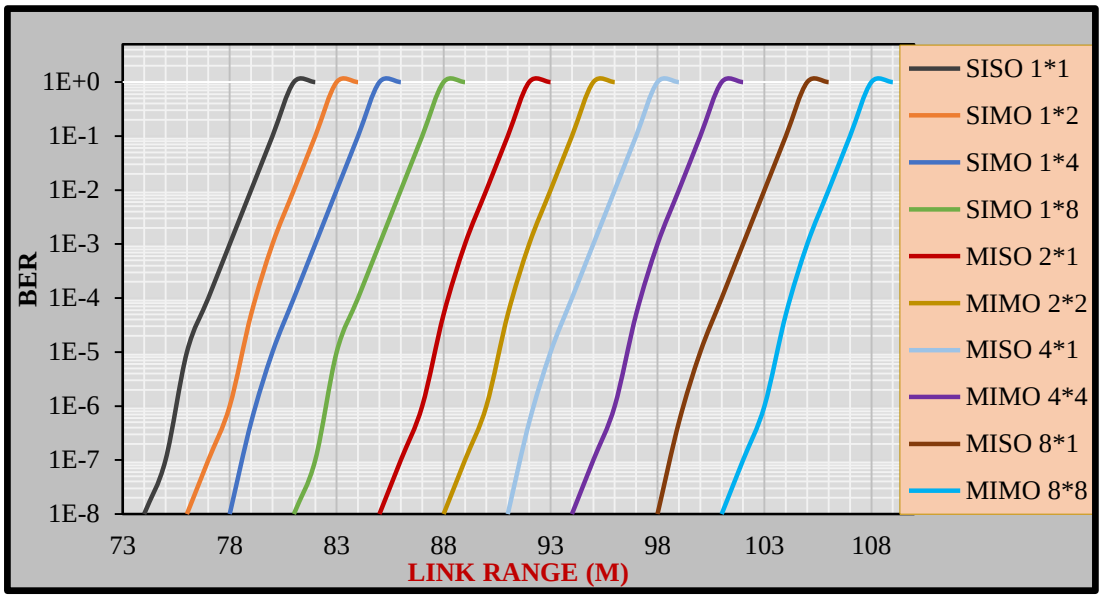

Fig. 4.2: Under coastal water, BER vs. Link Range for QPSK-OFDM with1×1SISO and various MIMO configurations.

The schematic diagram of BER vs link range for QPSK-OFDM is shown in Figure (4.2) with various MIMO techniques and 1×1SISO in coastal water. It is

clear from this figure that the transmission range is directly proportional to BER, as the BER increases when the link range increases. In addition, 8×8MIMO has achieved the best results by 101m with an BER approximately 10^{-8}.

Table (4.3) presents the numerical findings of BERs and links distance that has been achieved in turbid water while transmitting at 20Gbps.

Table (4.3): Results from simulations of QPSK-OFDM modulation.

Techniques	Max Link Range(m)	BER
1×1SISO	18	1×10^{-8}
1×2SIMO	18.2	1.2×10^{-8}
1×4SIMO	18.45	2.3×10^{-8}
1×8SIMO	18.6	1.1×10^{-8}
2×1MISO	19.5	5.6×10^{-8}
4×1MISO	20.9	1.2×10^{-8}
8×1MISO	21.9	2.7×10^{-8}
2×2MIMO	19.8	1.3×10^{-8}
4×4MIMO	21.1	3.9×10^{-8}
8×8MIMO	22.1	5.7×10^{-8}

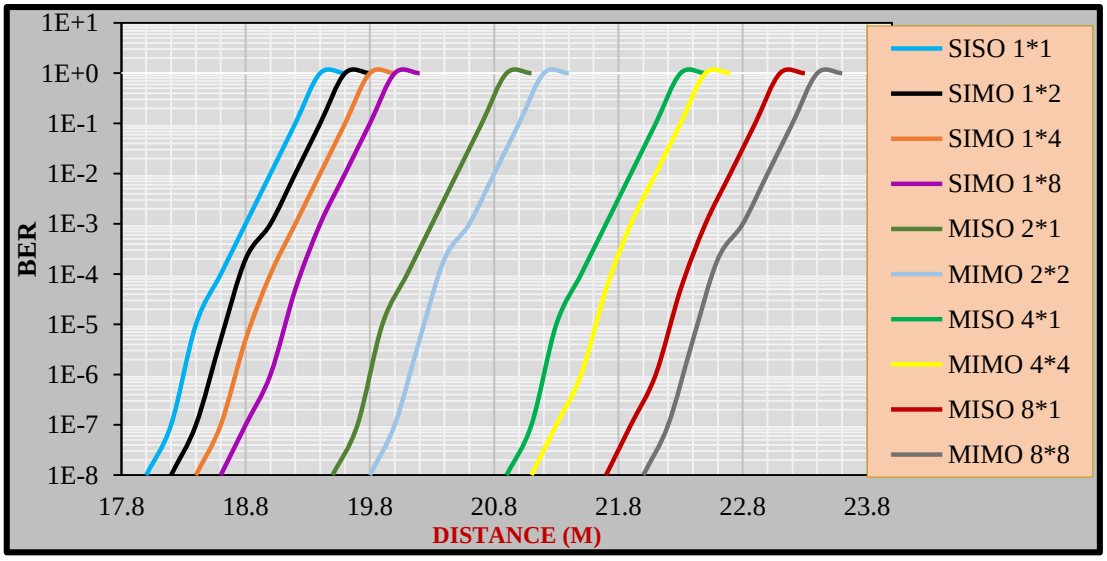

Fig.4.3: Link distance vs. BER for QPSK-OFDM with various MIMO configurations and 1×1SISO in turbid water.

It is evident from the figures presented previously (4.1), (4.2), and (4.3) that the performance of the 8×8MIMO and 8×1MISO systems under 3 different types of water (turbid, coastal, and clear) is the best compared to that of the other MIMO configurations. Therefore, the link range increased as a result of an increase in the number of receiver elements (photodetectors), while maintaining a very low BER about 10^{-8}.

Figure (4.4) displays the relationship between the link distance and the received power for QPSK-OFDM under three water types (turbid, coastal, and clear). It is important to note that the transmitted power is equal to 20dBm for all distances shown.

The figure below shows that the amount of power is inversely proportional to the link range and also depends directly on the type of water. In other words, it is greatly affected by the amount of attenuation caused by each type of water.

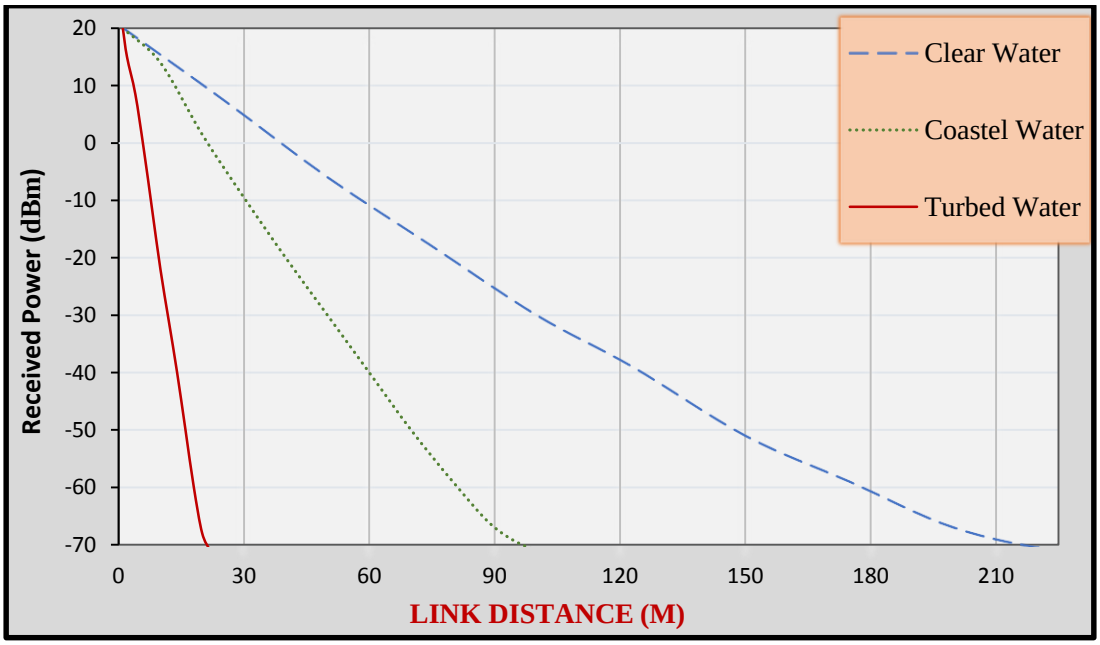

Fig.4.4: Link Range (m) vs. Received Power (dBm) of QPSK-OFDM at 8×8MIMO in three water types.

Using 8×8MIMO technology, Figure (4.5) displays a constellation diagram for QPSK modulation at a distance of 227m and 250m for clean water. It clear from the figure that the BER increases with increasing distance. When the constellation is far from the center, this indicates that the BER is very low

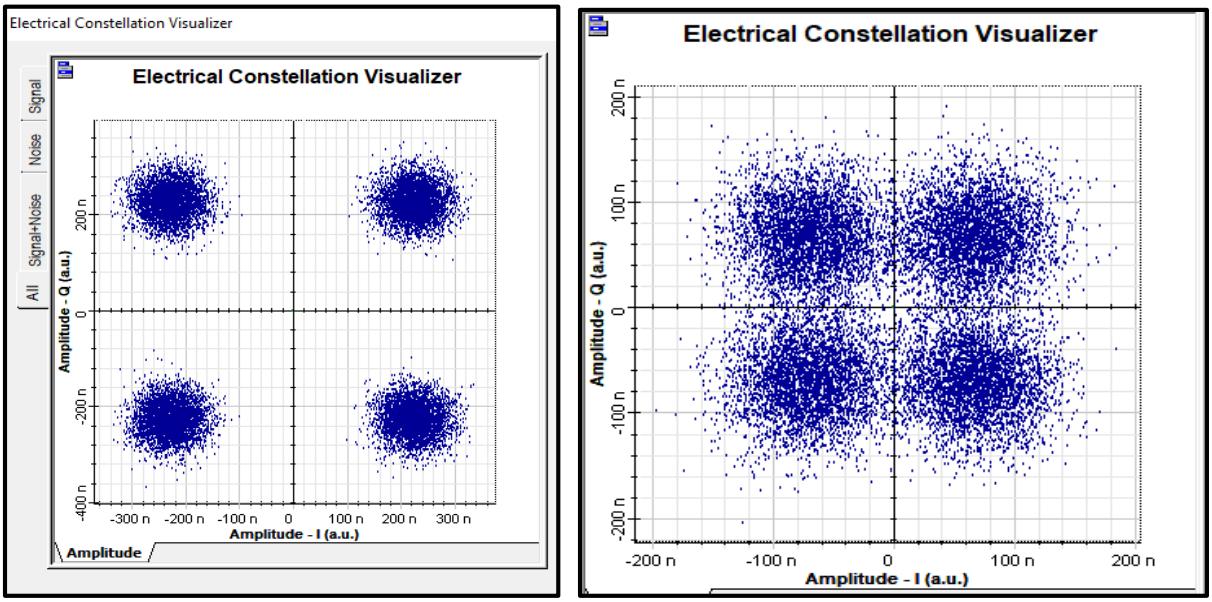

(a) (b)

Fig.4.5: constellation diagram for QPSK modulation using 8×8MIMO technique at (a) 227m in clearwater (b) 250m in clear water.

4.3 Simulation Results of OOK-NRZ

The data rate was gradually increased from 10Gbps to 40Gbps and then to 100Gbps as the outcomes of this modulation type were calculated for three situations.

4.3.1 Simulation Results of OOK-NRZ at 10Gbps

Three distinct types of water (turbid, coastal, and clear) are used to examine the BER performance of the proposed OOK-NRZ at a 10Gbps data rate and varied transmission lengths.

The numerical results of BERs and distances at 10Gbps are reported in table (4.4) format for the case of clear water.

Table (4.4): Simulation results of OOK-NRZ modulation under clear water.

Techniques	Max Link Range(m)	BER	Q Factor
1X1SISO	162	7.1×10^{-8}	5.25
1X2SIMO	164.3	8.6×10^{-8}	5.22
1X4SIMO	166.1	9×10^{-7}	4.9
1X8SIMO	168	1×10^{-8}	5.12
2X1MISO	178	1×10^{-8}	5.53
4X1MISO	192	7×10^{-8}	5.26
8X1MISO	210	3×10^{-8}	5.4
2X2MIMO	181	2×10^{-8}	5.49
4X4MIMO	195	1.6×10^{-8}	5.52
8X8MIMO	214	1.9×10^{-8}	5.49

Figure (4.6) displays the BER analyzer for OOK-NRZ at the 8×8MIMO technique in clear water with 20dB of transmitted power and the target of BER is 10^{-8}.

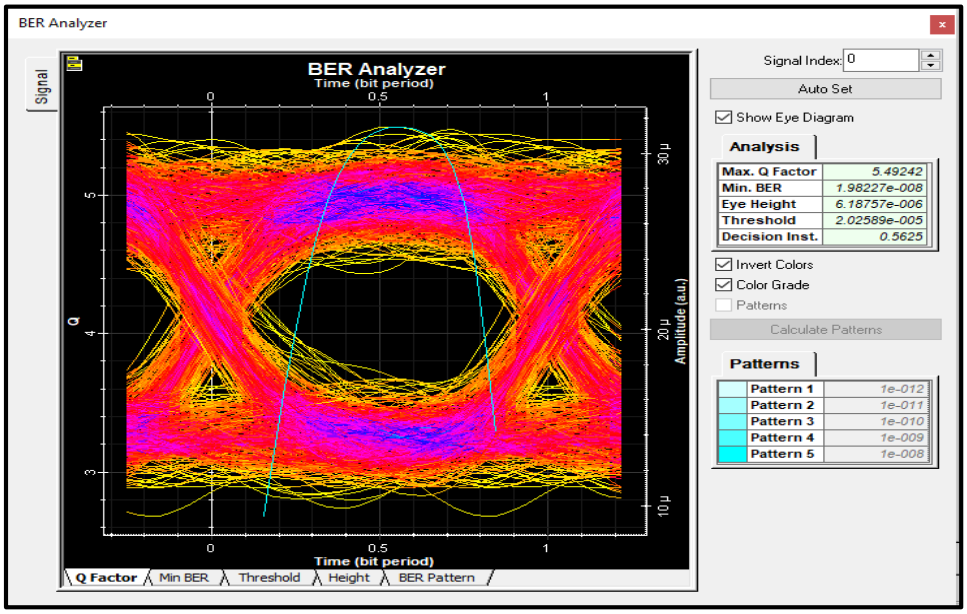

Fig.4.6: BER Analyzer for 8X8MIMO System in clearwater at10Gbps.

Figure (4.7) displays a schematic diagram of the relationship between BER and link range for OOK-NRZ at 10Gbps with various MIMO combinations and 1×1SISO in clear water. 8×8MIMO and 8×1MISO techniques was the best in terms of result in clear water, achieving a link range of 214m and 195m respectively with a very low BER approximately 10^{-8}.

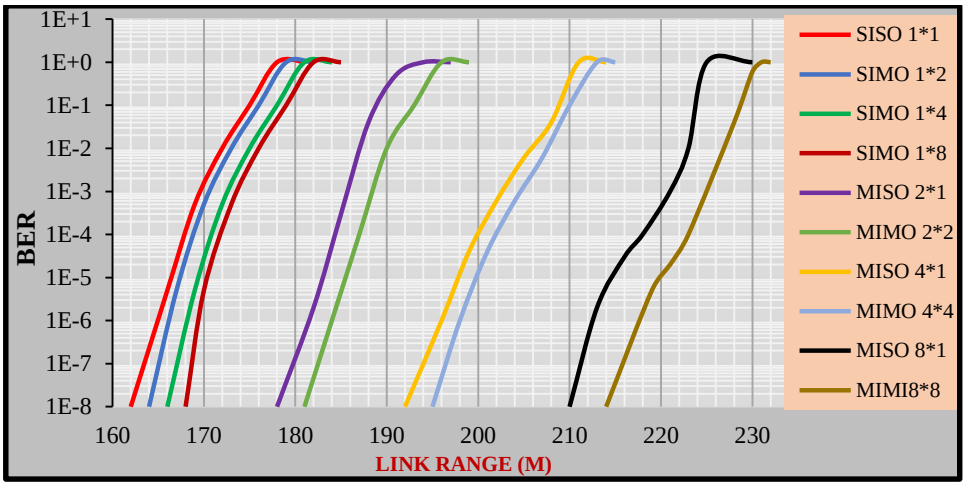

Fig.4.7: Link Range vs. BER for OOK-NRZ at 10Gbps with various MIMO configurations and 1×1SISO under clear water.

For coastal water at 10Gbps, the numerical results of distances and BERs have been obtained as shown in the table below (4.5).

Table (4.5): Simulation results of OOK-NRZ modulation under coastal water.

Techniques	Max Link Range(m)	BER	Q Factor
1×1SISO	72	6.34×10^{-8}	5.28
1×2SIMO	73	5.28×10^{-7}	4.88
1×4SIMO	74.5	8×10^{-7}	4.8
1×8SIMO	76	2.99×10^{-8}	5.4
2×1MISO	81	1.88×10^{-9}	5.89
4×1MISO	88	3.5×10^{-8}	5.38
8×1MISO	93.7	1×10^{-9}	5.98
2×2MIMO	83	7×10^{-8}	5.51
4×4MIMO	90	6.44×10^{-8}	5.27
8×8MIMO	95.5	2.3×10^{-7}	5.03

Figure (4.8) shows the relationship between the transmission range and the bit error rate at 10Gbps and under coastal water, as it becomes clear that increasing the transmission range leads to an increase in the error rate. 8×8MIMO technology achieved the best results compared to other technologies. It achieved a transmission distance equal to 95.5m and a BER of 2.3×10^{-7}

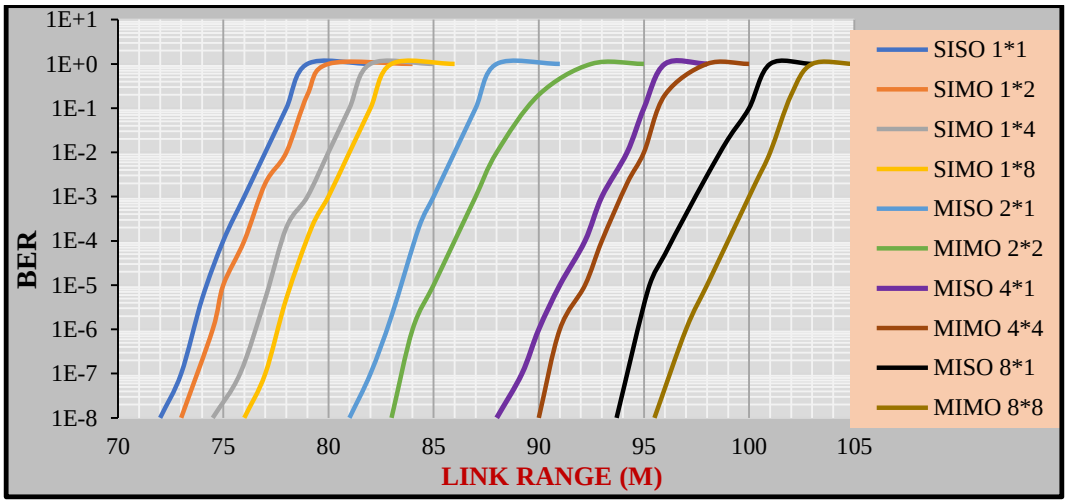

Fig.4.8: Link Range vs. BER for OOK-NRZ at 10Gbps with 1×1SISO and various MIMO techniques in coastal water.

for turbid water at 10Gbps, the numerical results of Q factor, link range, and BERs have been obtained as shown in the table below (4.6).

Table (4.6): Simulation results of OOK-NRZ modulation under turbid water.

Techniques	Max Link Range(m)	BER	Q Factor
1×1SISO	16.9	3.12×10^{-8}	5.41
1×2SIMO	17.15	1.97×10^{-7}	5.07
1×4SIMO	17.28	9.17×10^{-7}	4.77
1×8SIMO	17.4	3.78×10^{-7}	4.94
2×1MISO	18.3	6.7×10^{-9}	5.67
4×1MISO	19.6	9.18×10^{-7}	4.78
8×1MISO	20.9	3.73×10^{-8}	5.37
2×2MIMO	18.5	6.03×10^{-8}	5.29
4×4MIMO	19.9	4.42×10^{-8}	5.34
8×8MIMO	21.1	7.09×10^{-9}	5.67

Figure (4.9) displays the relation of the link range versus the BER of OOK-NRZ at 10Gbps with various MIMO combinations and 1×1SISO in turbid water. It is clear from this figure that the transmission range is directly proportional to BER, as the BER increases when the link range increases. In addition, 8×8MIMO has achieved the best results by 21.1m with a BER approximately 10^{-9}.

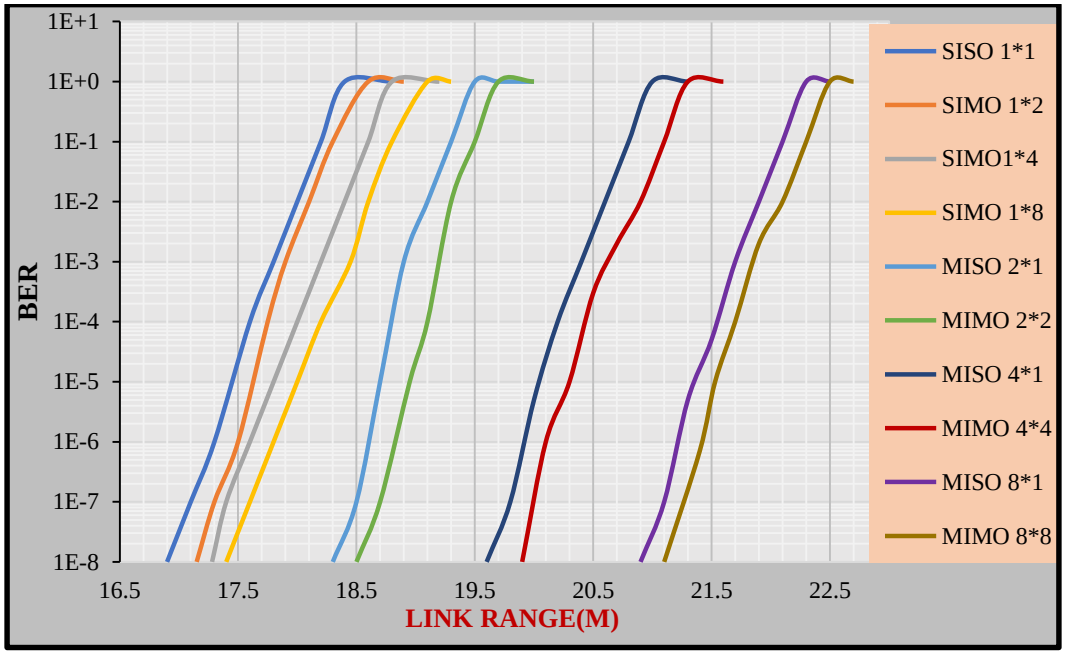

Fig.4.9: OOK-NRZ at 10Gbps BER vs. Link Range for 1×1SISO and various MIMO configurations in turbid water.

4.3.2 Simulation Results of OOK-NRZ at 40Gbps

The BER performance of the proposed OOK-NRZ is evaluated utilizing three distinct water types (clear, coastal, and turbid), at 40Gbps data rate, and varied transmission lengths.

For clear water, the numerical results of BERs and links range have been obtained as shown in the table below (4.7).

Table (4.7): Results from simulations of OOK-NRZ modulation under clear water at 40Gbps.

Techniques	Max Link Range(m)	BER	Q Factor
1×1SISO	145	8.7×10^{-8}	5.22
1×2SIMO	146.5	1.4×10^{-7}	5.12
1×4SIMO	148.1	4×10^{-7}	4.93
1×8SIMO	151.5	4.9×10^{-8}	5.32
2×1MISO	160	7.9×10^{-8}	5.25
4×1MISO	177	3.3×10^{-8}	5.4
8×1MISO	191.7	9.55×10^{-8}	5.2
2×2MIMO	165	3.19×10^{-8}	5.4
4×4MIMO	181	2.27×10^{-7}	5.04
8×8MIMO	196	2.76×10^{-8}	5.13

Figure (4.10) shows the OOK-NRZ connection range diagram of BER with various MIMO technique combinations and 1×1SISO at 40Gbps and under a low turbulence channel. 8×8MIMO was the best in terms of result in clear water, achieving a link range of 196m with a very low BER approximately 10^{-8}.

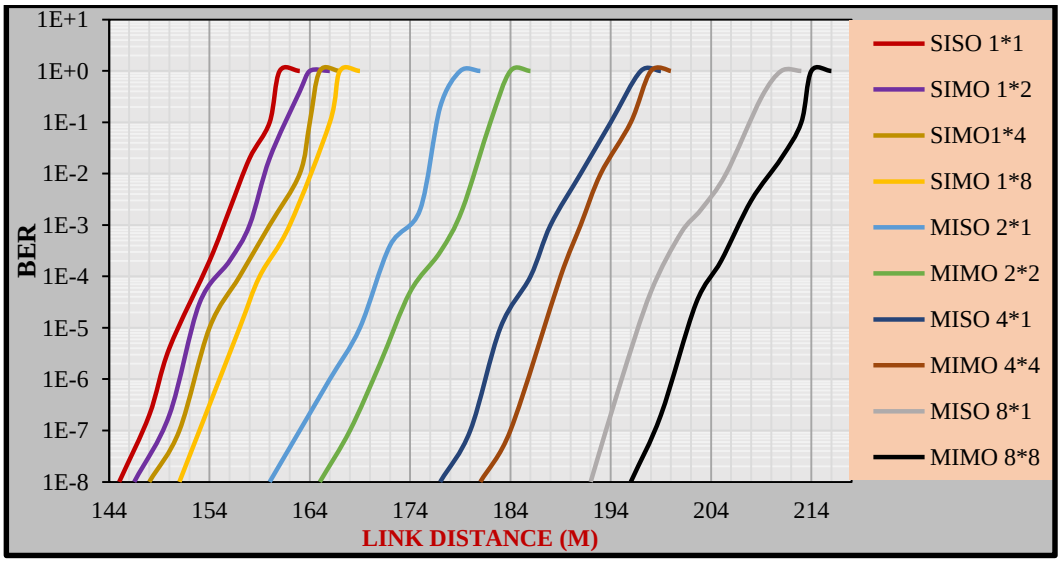

Fig.4.10: Link Distance vs. BER for OOK-NRZ at 40Gbps with SISO technique and various MIMO configurations in clear water.

Table (4.8) presents the simulated results of bit error rates (BERs), Q factor, and links range at 40 Gbps in coastal water (channel with medium turbulence)

Table (4.8): Results from simulations of OOK-NRZ modulation under coastal water at 40Gbps.

Techniques	Max Link Range(m)	BER	Q Factor
1×1SISO	67	3.27×10^{-8}	5.4
1×2SIMO	68	2.2×10^{-7}	5.04
1×4SIMO	69.5	1.89×10^{-7}	5.07
1×8SIMO	71	8.7×10^{-8}	5.22
2×1MISO	75	5.65×10^{-9}	5.7
4×1MISO	80	1.17×10^{-8}	5.58
8×1MISO	87	6.62×10^{-8}	5.27
2×2MIMO	77	9.61×10^{-8}	5.2
4×4MIMO	82	1.2×10^{-7}	5.15
8×8MIMO	88.5	6.4×10^{-8}	5.28

Figure (4.11) shows the relationship between the link range versus BER of OOK-NRZ at 40Gbps with various MIMO configurations and 1×1SISO in coastal water. 8×8MIMO was the better results, 88.5m link range and 6.4×10^{-8} BER.

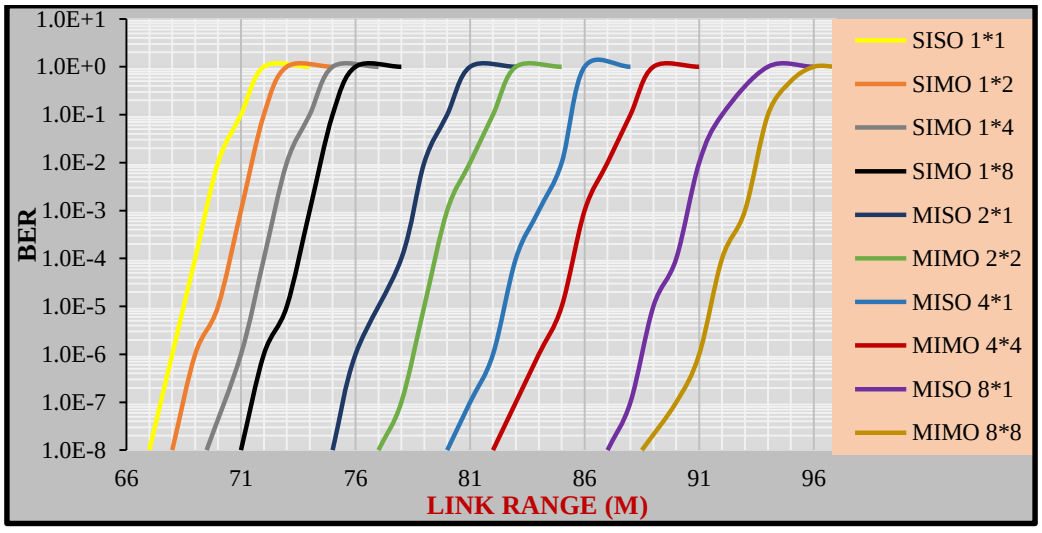

Fig.4.11: BER vs. Link Range for 40Gbps OOK-NRZ with 1×1SISO and MIMO under coastal water.

For turbid water, at 40Gbps the numerical results of BERs have been obtained as shown in the table below (4.9).

Table (4.9): OOK-NRZ modulation under turbid water simulation results 40Gbps.

Techniques	Max Link Range(m)	BER	Q Factor
1×1SISO	15.6	3.11×10^{-8}	5.41
1×2SIMO	15.8	1.75×10^{-7}	5.09
1×4SIMO	15.9	1.89×10^{-7}	5.07
1×8SIMO	16.1	5.59×10^{-8}	5.3
2×1MISO	16.9	4×10^{-8}	5.36
4×1MISO	18.4	1.89×10^{-7}	5.7
8×1MISO	19.6	1.24×10^{-8}	5.57
2×2MIMO	17.2	9.13×10^{-8}	5.21
4×4MIMO	18.6	1.39×10^{-8}	5.13
8×8MIMO	19.8	7.94×10^{-8}	5.24

Figure (4.12) shows the graphic chart of the link range vs BER_s of OOK-NRZ at 40Gbps with different MIMO configurations and 1×1SISO under turbid water. It has been shown that the relationship of the BER with the link range is a direct relationship and also shows that the 8×8MIMO technique gave the best results as the link range reached 19.8m with 7.9×10^{-8} BER.

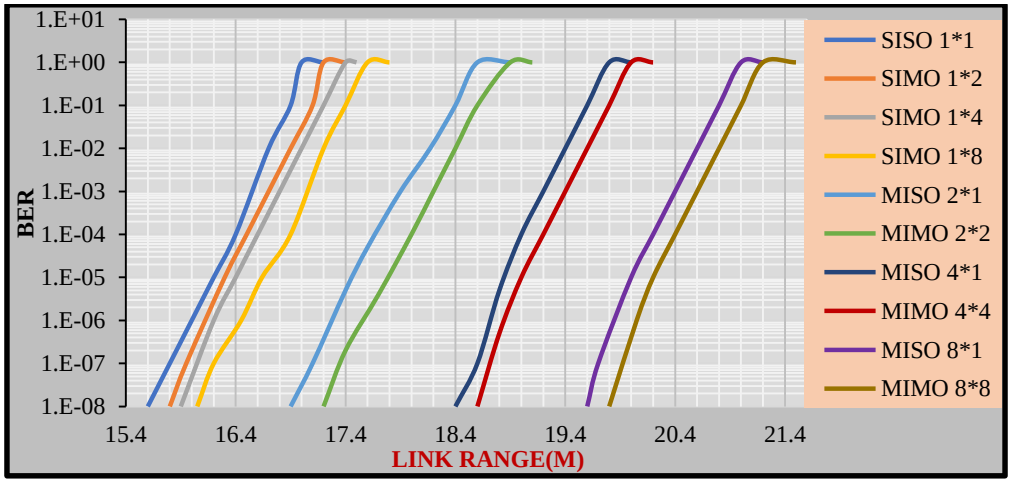

Fig.4.12: OOK-NRZ at 40Gbps BER vs. Link Range for 1×1SISO and various MIMO configurations in turbid water.

4.3.3 Simulation Results of OOK-NRZ at 100Gbps

The performance of the OOK-NRZ system has been studied by calculating the transmission range with the BER per distance at a data rate of 100Gbps and for all channel technologies and under three different types of water (clear, coastal, and turbid).

The following table (4.10) presents the numerical results that were achieved for BERs, Q factor, and links range in clear water.

Table 4.10: Simulation results of OOK-NRZ modulation under clear water at 100Gbps.

Techniques	Max Link Range(m)	BER	Q Factor
1×1SISO	135	4.37×10^{-8}	5.35
1×2SIMO	137	2.28×10^{-8}	5.46
1×4SIMO	138	2.4×10^{-8}	5.45
1×8SIMO	140	1.8×10^{-7}	5.08
2×1MISO	150	1.8×10^{-8}	5.5
4×1MISO	165	2.94×10^{-8}	5.42
8×1MISO	180	2.85×10^{-8}	5.42
2×2MIMO	155	1.1×10^{-7}	5.17
4×4MIMO	170	5.47×10^{-8}	5.3
8×8MIMO	185	1.37×10^{-8}	5.55

Figure (4.13) displays a schematic diagram of the relationship between BER and link range for OOK-NRZ at 10Gbps with various MIMO combinations and 1×1SISO in clear water. 8×8MIMO and 8×1MISO techniques was the best in terms of result in clear water, achieving a link range of 185m and 170m respectively with a very low BER approximately 10^{-8}.

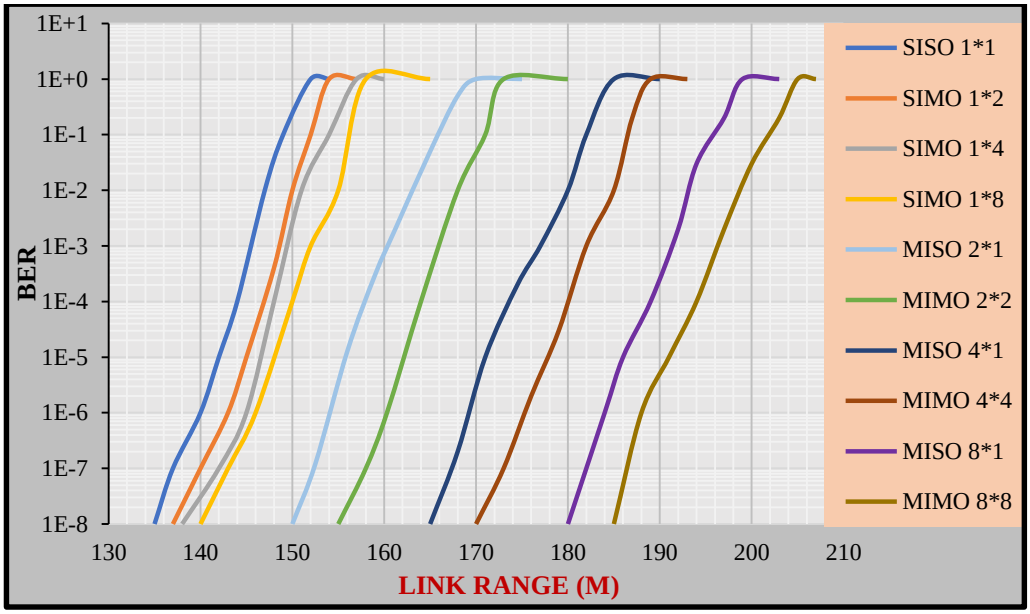

Fig.4.13: OOK-NRZ at 100Gbps BER vs. Link Range for 1×1SISO and various MIMO techniques in clear water.

For coastal water, at 100Gbps the numerical results of BERs, Q factor, and links range have been obtained as shown in the table below (4.11).

Table (4.11): Simulation results of OOK-NRZ modulation under coastal water.

Techniques	Max Link Range(m)	BER	Q Factor
1X1SISO	63	1.13×10^{-8}	5.58
1X2SIMO	64	1.66×10^{-7}	5.1
1X4SIMO	65	2.87×10^{-7}	4.99
1X8SIMO	66.2	1.69×10^{-7}	5.1
2X1MISO	70	1.6×10^{-8}	5.52
4X1MISO	77	1.7×10^{-8}	5.51
8X1MISO	82	1.5×10^{-8}	5.54
2X2MIMO	72	2.7×10^{-8}	5.43
4X4MIMO	79	2.34×10^{-7}	5.03
8X8MIMO	84	2.36×10^{-7}	5.03

Figure (4.14) shows the relationship between the link range versus BER of OOK-NRZ at 100Gbps with various MIMO configurations and 1×1SISO in coastal water. 8×8MIMO was the better results, 84m link range and 2×10^{-7} BER.

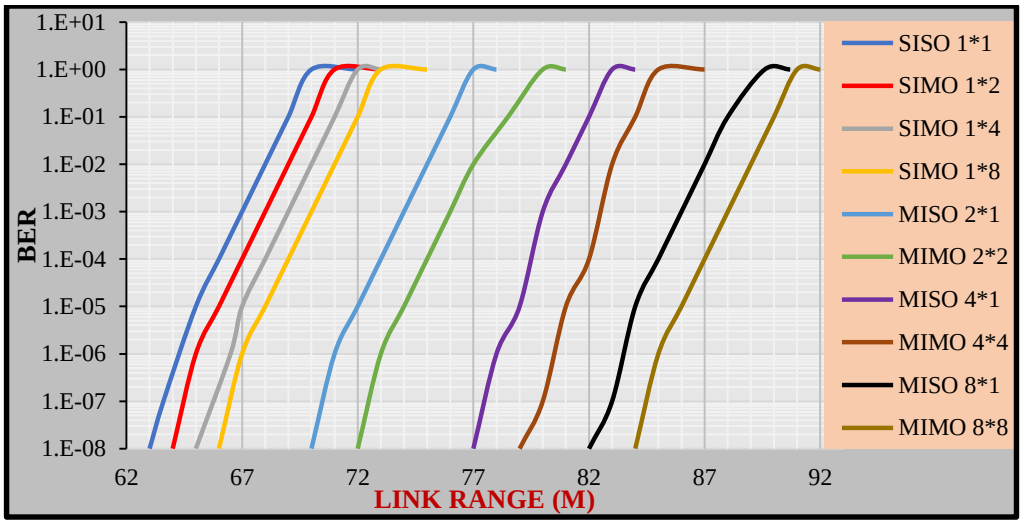

Fig.4.14: OOK-NRZ at 100Gbps with 1×1SISO and various MIMO techniques under coastal water: BER vs. Link Range.

In high turbulence channels (turbid water), at 100Gbps the numerical results of BERs, Q factor, and links range have been obtained as shown in the table below (4.12).

Table (4.12): Simulation results of OOK-NRZ modulation under turbid water.

Techniques	Max Link Range(m)	BER	Q Factor
1×1SISO	14.8	3.53×10^{-8}	5.38
1×2SIMO	14.95	1.79×10^{-7}	5.08
1×4SIMO	15.1	5.28×10^{-8}	5.31
1×8SIMO	15.25	7.34×10^{-8}	5.25
2×1MISO	16.2	1.56×10^{-8}	5.53
4×1MISO	17.4	5.28×10^{-8}	5.31
8×1MISO	18.7	3.11×10^{-9}	5.81
2×2MIMO	16.5	1.5×10^{-8}	5.54
4×4MIMO	17.7	2.94×10^{-8}	5.42
8×8MIMO	19	2.46×10^{-8}	5.45

Figure (4.15) presents the schematic graphic of the link range versus BER of OOK-NRZ at 100Gbps with SISO and different MIMO techniques in turbid water.

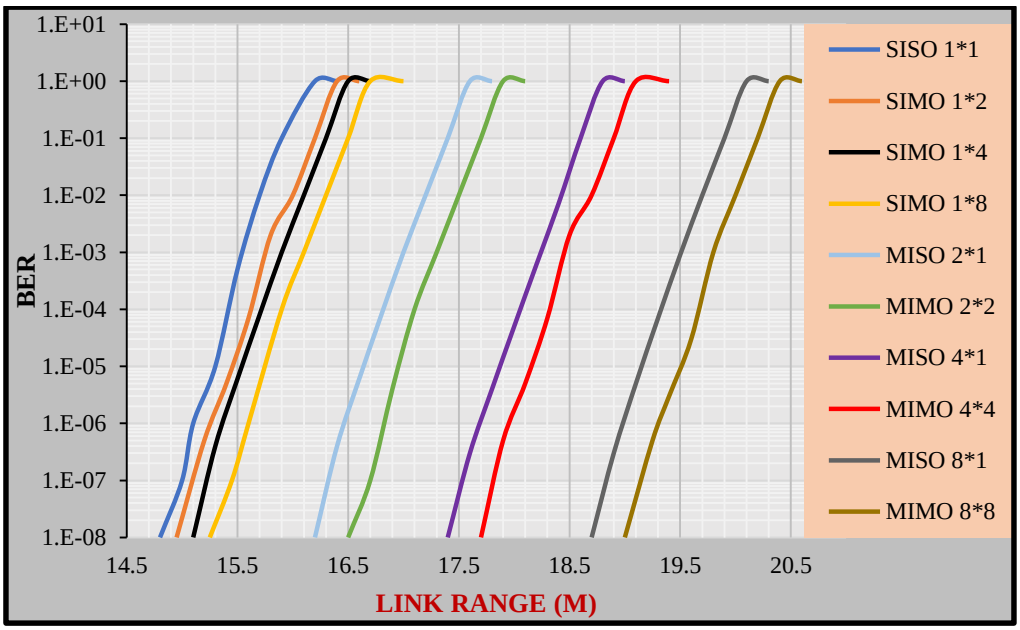

Fig.4.15: OOK-NRZ at 100Gbps BER vs. Link Range for 1✕1SISO and various MIMO configurations in turbid water.

Based on the preceding data, it is evident that 8×8MIMO and 8×1MISO techniques gave the best results better than other MIMO configurations in three water types (clear, coastal, and turbid). Observably, increasing the number of receiver elements (photodetectors) increased the link range, whereas raising the data rate at the target BER =10^{-8} lowered the link range.

Figure (4.16) displays the relationship between the received power and the link range for OOK-NRZ under 3 distinct types of water (clear, coastal, and turbid). It is essential to note that the transmitted power remains constant at 20 dB for all distances specified.

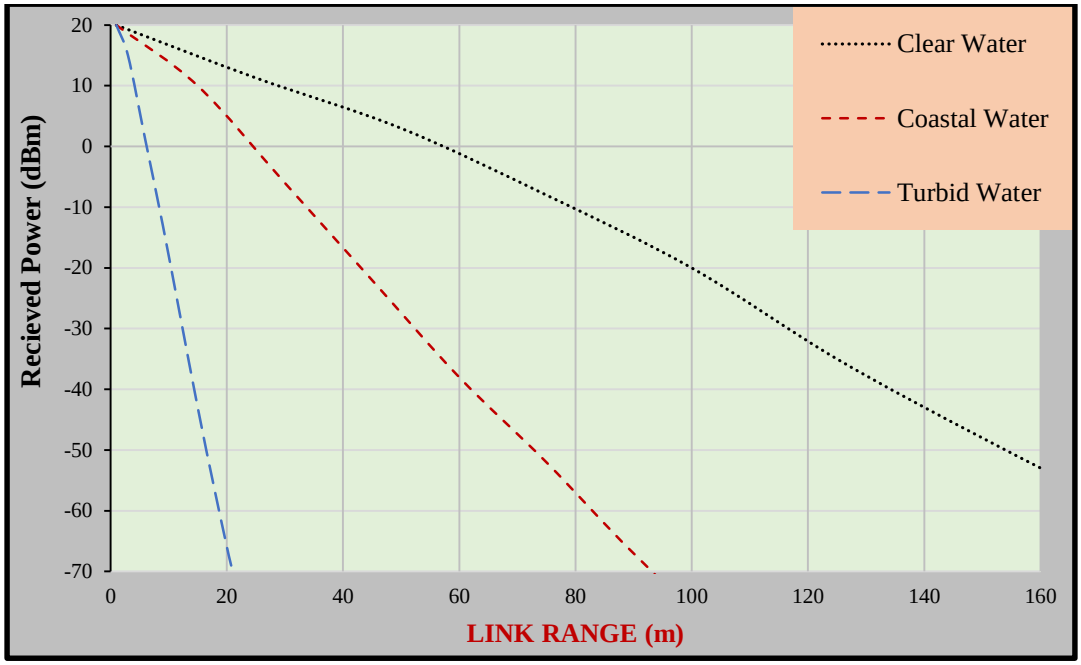

Fig.4.16: Link Range (m) vs. Received Power (dBm) of OOK-NRZ with 8×8MIMO under three water types (clearwater, coastal water, and turbid water).

4.4 Simulation Results of OOK-CSRZ

A data rate of 10 Gbps, gradually increasing it to 40 Gbps, and finally reaching 100 Gbps, the results of this particular sort of modulation were computed for three different data rates.

4.4.1 Simulation Results of OOK-CSRZ at 10Gbps

The BER performance of the proposed OOK-CSRZ is evaluated using three distinct types of water (clear, coastal, and turbid) at several different transmission lengths. In clear water, at 10Gbps the numerical results of BERs have been obtained as shown in the table below (4.13).

Table (4.13): Simulation results of OOK-CSRZ modulation under clear water at 10Gbps.

Techniques	Max Link Range(m)	BER	Q Factor
1×1SISO	129	2.23×10^{-8}	5.47
1×2SIMO	131	7.45×10^{-9}	5.66
1×4SIMO	133	2.12×10^{-9}	5.87
1×8SIMO	135	6.67×10^{-9}	5.68
2×1MISO	145	1.3×10^{-8}	5.56
4×1MISO	160	4.8×10^{-9}	5.73
8×1MISO	175	8×10^{-9}	5.64
2×2MIMO	150	2.1×10^{-8}	5.47
4×4MIMO	165	7.14×10^{-8}	5.26
8×8MIMO	179	6.7×10^{-8}	5.27

The BER analyzer for OOK-CSRZ at10Gbps 8×8MIMO in clear water with transmitted power is 20dBm for goal BER=10^{-8} is displayed in Figure (4.17).

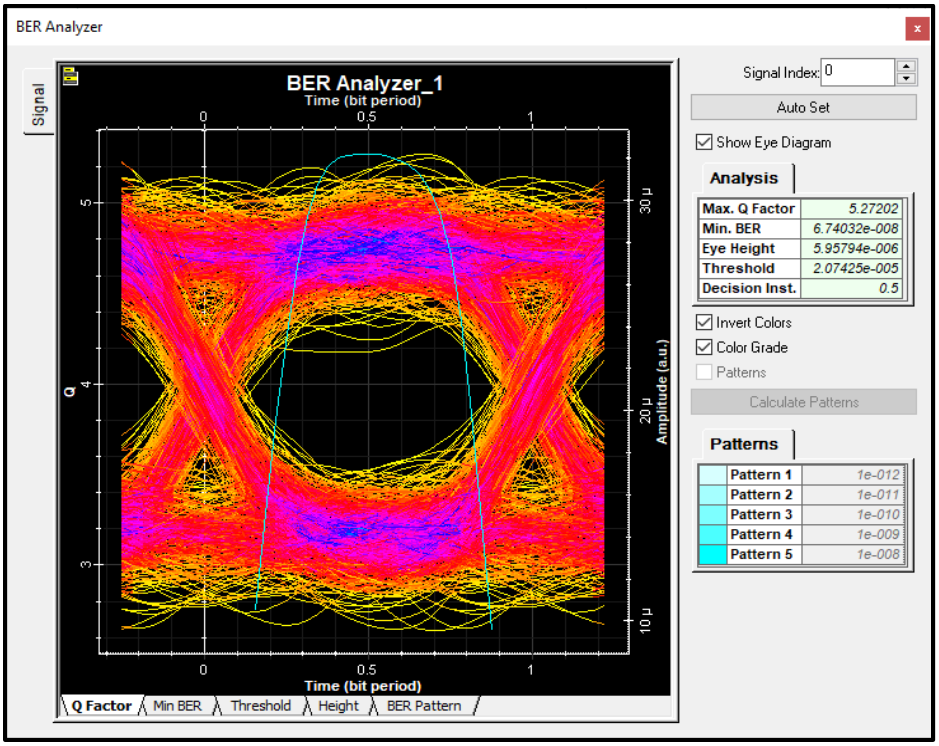

Fig.4.17: BER Analyzer for 8×8MIMO System in clearwater at10Gbps.

Figure (4.18) presents the schematic diagram of the link distance versus BER of OOK-CSRZ at 10Gbps with SISO1×1 and various MIMO technique configurations in clear water.

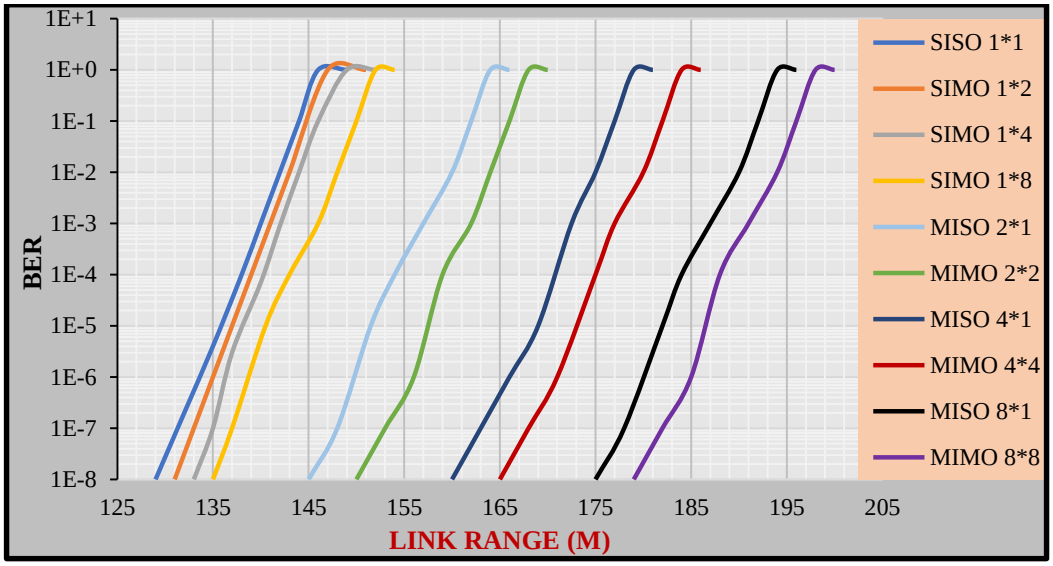

Fig.4.18: Link Range vs. BER for OOK-CSRZ at 10Gbps with SISO technique and various MIMO configurations in clear water.

Table (4.14) shows the numerical values for BERs, Q factors, and distances for coastal water at 10Gbps.

Table (4.14): Simulations results of OOK-CSRZ modulation under coastal water.

Techniques	Max Link Range(m)	BER	Q Factor
1×1SISO	60	2.05×10^{-8}	5.48
1×2SIMO	61	2.63×10^{-8}	5.44
1×4SIMO	62	4.67×10^{-7}	4.9
1×8SIMO	63.5	4.85×10^{-7}	4.89
2×1MISO	68	7.66×10^{-8}	5.24
4×1MISO	74	1.53×10^{-8}	5.53
8×1MISO	80	5.92×10^{-8}	5.29
2×2MIMO	70	1.17×10^{-7}	5.16
4×4MIMO	76	7.24×10^{-8}	5.25
8×8MIMO	82	6.77×10^{-8}	5.27

Figure (4.19) presents the schematic diagram of the link range versus BER of OOK-CSRZ at 10Gbps with SISO1×1 and various MIMO combinations.

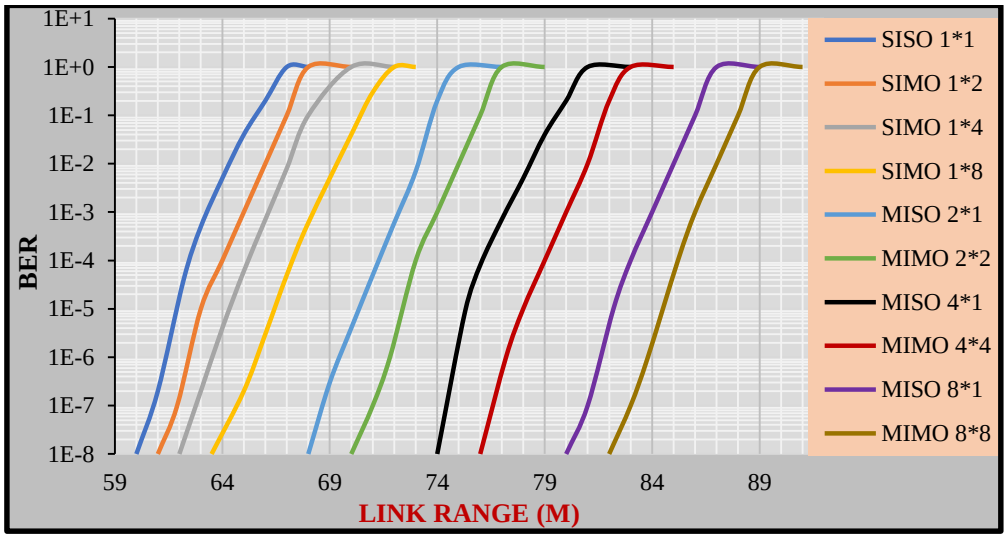

Fig.4.19: Link Range vs. BER for OOK-CSRZ at 10Gbps with 1×1SISO and various MIMO technique combinations under mid-water.

Table (4.15) shows the numerical results for BERs, distances, and Q factors at 10Gbps in turbid water for various MIMO configurations and SISO technique.

Table (4.15): Results from simulations of OOK-CSRZ modulation under turbid water at 10Gbps.

Techniques	Max Link Range(m)	BER	Q Factor
1×1SISO	14.3	1.5×10^{-8}	5.54
1×2SIMO	14.5	1.27×10^{-8}	5.57
1×4SIMO	14.7	5.99×10^{-8}	5.29
1×8SIMO	15	2×10^{-7}	5.06
2×1MISO	15.8	4.09×10^{-9}	5.76
4×1MISO	17	5.82×10^{-9}	5.7
8×1MISO	18.2	6.2×10^{-9}	5.69
2×2MIMO	16.1	3.55×10^{-7}	4.95
4×4MIMO	17.3	3×10^{-8}	5.41
8×8MIMO	18.6	2.08×10^{-7}	5.06

Figure (4.20) displays the relation of the link range versus the BER of OOK-CSRZ at 10Gbps with various MIMO combinations and 1×1SISO in turbid water. It is clear from this figure that the link range is directly proportional to BER, as the BER increases when the link range increases. In addition, 8×8MIMO has achieved the best results by 18.6m with a BER approximately 10^{-8}.

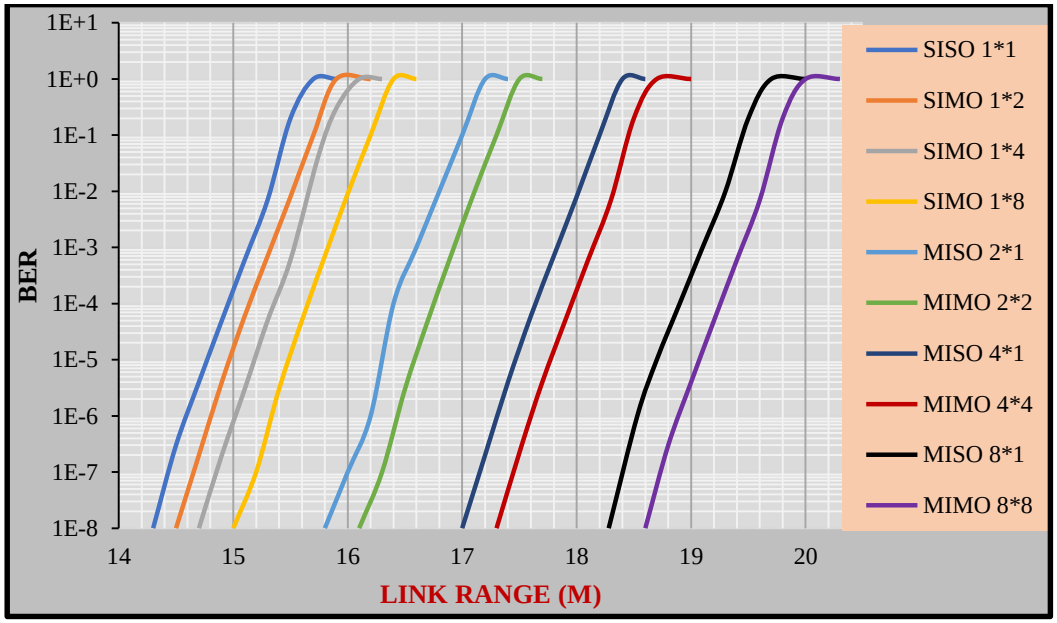

Fig.4.20: Link Range vs. BER for OOK-CSRZ at 10Gbps with SISO technique and various MIMO configurations in turbid water.

4.4.2 Simulation Results of OOK-CSRZ at 40Gbps

To analyze the bit error rate (BER) performances of the proposed OOK-CSRZ, three distinct kinds of water clear, coastal, and turbid are used, together with a data rate of 40Gbps and a variety of transmission lengths.

In clear water, the numerical values of BERs, distances, and Q factors have been obtained as shown in table (4.16) for various MIMO technique configurations.

Table (4.16): Simulations results of OOK-CSRZ modulation under clear water.

Techniques	Max Link Range(m)	BER	Q Factor
1✕1SISO	105	6.2×10^{-8}	5.28
1✕2SIMO	107	6.2×10^{-8}	5.28
1✕4SIMO	109	6×10^{-8}	5.29
1✕8SIMO	111	1.38×10^{-7}	5.13
2✕1MISO	125	3.89×10^{-8}	5.37
4✕1MISO	140	8.2×10^{-8}	5.23
8✕1MISO	152	5.9×10^{-8}	5.29
2✕2MIMO	128	9.4×10^{-8}	5.2
4✕4MIMO	144	1.74×10^{-7}	5.09
8✕8MIMO	155	2.7×10^{-7}	5

Figure (4.21) displays a schematic diagram of the relationship between BER and link range for OOK-NRZ at 40Gbps with various MIMO combinations and 1✕1SISO in clear water. 8✕8MIMO and 8✕1MISO techniques was the best in terms of result in clear water, achieving a link range of 155m and 144m respectively with a very low BER approximately 10^{-8}.

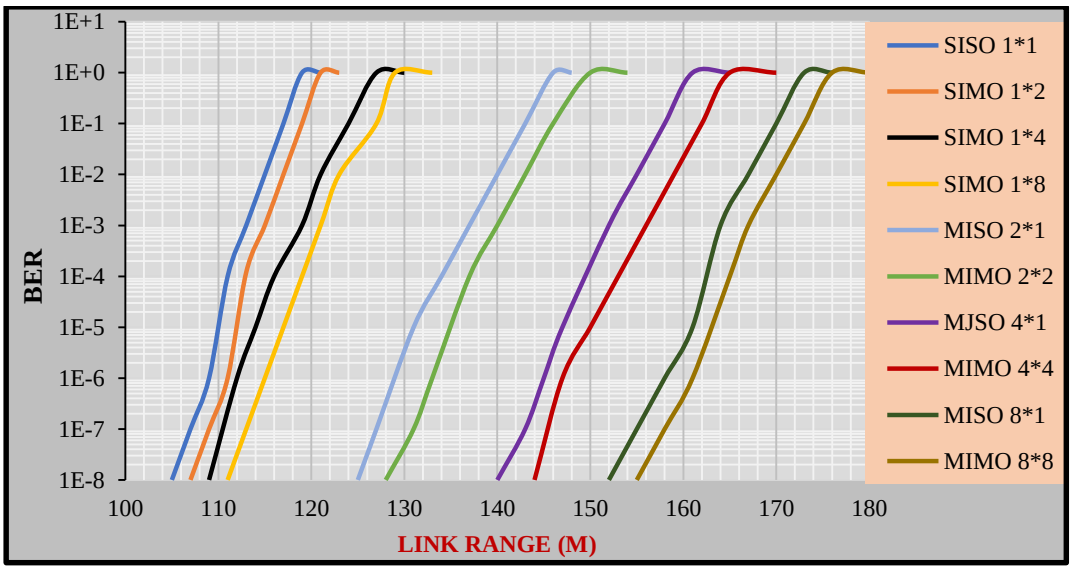

Fig.4.21: Link Range vs. BER for OOK-CSRZ at 40Gbps with SISO technique and various MIMO technique configurations in clear water.

For the mid-turbulence channel (coastal water), at 40Gbps the numerical results of BERs have been obtained as shown in the table below (4.17).

Table (4.17): Simulation results of OOK-CSRZ modulation under coastal water.

Techniques	Max Link Range(m)	BER	Q Factor
1×1SISO	50	1.16×10^{-8}	5.58
1×2SIMO	51	4.84×10^{-8}	5.33
1×4SIMO	52	1.84×10^{-7}	5.08
1×8SIMO	53	6.2×10^{-7}	4.8
2×1MISO	57	1.7×10^{-8}	5.5
4×1MISO	64	3.9×10^{-8}	5.3
8×1MISO	71	7.14×10^{-8}	5.26
2×2MIMO	60	1.17×10^{-7}	5.16
4×4MIMO	67	9.24×10^{-8}	5.2
8×8MIMO	73	2.38×10^{-7}	5.03

Figure (4.22) shows the relation between the link range versus BER of OOK-CSRZ at 40Gbps with various MIMO configurations and 1×1SISO in coastal water. 8×8MIMO was the better results, 73m link range and 2×10^{-7} BER.

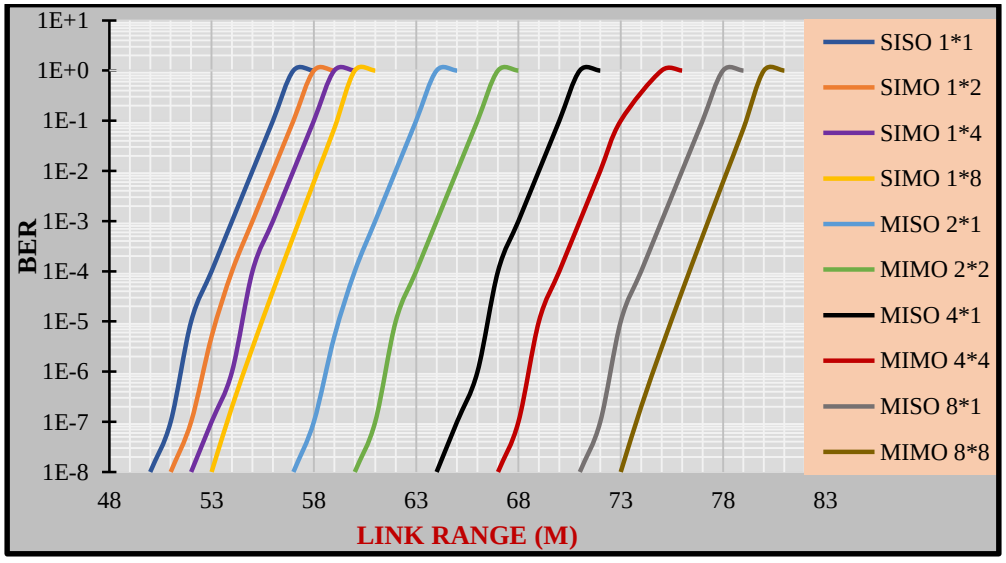

Fig.4.22: Link Range vs. BER for OOK-CSRZ at 40Gbps with 1×1SISO and various MIMO technique configurations in coastal water.

In high turbulence channels (turbid water), the numerical findings of BERs, Q factors, and links range at 40Gbps are presented in the table (4.18) for SISO and various MIMO techniques.

Table (4.18): Simulation results of OOK-CSRZ modulation under turbid water.

Techniques	Max Link Range(m)	BER	Q Factor
1×1SISO	12.5	6.77×10^{-9}	5.67
1×2SIMO	12.7	2.26×10^{-9}	5.86
1×4SIMO	12.9	5×10^{-9}	5.7
1×8SIMO	13.1	1.3×10^{-8}	5.56
2×1MISO	14	1.7×10^{-8}	5.51
4×1MISO	15	2.04×10^{-8}	5.48
8×1MISO	16.1	1.02×10^{-9}	5.99
2×2MIMO	14.5	8.07×10^{-8}	5.23
4×4MIMO	15.4	4.57×10^{-8}	5.34
8×8MIMO	16.5	2.9×10^{-9}	5.81

Figure (4.23) shows the graphic chart of the link range vs BER_s of OOK-NRZ at 40Gbps with different MIMO configurations under turbid water. It has been shown that the relation of the BER with the link range is a direct relationship.

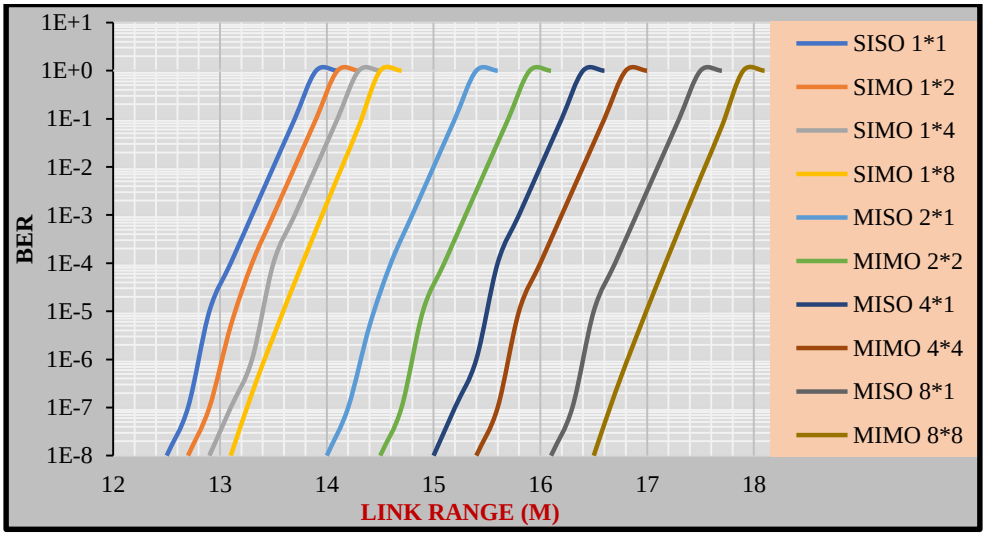

Fig.4.23: Link Range vs. BER for OOK-CSRZ at 40Gbps with SISO & various MIMO configurations in turbid water.

4.4.3 Simulation Results of OOK-CSRZ at 100Gbps

When the data rate is increased from 40 to 100 Gbps, the BER value is one and the value of the Q factor is zero at any distance used for 1✕1SISO and various MIMO combinations. This means that the process of sending and receiving has failed, and the figure (4.24) shows the amount of distortion in the signal.

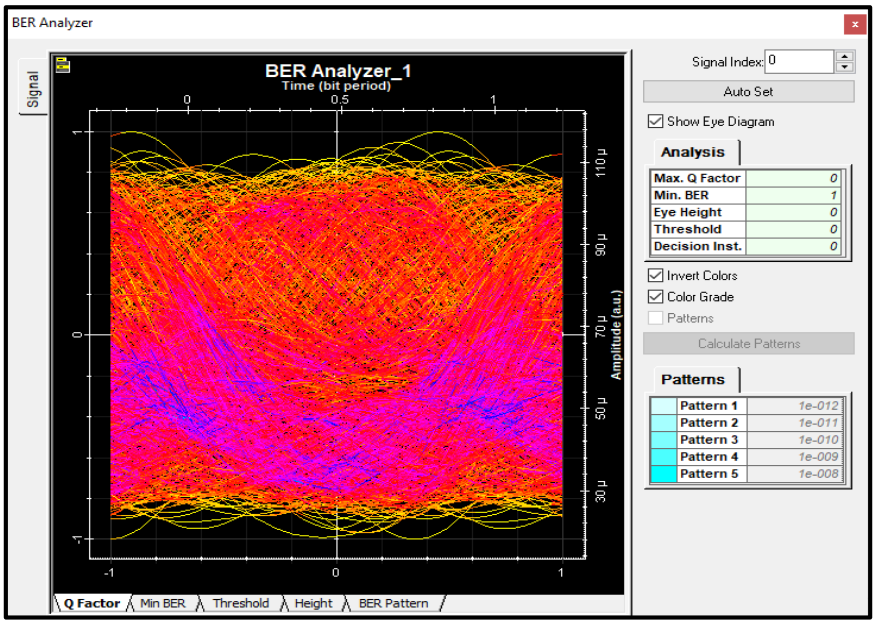

Fig.4.24: BER Analyzer for8✕8MIMO System in turbid water at 100Gbps.

It is evident from the preceding data that 8×8MIMO and 8×1MISO systems perform better than the other configurations in all three water types (turbid, coastal, and clear). Consequently, the link range increased as the number of receiver elements (photodetectors) increased, and the link range decreased as the data rate increased. However, when the data rate was increased to 100Gbps, there was no result for BERs (BER=1) at any distance.

Figure (4.25) presents the relationship between the received power and the link distance for OOK-CSRZ under three water types (turbid, coastal, and clear) at

40Gbps. It is important to note that the transmitted power is equal to 20dBm for all distances shown.

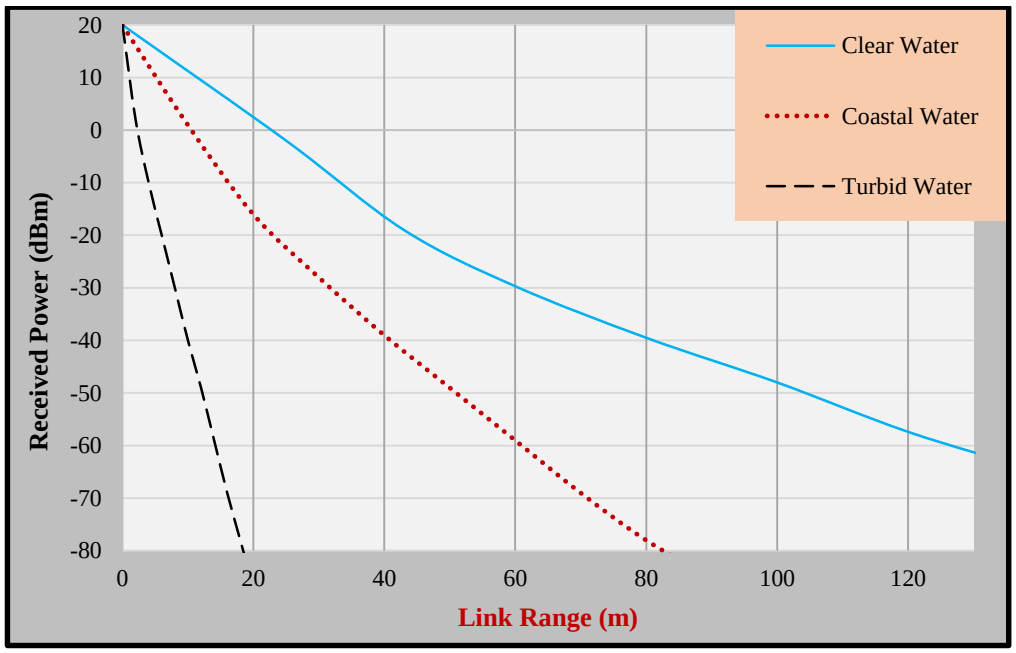

Fig.4.25: Link Range (m) vs. Received Power (dBm) of OOK-CSRZ with 8×8MIMO under three types of water.

4.5 Simulation Results of OOK-Manchester code

The results of this modulation type were calculated for three cases from the date rate, and the data rate was gradually increased from 10Gbps to 40Gbps and then to 100Gbps.

4.5.1 Simulation Results of OOK-Manchester at 10Gbps

The BER performance of the proposed OOK-Manchester coding is investigated using three distinct types of water and various transmission lengths (turbid, coastal, and clear).

In low turbulence channels (clear water), the numerical findings of BERs, Q factor, and links range at 10Gbps are presented in the table below (4.19).

Table (4.19): Simulation results of OOK-Manchester code modulation under clear.

Techniques	Max Link Range(m)	BER	Q Factor
1×1SISO	200	6.19×10^{-8}	5.28
1×2SIMO	203	6.84×10^{-8}	5.26
1×4SIMO	206	4.94×10^{-8}	5.32
1×8SIMO	209	1.52×10^{-7}	5.12
2×1MISO	220	3.94×10^{-9}	5.77
4×1MISO	235	2.11×10^{-9}	5.87
8×1MISO	250	1×10^{-8}	5.6
2×2MIMO	225	1.48×10^{-8}	5.54
4×4MIMO	241	2.38×10^{-8}	5.45
8×8MIMO	257	1.55×10^{-7}	5.11

Figure (4.26) shows the BER analyzer for OOK-Manchester code at 10Gbps with 8×8MIMO in turbid water with transmitted power are 100mW (20dBm) for target BER=10^{-8}.

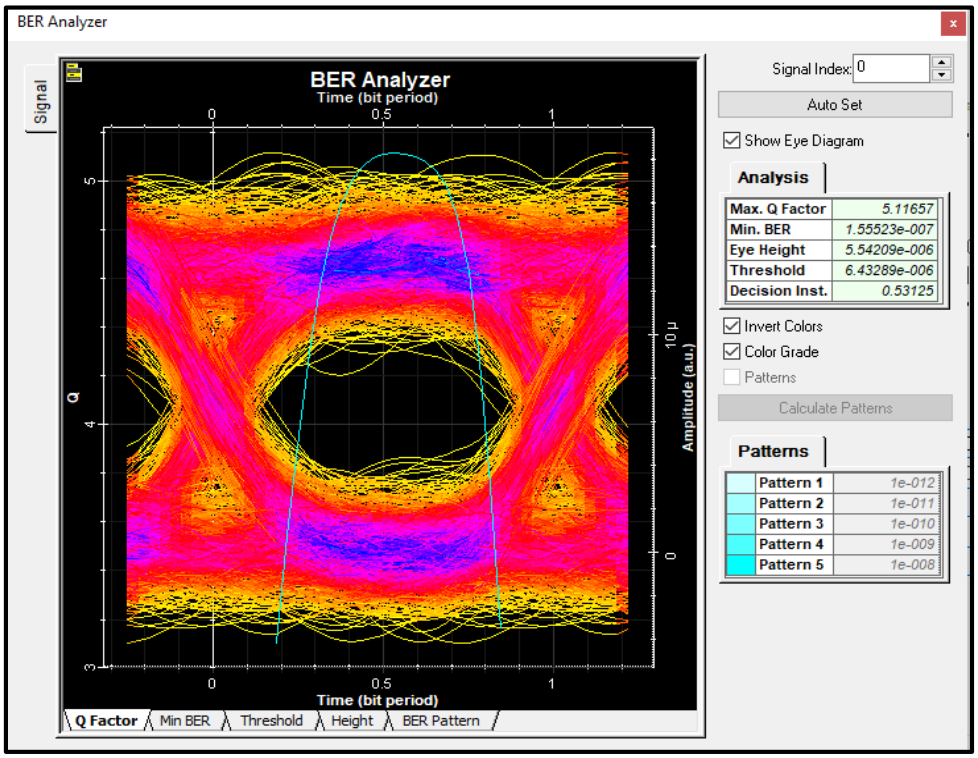

Fig.4.26: BER Analyzer for 8×8MIMO System in clear water at 10Gbps.

Figure (4.27) shows the schematic graphic of the link range versus BER of OOK-Manchester at 10Gbps with the SISO technique and multiple MIMO configurations in clearwater. the 8×8MIMO showed the best result about 257m link range and 10^{-8} BER.

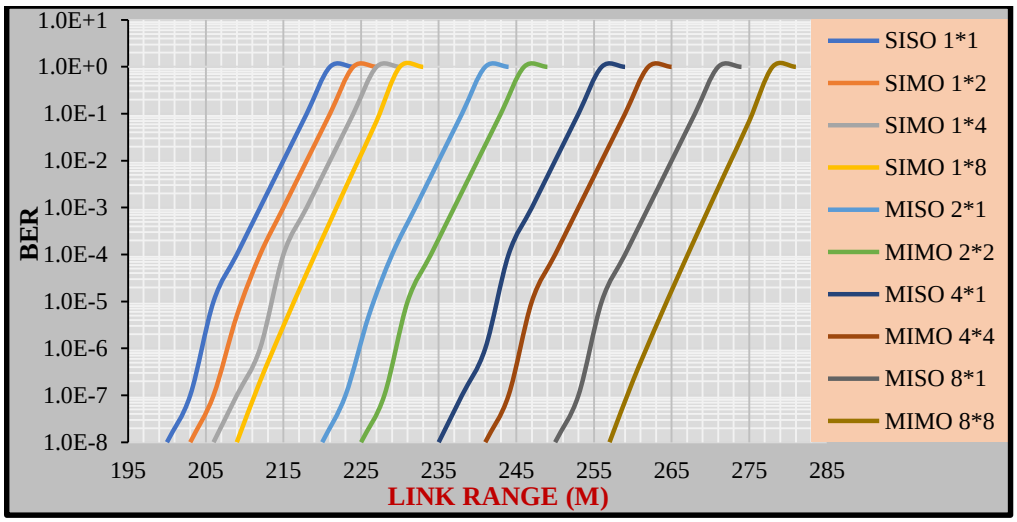

Fig.4.27: Link Range vs BER for OOK-Manchester code at 10Gbps with SISO and multiple MIMO configurations in clear water.

In the mid-turbulence channel (coastal water), at 10Gbps the numerical values of BERs, Q factor, and links range have been obtained as shown in the table (4.20).

Table (4.20): Simulation results of OOK-Manchester under coastal water.

Techniques	Max Link Range(m)	BER	Q Factor
1×1SISO	90	3.3×10^{-8}	5.4
1×2SIMO	91	5.27×10^{-8}	5.31
1×4SIMO	92	7.62×10^{-8}	5.24
1×8SIMO	93	2×10^{-7}	5.06
2×1MISO	98	5×10^{-9}	5.72
4×1MISO	104	1×10^{-8}	5.6
8×1MISO	110	1.48×10^{-8}	5.54
2×2MIMO	100	2.15×10^{-8}	5.47
4×4MIMO	106	1.8×10^{-8}	5.5
8×8MIMO	113	1.72×10^{-7}	5.09

Figure (4.28) shows the graphic chart of the link range versus BER of the OOK-Manchester code (with 10Gbps) with SISO technique and multiple MIMO configurations in coastal water.

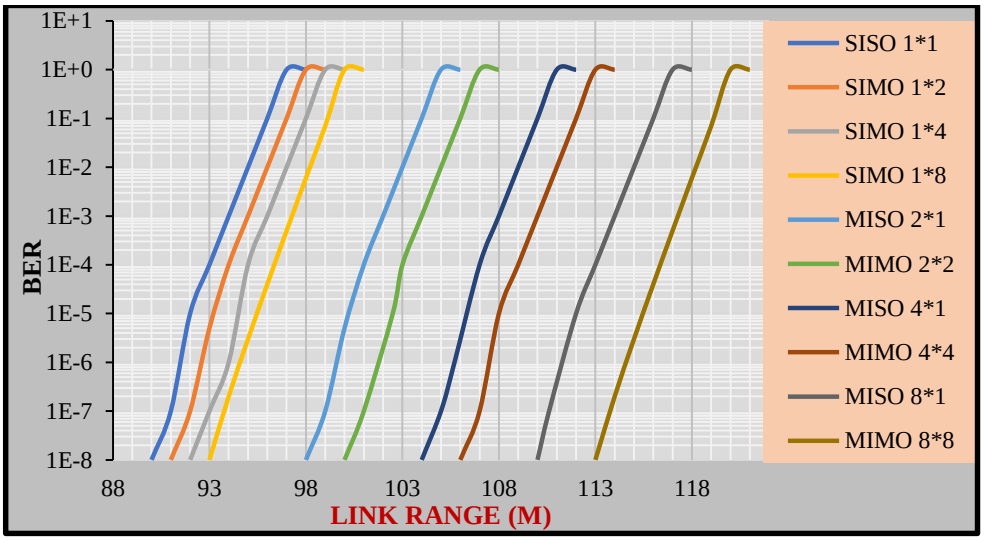

Fig.4.28: Link Range vs BER for OOK-Manchester code at 10Gbps with 1×1SISO and multiple MIMO configurations in coastal water.

For turbid water, at 10Gbps the numerical results of BERs, Q factor, and links range have been obtained as shown in the table below (4.21).

Table (4.21): Simulation results of OOK-Manchester code modulation under turbid water at 10Gbps.

Techniques	Max Link Range(m)	BER	Q Factor
1×1SISO	20	2×10^{-8}	5.48
1×2SIMO	20.2	1.91×10^{-8}	5.49
1×4SIMO	20.4	6.94×10^{-8}	5.26
1×8SIMO	20.6	1.12×10^{-7}	5.17
2×1MISO	21.6	2.1×10^{-8}	5.48
4×1MISO	23	6.27×10^{-8}	5.28
8×1MISO	24.1	6.77×10^{-8}	5.27
2×2MIMO	22	1.1×10^{-8}	5.59
4×4MIMO	23.3	3.96×10^{-8}	5.36
8×8MIMO	24.5	2.38×10^{-7}	5.03

Figure (4.29) displays the relation of the link range versus the BER of OOK-Manchester code at 10Gbps with various MIMO combinations and 1✕1SISO in turbid water. It is clear from this figure that the link range is directly proportional to BER, as the BER increases when the link range increases. In addition, 8✕8MIMO has achieved the best results by 24.5m with a BER approximately 10^{-8}.

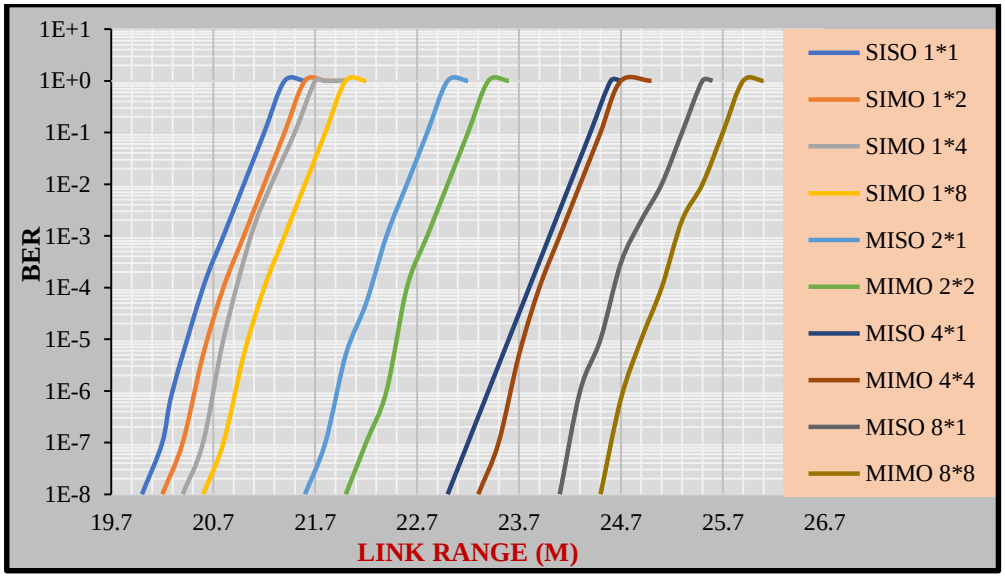

Fig.4.29: Link Range vs BER for OOK-Manchester code at 10Gbps with SISO technique and various MIMO configurations in turbid water.

4.5.2 Simulation Results of OOK-Manchester at 40Gbps

The proposed OOK-Manchester code's BER performance is examined for different transmission lengths and 3 different types of water (turbid, coastal, and clear).

In low turbulence channels (clear water), at 40Gbps the numerical values of BERs, Q factor, and links range have been obtained as shown in the table below (4.22).

Table (4.22): Simulation results of OOK-Manchester code modulation under clear water at 40Gbps.

Techniques	Max Link Range(m)	BER	Q Factor
1×1SISO	185	1.35×10^{-8}	5.55
1×2SIMO	188	3.35×10^{-8}	5.39
1×4SIMO	191	5.35×10^{-8}	5.31
1×8SIMO	194	2.2×10^{-7}	5.05
2×1MISO	205	2.47×10^{-9}	5.84
4×1MISO	220	6.9×10^{-8}	5.26
8×1MISO	235	3.91×10^{-8}	5.37
2×2MIMO	210	4.9×10^{-9}	5.73
4×4MIMO	225	1.61×10^{-7}	5.1
8×8MIMO	241	1.1×10^{-7}	5.18

Figure (4.30) shows the graphic chart of BER vs the link range of the OOK-Manchester code at 40Gbps with SISO and various MIMO configurations in clearwater. 8×8MIMO showed the best results, about 241m and 10^{-7} BER.

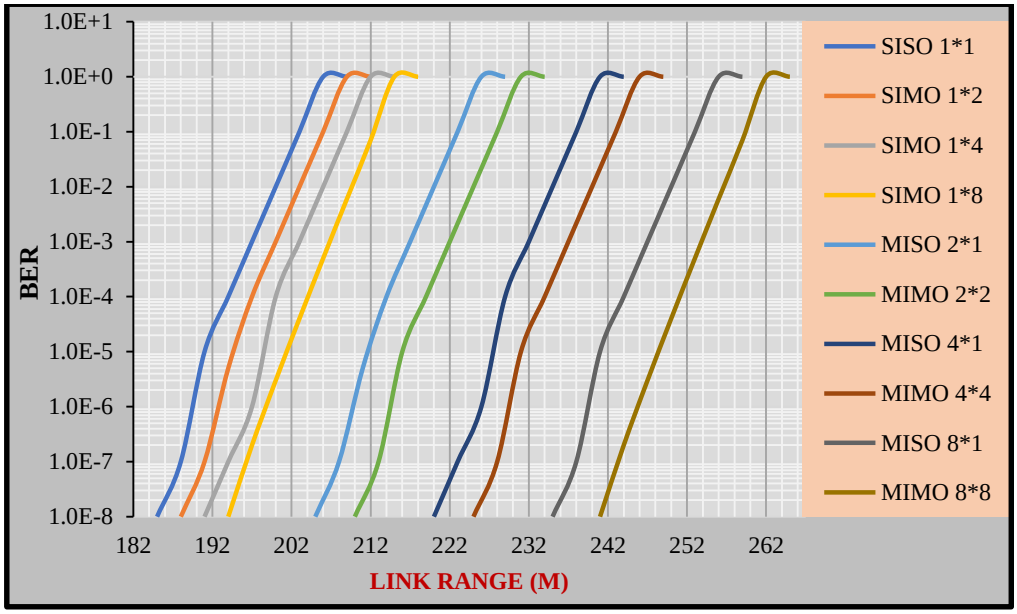

Fig.4.30: Link Range vs BER for OOK-Manchester code at 40Gbps with SISO and multiple MIMO configurations in clear water.

In coastal water at 40Gbps, the numerical values of BERs, Q factor, and links range have been obtained as shown in the table below (4.23).

Table (4.23): Simulation results of OOK-Manchester code modulation under coastal water at 40Gbps.

Techniques	Max Link Range(m)	BER	Q Factor
1×1SISO	82	1.54×10^{-8}	5.53
1×2SIMO	83	7.94×10^{-9}	5.65
1×4SIMO	84	3.88×10^{-8}	5.37
1×8SIMO	86	7.04×10^{-8}	5.26
2×1MISO	91	2.77×10^{-9}	5.82
4×1MISO	97	8.77×10^{-9}	5.63
8×1MISO	104	1.33×10^{-8}	5.56
2×2MIMO	94	4.11×10^{-8}	5.36
4×4MIMO	100	9.06×10^{-8}	5.21
8×8MIMO	106	1.11×10^{-7}	5.17

Figure (4.31) shows the graphic chart of the link range versus BER of the OOK-Manchester code at 40Gbps with SISO and multiple MIMO configurations in coastal water.

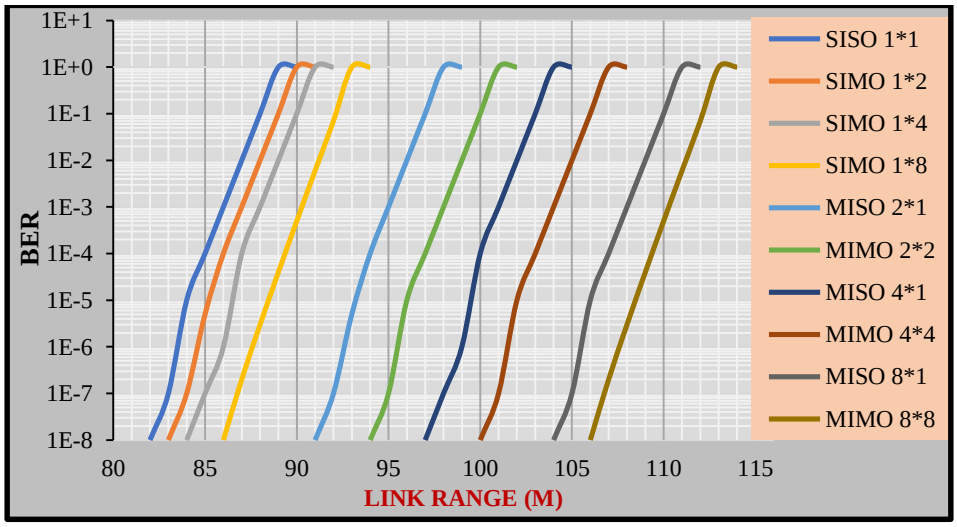

Fig.4.31: Link Range vs BER for OOK-Manchester code at 40Gbps with SISO and multiple MIMO configurations in coastal water.

In turbid water at 40Gbps, the numerical results of bit error rate BERs, Q factor, and links range is presented in the table below (4.24).

Table (4.24): Simulation results of OOK-Manchester code modulation under turbid water at 40Gbps.

Techniques	Max Link Range(m)	BER	Q Factor
1X1SISO	18.8	4.81×10^{-9}	5.73
1X2SIMO	19	4.22×10^{-8}	5.35
1X4SIMO	19.2	1.16×10^{-7}	5.17
1X8SIMO	19.5	3.45×10^{-7}	4.96
2X1MISO	20.5	3.93×10^{-8}	5.36
4X1MISO	21.8	1.37×10^{-8}	5.55
8X1MISO	23.2	3.45×10^{-7}	4.96
2X2MIMO	20.9	5.46×10^{-8}	5.31
4X4MIMO	22.2	4.6×10^{-8}	5.34
8X8MIMO	23.5	3.12×10^{-7}	4.98

Figure (4.32) presents the schematic graphic of the link range versus BER_s of the OOK-Manchester code at 40Gbps with SISO and various MIMO configurations in turbid water.

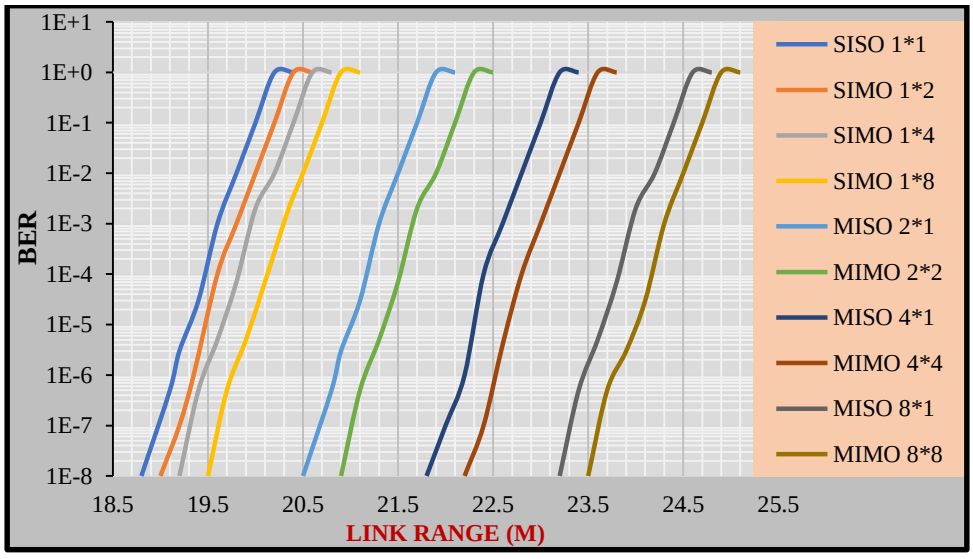

Fig.4.32: Link Range vs BER for OOK-Manchester code at 40Gbps with SISO technique and various MIMO configurations in turbid water.

4.5.3 Simulation Results of OOK-Manchester code at 100Gbps

Under several transmission lengths and three different types of water, the proposed OOK-Manchester code's BER performance is examined (turbid, coastal, and clear).

In low turbulence channels (clear water), at 100Gbps the numerical results of BERs, Q factor, and links range have been obtained as shown in the table below (4.25).

Table (4.25): Simulation results of OOK-Manchester code modulation under clear water at100Gbps.

Techniques	Max Link Range(m)	BER	Q Factor
1×1SISO	175	2.74×10^{-8}	5.43
1×2SIMO	178	9.51×10^{-8}	5.2
1×4SIMO	181	7×10^{-8}	5.26
1×8SIMO	184	3.46×10^{-8}	5.39
2×1MISO	192	1.68×10^{-8}	5.52
4×1MISO	210	7.91×10^{-8}	5.24
8×1MISO	225	8.27×10^{-8}	5.23
2×2MIMO	199	2.38×10^{-8}	5.45
4×4MIMO	215	9.72×10^{-7}	4.75
8×8MIMO	230	1.78×10^{-7}	5.09

Figure (4.33) displays a schematic diagram of the relationship between BER and link range for OOK-Manchester code at 10Gbps with various MIMO combinations and 1×1SISO in clear water. 8×8MIMO and 8×1MISO techniques was the best in terms of result in clear water, achieving a link range of 230m and 215m respectively with a very low BER approximately 10^{-8}.

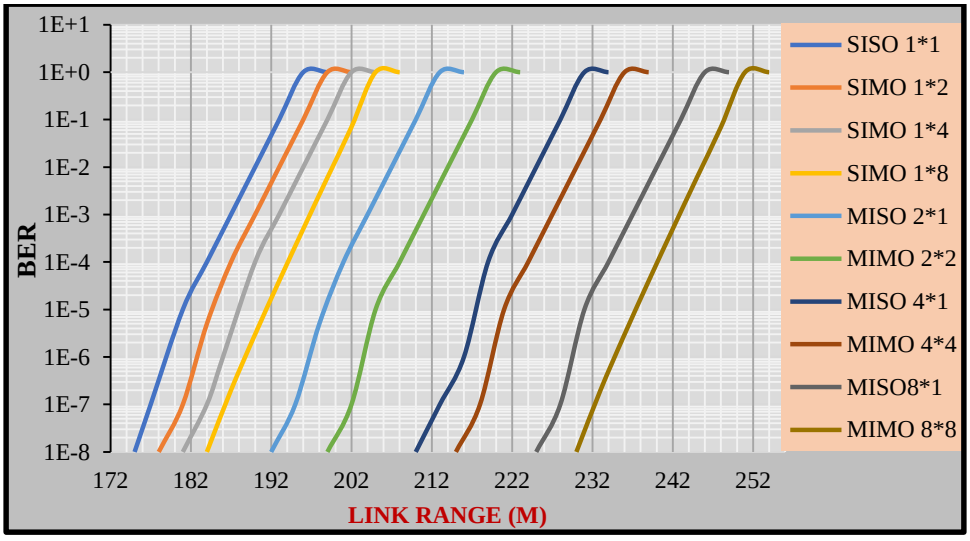

Fig.4.33: Link Range vs BER for OOK-Manchester code at 100Gbps with SISO technique and various MIMO configurations in clear water.

In mid-turbulence channels (coastal water), at 100Gbps the numerical results of BERs, Q factor, and links range have been obtained as shown in the table below (4.26).

Table (4.26): Simulation results of OOK-Manchester code modulation under coastal water at 100Gbps

Techniques	Max Link Range(m)	BER	Q Factor
1X1SISO	79	1.54×10^{-9}	5.72
1X2SIMO	80	3×10^{-8}	5.41
1X4SIMO	81	3.77×10^{-8}	5.37
1X8SIMO	83	1.43×10^{-7}	5.13
2X1MISO	86	2.29×10^{-8}	5.46
4X1MISO	94	6.22×10^{-8}	5.28
8X1MISO	98	5.7×10^{-9}	5.7
2X2MIMO	89	1.78×10^{-8}	5.51
4X4MIMO	96	6.61×10^{-8}	5.27
8X8MIMO	101	1.67×10^{-8}	5.52

Figure (4.34) presents the schematic graphic of the link range versus BER of the OOK-Manchester code 100Gbps with 1✕1SISO and different MIMO configurations in coastal water.

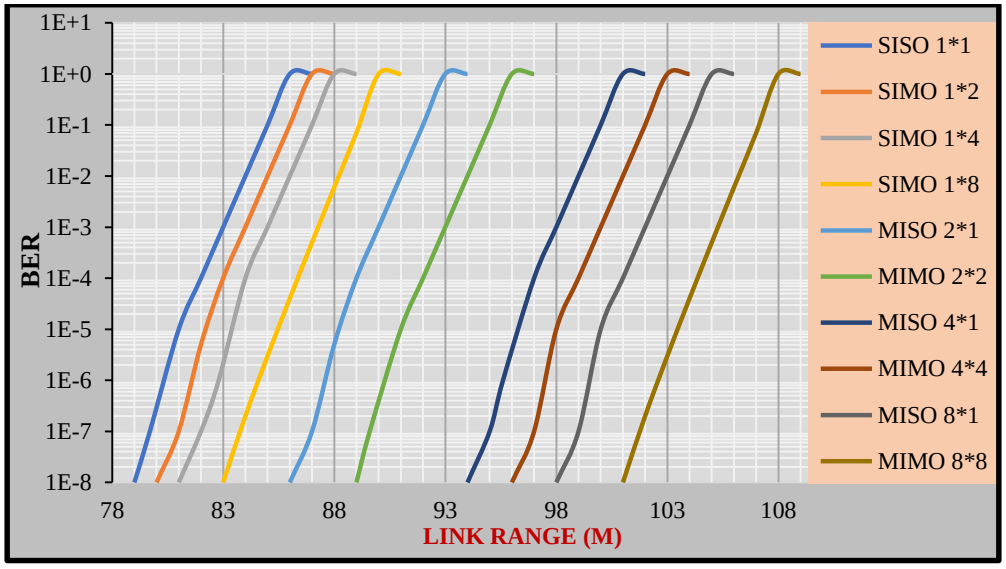

Fig.4.34: Link Range vs BER for OOK-Manchester code at 100Gbps with 1✕1SISO and multiple MIMO configurations in coastal water.

In a high turbulence channel (turbid water), at 100Gbps the numerical values of BERs, Q factor, and links range have been obtained as shown in the table (4.27).

Table (4.27): Simulation results of OOK-Manchester code modulation under turbid water at 100Gbps.

Techniques	Max Link Range(m)	BER	Q Factor
1✕1SISO	18	8.07×10^{-9}	5.64
1✕2SIMO	18.2	2×10^{-8}	5.48
1✕4SIMO	18.4	4.93×10^{-8}	5.32
1✕8SIMO	18.6	1.98×10^{-7}	5.07
2✕1MISO	19.6	1.6×10^{-8}	5.52
4✕1MISO	21	1.15×10^{-8}	5.58
8✕1MISO	22.2	1.11×10^{-8}	5.59
2✕2MIMO	19.9	3.1×10^{-8}	5.41
4✕4MIMO	21.3	3.23×10^{-8}	5.4
8✕8MIMO	22.5	3.91×10^{-8}	5.37

Figure (4.36) shows the schematic graphic of the link range versus BER of the OOK-Manchester code at 100Gbps with SISO and multiple MIMO configurations.

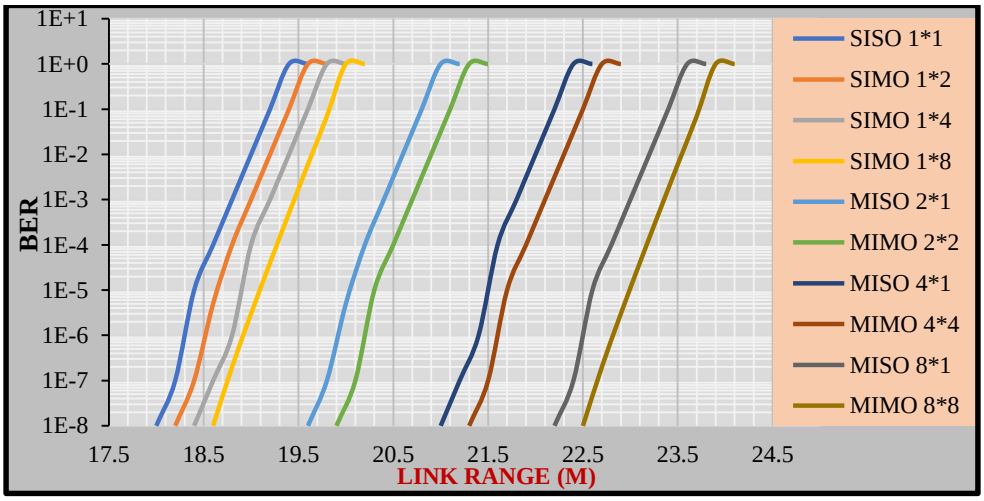

Fig.4.35: Link Range vs BER for OOK-Manchester code at 100Gbps with SISO technique and various MIMO configurations in turbid water.

Figure (4.37) presents the graphic chart of the received power vs the link distance for the OOK-Manchester code under 3 water types correspondingly (turbid, coastal, and clear). It is essential to note that the transmitted power remains constant at 20 dB for all distances specified.

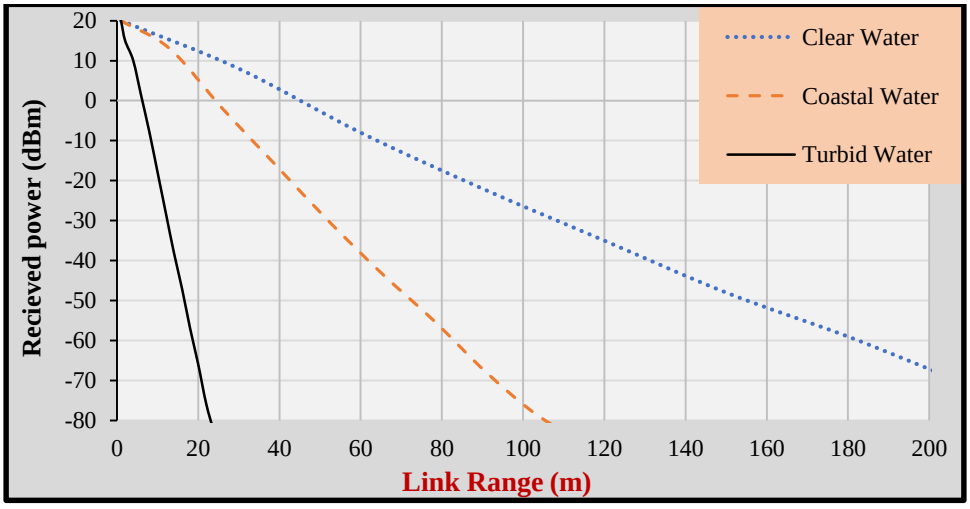

Fig.4.36: Link Range vs Received Power of OOK-Manchester with 8×8MIMO under three water types.

From the previous figures, the performance of 8×8MIMO and 8×1MISO systems under 3 types of water (turbid, coastal, and clear) is superior to the other techniques (SISO1×1, SIMO1×2, SIMO1×4, SIMO1×8, MISO2×1, MISO4×1, MIMO2×2 and MIMO4×4 respectively). Thus, it can be seen that increasing the receiver elements (photodetectors) improved the link range, and also the link range decreased by increasing the data rate.

4.6 Summarization and Comparison of Simulation Results

Table (4.28) shows a summary of the results comparison of QPSK-OFDM and OOK Modulation with three types of encoding techniques (NRZ, CSRZ, Manchester code) for 1×1SISO and 8×8MIMO techniques in 3 types of water.

Table (4.28): Comparison summary of QPSK-OFDM and OQK modulation results

UWOC System		**Clearwater**			**Coastal water**			**Turbid water**		
		Range (m)	BER	P_R (dBm)	Range (m)	BER	P_R (dBm)	Range (m)	BER	P_R (dBm)
QPSK-OFDM (20Gbps)	1×1SISO	174	1×10^{-8}	-56	74	2×10^{-8}	-53	18	1×10^{-8}	-55
	8×8MIMO	230	3×10^{-8}	-58	101	2×10^{-8}	-54	22.1	6×10^{-8}	-57

OOK-NRZ (10Gbps)	1×1SISO	162	7×10^{-8}	-50	72	6×10^{-8}	-48	16.9	3×10^{-8}	-55
	8×8MIMO	214	2×10^{-7}	-54	95.5	2×10^{-7}	-50	21.1	7×10^{-9}	-57
OOK-CSRZ (10Gbps)	1×1SISO	129	2×10^{-8}	-60	60	2×10^{-8}	-58	14.3	1×10^{-8}	-62
	8×8MIMO	179	7×10^{-8}	-60	82	7×10^{-8}	-59	18.6	2×10^{-7}	-65
OOK-Manchester (10Gbps)	1×1SISO	200	6×10^{-8}	-65	90	3×10^{-8}	-61	20	2×10^{-8}	-66
	8×8MIMO	257	1×10^{-7}	-67	113	2×10^{-7}	-64	24.5	2×10^{-7}	-68

In terms of bit error rate (BER) and link range, the performance of the UWOC system with 8×8MIMO is better than to that of the UWOC system with the SISO technique in the undersea environment. The results indicate that the effect of spatial diversity can significantly improve the system performance and also increase the link range, the performance of the proposed QPSK-OFDM and OOK-Manchester code with 8×8MIMO are better than OOK-NRZ and OOK-CSRZ with

8×8MIMO in terms of link range and BER for the underwater environment. Table (4.29) presents a comparison of published and proposed work.

Table 4.29: A comparison between suggested work with published works.

Authors	Transmitter type	Light power (mW)	BER	Modulation technique	Data rate	Distance (m)	Type of water
[11]	450nm LED	100mw	10^{-3}	64QAM-OFDM	127.07 Mbps	40	Coastal
[12]	532nm LD	25-100 mw	10^{-9}	OOK-3×1MISO	(0.5-50) Gbps	11-25	Coastal
[15]	450nm LD	100mW	10^{-3}	4QAM-4DPSK – OFDM	40Gbps	270 45 12	Clear Coastal turbid
[57]	450nm LD	100mw	10^{-5}	DPSK-OFDM-DD 4×4MIMO	10 Gbps	130 31.5 10.50	Clear Coastal Turbid
			10^{-5}	DPSK-OFDM-CD 4×4 MIMO		156.3 38.6 12.1	Clear Coastal Turbid
suggested work	450nm LD	100mw	10^{-8}	QPSK-OFDM 8×8MIMO	20 Gbps	230 101 22.1	Clear Coastal Turbid
				OOK-NRZ 8×8MIMO	10 Gbps	214 95.5 21.1	Clear Coastal Turbid
				OOK-CSRZ 8×8MIMO		179 82 18.6	Clear Coastal Turbid
				OOK-Manchester code 8×8MIMO		257 113 24.5	Clear Coastal Turbid

suggested work	450nm LD	100mw	10^{-8}	OOK-NRZ 8×8MIMO	40 Gbps	196 88.5 19.8	Clear Coastal Turbid
				OOK-CSRZ 8×8MIMO		155 73 16.5	Clear Coastal Turbid
				OOK-Manchester code 8×8MIMO		241 106 23.5	Clear Coastal Turbid
				OOK-NRZ 8×8MIMO	100 Gbps	185 84 19	Clear Coastal Turbid
				OOK-CSRZ 8×8MIMO		0 0 0	Clear Coastal Turbid
				OOK-Manchester code 8×8MIMO		230 101 22.5	Clear Coastal Turbid

Table (4.29) compared the suggested work with [11,12,15,57] in term of link range and BER performance at same parameters. The link range of suggested work in coastal water is better than link range of literatures [11, 12, 15, 57] that achieved with OOK-Manchester code is 113m and BER is 10^{-8} compared to that in literatures [11, 12, 15, 57] which are 40m, 25m, 31m, and 38m respectively with BER are 10^{-3}, 10^{-9}, 10^{-3}, and 10^{-5} respectively. The suggested work employed many data rate started with 10Gbps up to 100Gbps, while the literature [11,12,15,57] employed 127Mbps, 50Gbps, 40Gbps, and 10Gbps respectively. Thus, the proposed systems transmitted data with high rate compared with literatures work.

Chapter Five

Conclusions and Suggestions for Future Works

Chapter five

Conclusions and Future Research Suggestions

5.1 Conclusions

From the simulation results of the techniques adopted in this work and the system performance values, the following points can be concluded:

1) In this work, two main valuable modulation schemes have been suggested to improve the UWOC performance which is QPSK- OFDM and OOK modulation shapes for different MIMO configuration. The strength of the UWOC system is tested over a range of transmission distances and different water types
2) The results show that the performance of the UOWC system with 8×8MIMO is better than the UOWC system with 1×1SISO in terms of BER and link range
3) In the case of turbid water, the OOK-Manchester code offered a better link range around 23.5 m with BER equal to 2×10^{-7} at 40 Gb/s data rate
4) In the case of clean water, the OOK-Manchester code offered a better link range around 240 m with BER equal to 1×10^{-7} at 40 Gb/s data rate
5) The performance of QPSK-OFDM is close to the performance of the OOK-Manchester code where the linked ranges achieved were 230 m and 22.1m for clean and turbid water and BER equals approximately 1×10^{-8}
6) In the OOK-NRZ and OOK-Manchester code system, the results were explained with an increase in the data rate to 100Gbps, while in the OOK-CSRZ system the data rate was increased to 40Gbps and after that, the Link Range=0 and BER=1 when the data rate was increased.

7) Comparatively to earlier work, the proposed method provides better system performance and link range under similar testing conditions.

5.2 Future Works Recommendations

The following is a summary of this work's proposals:

1) Design and testing of an underwater wireless communication system using Transceiver based Space Time Block Coding (STBC).

2) Improving the Underwater Wireless Optical Communication Channel Based on (DQPSK) differentially encoded quadrature phase shift keying modulated (OFDM) orthogonal frequency division multiplexing.

3) Design and testing of an underwater wireless communication system using a Polarization Modulation technique.

References

[1] X. Zhang, J. H. Cui, S. Das, M. Gerla, and M. Chitre, “Underwater Wireless Communications and Networks: Theory and Application: Part 2,” *IEEE Commun. Mag.*, vol. 54, no. 2, pp. 30–31, Feb. 2016, doi: 10.1109/MCOM.2016.7402257.

[2] M. Al-Rubaiai and X. Tan, “Design and development of an LED-based optical communication system with active alignment control,” *IEEE/ASME Int. Conf. Adv. Intell. Mechatronics, AIM*, vol. 2016-September, no. 2, pp. 160–165, Jul. 2016, doi: 10.1109/AIM.2016.7576760.

[3] Rabee M. Hagem, “Real Time Evaluation of Swimmers Performance Based on an Optical Wireless Communication System,” Griffith University, 2013. doi: https://doi.org/10.25904/1912/766.

[4] H. Kaushal and G. Kaddoum, “Underwater Optical Wireless Communication,” *IEEE Access*, vol. 4, pp. 1518–1547, 2016, doi: 10.1109/ACCESS.2016.2552538.

[5] F. Schill, U. R. Zimmer, and J. Trumpf, “Visible Spectrum OpticalCommunication and Distance Sensing for Underwater Applications Felix,” *Proc. ofACRA2004*, vol. 3, pp. 234–241, 2004.

[6] L. Liu, S. Zhou, and J. H. Cui, “Prospects and problems of wireless communication for underwater sensor networks,” Italy, 2008. doi: 10.1002/wcm.654.

[7] G. Baiden, Y. Bissiri, and A. Masoti, “Paving the way for a future underwater omni-directional wireless optical communication systems,” *Ocean Eng.*, vol. 36, no. 9–10, pp. 633–640, 2009, doi: 10.1016/j.oceaneng.2009.03.007.

References

[8] H. D. Trung and V. D. Nguyen, “An analysis of MIMO-OFDM for underwater communications,” in *International Congress on Ultra Modern Telecommunications and Control Systems and Workshops*, 2011, no. January.

[9] J. Bayarri, “Contribution to Research on Underwater Sensor Networks Architectures by Means of Simulation,” POLITECNICA DE VALENCIA, 2013.

[10] H. M. Oubei, C. Li, K.-H. Park, T. K. Ng, M.-S. Alouini, and B. S. Ooi, “23 Gbit/s underwater wireless optical communications using directly modulated 520 nm laser diode,” *Opt. Express*, vol. 23, no. 16, p. 20743, 2015, doi: 10.1364/oe.23.020743.

[11] J. Xu *et al.*, “OFDM-based broadband underwater wireless optical communication system using a compact blue LED,” *Opt. Commun.*, vol. 369, pp. 100–105, 2016, doi: 10.1016/j.optcom.2016.02.044.

[12] M. V. Jamali, J. A. Salehi, and F. Akhoundi, “Performance studies of underwater wireless optical communication systems with spatial diversity: MIMO Scheme,” *IEEE Trans. Commun.*, vol. 65, no. 3, pp. 1176–1192, 2017, doi: 10.1109/TCOMM.2016.2642943.

[13] F. Wang, Y. Liu, F. Jiang, and Nan Chi, “High speed underwater visible light communication system based on LED employing maximum ratio combination with multi-PIN reception,” *Opt. Commun.*, vol. 425, no. April, pp. 106–112, 2018, doi: 10.1016/j.optcom.2018.04.073.

[14] J. Wang, C. Lu, S. Li, and Z. Xu, “100 m/500 Mbps underwater optical wireless communication using an NRZ-OOK modulated 520 nm laser diode,” *Opt. Express*, vol. 27, no. 9, p. 12171, 2019, doi: 10.1364/oe.27.012171.

[15] H. M. Azzawi, A. H. Ali, S. A. Gitaffa, S. A. Kadhim, and H. A. Azawi,

References

"Performance Evaluation of Dual Polarization Coherent Detection Optical for Next Generation of UWOC Systems," in *2020 International Conference on Computer Science and Software Engineering (CSASE)*, Apr. 2020, pp. 117–122. doi: 10.1109/CSASE48920.2020.9142086.

[16] M. N. Hasan, A. G. Wadday, F. M. Ali, and H. M. Azzawi, "Performance Evaluating of DD-OFDM Based on MIMO System for Underwater Optical Wireless Communications," *Test Eng. Manag.*, vol. 83, no. November, pp. 25589–25598, 2020.

[17] S. Chakri D, O. S. Harsha Ambati, S. Reddy Putlur, and S. K, "Performance Analysis of Uwoc-4Qamofdm System With Mimo," *Int. J. Eng. Appl. Sci. Technol.*, vol. 6, no. 4, pp. 239–245, 2021, doi: 10.33564/ijeast.2021.v06i04.028.

[18] F. Kaeib, O. A. Alshawish, S. Ali Altayf, and M. A. Gamoudi, "Designing and Analysis of Underwater Optical Wireless communication system," in *2022 IEEE 2nd International Maghreb Meeting of the Conference on Sciences and Techniques of Automatic Control and Computer Engineering (MI-STA)*, May 2022, pp. 441–446. doi: 10.1109/MI-STA54861.2022.9837554.

[19] H. Brundage, "Designing a Wireless Underwater Optical Communication System," Massachusetts Institute of Technology, 2010.

[20] S. Hranilovic, *Wireless optical communication systems*. New York: Springer New York, 2005. doi: 10.1007/b99592.

[21] J. A. Simpson, "A 1 Mbps Underwater Communications System using LEDs and Photodiodes with Signal Processing Capability," North Carolina State University, 2007.

[22] M. H. Langaroodi, "Design and Performance of a 1550nm Free Space Optical Communication Link," CALIFORNIA STATE UNIVERSITY,

References

2013. doi: 10.1088/1751-8113/44/8/085201.

[23] G. P. Agrawal, *Fiber- Optic Communication Systems*, Third Edit., vol. 6. Wiley, 2010. doi: 10.1002/9780470918524.

[24] Xiaoyong Chen, "Design and Otimization of Optical Fiber Based PSK Demodulation for High bit rate optical networks," University of Politécnica de Madrid, 2015.

[25] A. Hraghi, "Application of Mach-Zehnder Modulator for High Speed Optical Communication Network," 2016.

[26] C. M. G. Gussen, P. S. R. Diniz, M. L. R. Campos, W. A. Martins, F. M. Costa, and J. N. Gois, "A Survey of Underwater Wireless Communication Technologies," *J. Commun. Inf. Syst.*, vol. 31, no. 1, pp. 242–255, 2016, doi: 10.14209/jcis.2016.22.

[27] E. Biglieri, "Digital Modulation Techniques," in *The Communications Handbook*, Second edi., CRC Press, 2002, pp. 1–686. doi: 10.1201/9781420041163-22.

[28] T. D. Memon, W. Ghangro, B. S. Chowdhry, and A. A. Shaikh, "Quadrature phase shift keying modulator & demodulator for wireless modem," *2009 2nd Int. Conf. Comput. Control Commun. IC4 2009*, vol. 4, no. 1, pp. 2–7, 2009, doi: 10.1109/IC4.2009.4909180.

[29] J. Wu, Y. L. Xie, and S. Ouyang, "Performance of decision feedback differential detection for ADQAM-OFDM in high mobility environments," *ACM Int. Conf. Proceeding Ser.*, pp. 4–10, 2019, doi: 10.1145/3386415.3387056.

[30] K. Kim and A. Polydoros, "Digital modulation classification: The BPSK versus QPSK case," *Proc. - IEEE Mil. Commun. Conf.*, vol. 2, pp. 431–436, 1988, doi: 10.1109/milcom.1988.13427.

References

[31] B. Sklar, *DIGITAL COMMUNICATIONS Fundamentals and Applications*, Second Edi. Prentice Hall PTR, 2013.

[32] S. Rajbhandari, *Optical Wireless Communications*, Second Edi. CRC Press, 2012. doi: 10.1201/b12687.

[33] N. M. Aldibbiat, Z. Ghassemlooy, and R. McLaughlin, "Indoor optical wireless systems employing dual header pulse interval modulation (DH-PIM)," *Int. J. Commun. Syst.*, vol. 18, no. 3, pp. 285–305, Apr. 2005, doi: 10.1002/dac.704.

[34] M. Pfennigbauer, M. Pauer, P. J. Winzer, and M. M. Strasser, "Performance optimization of optically preamplified receivers for return-to-zero and non return-to-zero coding," *AEU-Archiv fur Elektron. und Ubertragungstechnik*, vol. 56, no. 4, pp. 261–267, 2002, doi: 10.1078/1434-8411-54100106.

[35] G. Castanon and T. Hoshida, "Impact of Filter Dispersion Slope in NRZ , CS-RZ , IMDPSK and RZ formats on Ultra High Bit-rate Systems," in *2002 28TH European Conference on Optical Communication*, 2002, pp. 8–9. doi: 10.1109/ECOC.2002.204762.

[36] R. Forster, "Manchester encoding: opposing definitions resolved," *Eng. Sci. Educ. J.*, vol. 9, no. 6, pp. 278–280, Dec. 2000, doi: 10.1049/esej:20000609.

[37] G. S. Hura and M. Singhal, *Data and Computer Communications*, Eighth Edi. CRC Press, 2001. doi: 10.1201/9781420041316.

[38] Z. Zeng, S. Fu, H. Zhang, Y. Dong, and J. Cheng, "A Survey of Underwater Optical Wireless Communications," *IEEE Commun. Surv. Tutorials*, vol. 19, no. 1, pp. 204–238, 2017, doi: 10.1109/COMST.2016.2618841.

References

[39] G. S. Spagnolo, L. Cozzella, and F. Leccese, "Underwater optical wireless communications: Overview," *Sensors (Switzerland)*, vol. 20, no. 8, pp. 1–14, 2020, doi: 10.3390/s20082261.

[40] M. Massot-Campos and G. Oliver-Codina, "Optical sensors and methods for underwater 3D reconstruction," *Sensors (Switzerland)*, vol. 15, no. 12, pp. 31525–31557, 2015, doi: 10.3390/s151229864.

[41] S. Jaruwatanadilok, "Underwater wireless optical communication channel modeling and performance evaluation using vector radiative transfer theory," *IEEE J. Sel. Areas Commun.*, vol. 26, no. 9, pp. 1620–1627, 2008, doi: 10.1109/JSAC.2008.081202.

[42] L. J. Johnson, F. Jasman, R. J. Green, and M. S. Leeson, "Recent advances in underwater optical wireless communications," *Underw. Technol.*, vol. 32, no. 3, pp. 167–175, 2014, doi: 10.3723/ut.32.167.

[43] S. Arnon, "Underwater optical wireless communication network," *Opt. Eng.*, vol. 49, no. 1, p. 015001, 2010, doi: 10.1117/1.3280288.

[44] H. M. Oubei, "Underwater Wireless Optical Communications Systems : from System- Level Demonstrations to Channel Modeling," King Abdullah University of Science and Technology, 2018.

[45] E. Zedini, H. M. Oubei, A. Kammoun, M. Hamdi, B. S. Ooi, and M. S. Alouini, "Unified Statistical Channel Model for Turbulence-Induced Fading in Underwater Wireless Optical Communication Systems," *IEEE Trans. Commun.*, vol. 67, no. 4, pp. 2893–2907, 2019, doi: 10.1109/TCOMM.2019.2891542.

[46] H. T. Belay, H. Zhao, and A. A. Okine, "On the Performance Analysis of Multi-Hop Hybrid FSO/RF Systems Using DPSK-SIM over Gamma-Gamma Turbulence Channel," in *ACM International Conference Proceeding Series*, Dec. 2021, pp. 201–206. doi:

10.1145/3507971.3508014.

[47] W. Shieh, *OFDM for Optical Communications*, First Edit. Elsevier, 2010. doi: 10.1016/C2009-0-19354-6.

[48] B. Zid and R. Kosai, "Multi User MIMO Communication: Basic Aspects, Benefits and Challenges," in *Recent Trends in Multi-user MIMO Communications*, InTech, 2013, pp. 3–24. doi: 10.5772/57133.

[49] A. Aled, "High Data Rate Coherent Optical Ofdm System for Long Haul Transmission," University of Denver, 2013.

[50] A. S. AL SHANTTi, "Optical Orthogonal Frequency Division Multiplexing Direct Detection for Improving Capacity of Radio over Fiber Transmission System," The Islamic University of Gaza, 2012.

[51] S. K. Rony, F. A. Mou, and M. Rahman, "Performance Analysis of OFDM Signal Using BPSK and QPSK Modulation Techniques," *Am. J. Eng. Res.*, no. 6, pp. 108–117, 2017, [Online]. Available: www.ajer.org

[52] Z. Wang, Y. Hou, and Z. Wang, "Compressed image transmission in precoded OFDM VLC systems," no. Vlc, pp. 0–22, 2022, doi: https://doi.org/10.21203/rs.3.rs-1053273/v1.

[53] M. Ben Zeglam, "A Novel Multi-band CO-OFDM based Long Reach Passive Optical Network Architecture," University of Waterloo, 2017.

[54] M. Abraham, "Analysis of Underwater Environment and Establishment of Underwater Wireless Optical Communication link," *EuroJournals Publ.*, vol. 87, no. April 2017, pp. 349–358, 2012.

[55] T. C. Wu, Y. C. Chi, H. Y. Wang, C. T. Tsai, and G. R. Lin, "Blue laser diode enables underwater communication at 12.4 gbps," *Sci. Rep.*, vol. 7, no. August 2016, pp. 1–10, 2017, doi: 10.1038/srep40480.

[56] C. D. Q. Mendez, E. F. H. Zuniga, and G. A. G. Agredo, "Effect of M-

References

QAM Modulation Technique for a Converged Network Infrastructure Radio over Fiber (RoF),” *Ing. y Desarro.*, vol. 39, no. April, p. 20, 2021.

[57] A.-F. Al-Awsat and M. N. Hasan, “REPUBLIC OF IRAQ MINISTRY OF HIGHER EDUCATION AND SCIENTIFIC RESEARCH Investigation the Performance of Underwater Optical Wireless Communication Under Impacts of Different Modulation Schemes and MIMO Configuration,” AL-FURAT AL-AWSAT TECHNICAL UNIVERSITY, 2020.

الخلاصة

أن إرسال واستقبال البيانات والمعلومات لاسلكياً في البيئة المائية يدعى بالاتصال اللاسلكي تحت الماء (UWC) والذي يتم بواسطة استخدام الحاملات اللاسلكية والتي تقسم إلى ثلاث انواع : الموجات الصوتية، والموجات الراديوية، والموجات الضوئية. في هذا العمل تم التركيز على الموجات الضوئية واستخدامها كحاملات لاسلكية لتصميم وتشكيل نظام اتصال لاسلكي ضوئي تحت الماء (UWOC). إن استخدام هذا النوع من الحاملات اللاسلكية في هذا العمل بسبب نطاق الإرسال الواسع الذي تملكه وبالتالي فأن معدل إرسال البينات سوف يكون كبير جداً مقارنتاً بالنوعين الآخرين (الحاملات الصوتية والحاملات الراديوية) وبسبب هذه الميزة فإن العديد من الباحثين اهتمو بتصميم انواع مختلفة من أنظمة الاتصال اللاسلكي الضوئي تحت الماء والتي لها استخدامات عديده مثل الاستكشافات البحرية والرصد البيئي والاستخدامات العسكرية وغيرها. ورغم هذه المميزات لهذا النوع من الإتصال اللاسلكي الا ان امتصاص الماء للضوء وتشتته بواسطة الجسيمات والاحياء الموجوده في البيئة المائية والضوضاء المصاحبة لعملية الإرسال والاستقبال تعد أبرز العوائق التي تواجه هذا النظام.

في هذا العمل تم اقتراح نوعين من التضمين بالإضافة إلى التقنيات الساندة الأخرى. النوع الأول هو QPSK مع تقنية OFDM والنوع الثاني هو OOK واستُخدم معه ثلاث أشكال من النبضات (NRZ, CSRZ, Manchester code) ويتم التحقق من فعالية نظام الاتصال اللاسلكي الضوئي من خلال استخدام مسافات إرسال متعدده مع انواع الماء المختلفة (الماء الصافي، الماء الساحلي، والماء العكر). بالإضافة إلى ذالك تم محكاه النظام باستخدام SISO ١×١ و تكوينات مختلفة من MIMO وبمعدلات بينات مختلفة.

قدم النظام المقترح ان استخدام تقنية MIMO ٨×٨ مع نظام UWOC هو أفضل من التقنيات المستخدمة الأخرى من حيث أقصى مسافة إرسال ومعدل الخطأ في البيانات BER. وقد أظهر النظام ان أداء نوعي التضمين المقترح QPSK-OFDM و OOK-Manchester code مع تقنية MIMO ٨×٨ افضل من NRZ-OOK و CSRZ-OOK تحت نفس الظروف. فقد حقق QPSK-OFDM مع MIMO 8×8 مسافة ارسال تقريبا ٢٢,١م ومعدل خطا (BER) يساوي 6×10^{-8} عند معدل ارسال ٢٠ جيجابت في الثانية في الماء العكر اما في OOK-Manchester فقد حقق مسافة ٢٤,٥م ومعدل خطا (BER) يساوي 2×10^{-7} عند معدل ارسال ١٠ جيجابت في الثانية وفي الماء العكر. بالمقارنة فان التقنيات المقترحة في هذا العمل تحقق مسافات ارسال ومعدلات خطا افضل من الاعمال السابقة عند نفس الظروف.

وزارة التعليم العالي والبحث العلمي

جامعة بابل / كلية الهندسة

قسم الهندسة الكهربائية

تحسين المحاكاة لنظام الاتصالات الضوئية اللاسلكية تحت الماء

رســـالـــــة

مقدمة الى كلية الهندسة في جامعة بابل

كجزء من متطلبات نيل درجة الماجستير في علوم الهندسة الكهربائية/اتصالات

من قبل

علي محمد عبد الساده عبد الواحد

اشراف

الاستاذ الدكتور حيدر جبار عبد نصار

١٤٤٤هـ **٢٠٢٣م**